THESIS

SOME ASPECTS OF THE COMPUTATIONAL COMPLEXITY IN THE DESIGN OF ISLANDED MICROGRIDS, DESIGN AND ANALYSIS OF BLACKSTART SEQUENCES FOR A NOTIONAL MICROGRID

Submitted by

Sudarshan Ananda Natarajan

Department of Electrical and Computer Engineering

In partial fulfillment of the requirements

For the Degree of Master of Science

Colorado State University

Fort Collins, Colorado

Summer 2012

Master's Committee:

Advisor: Siddharth Suryanarayanan
Co-Advisor: Sanjay Rajopadhye

Dan Zimmerle
Vakhtang Putkaradze

ABSTRACT

SOME ASPECTS OF THE COMPUTATIONAL COMPLEXITY IN THE DESIGN OF ISLANDED MICROGRIDS, DESIGN AND ANALYSIS OF BLACKSTART SEQUENCES FOR A NOTIONAL MICROGRID

The US grid represents more than $1 trillion in assets and serves over 100 million customers. But the grid is an aging system, and was built as centralized system architecture. The Title XIII of the Energy Independence and Security Act of 2007 outlined the 'Smart Grid Initiative' (SGI) as an official policy for modernization of the United States electricity transmission and distribution system to improve reliability and upgrade infrastructure to meet the ever increasing demand in electricity. The distribution feeder is the final link between the generation units and the end user. Distribution networks were traditionally designed in a radial topology since such configurations resulted in simpler protective schemes. More recently, there has been a renewed focus on distribution feeder reconfiguration. Reconfiguration at the distribution level can be achieved by the use of switches and sectionalizers. This enables portions of the distribution network to be reconfigured dynamically to improve reliability, hence enabling control on the topological structure of the distribution feeder. A related feature is the *microgrid,* or an islanded distributed resource (DR). The IEEE 1547.4 Standard on 'The guide for design, operation and integration of DR island systems with electric power supply' defines a microgrid as an electric power system that has the following properties:

- a local distributed resource and load
- the ability to disconnect from and parallel with the area electric power supply
- include the local electric power supply and portions of area electric power supply

A microgrid is capable of disconnecting from the main grid, on sensing a disturbance on the main grid, to maintain reliable supply of electricity to the constituent end-user loads. In this work, the computational complexity of the design of islanded microgrids by the optimal addition of network feeders in a legacy

radial electric distribution system is identified, and a technique to accelerate the process of finding Pareto optimal solutions to the problem is provided. The next part of this thesis models a notional microgrid with blackstart capabilities. Microgrids that cannot continue uninterrupted supply to all local loads on disconnection from main grid are required to follow a sequence for startup which is known as the blackstart sequence. In this work, the various generation resources in the notional microgrid are studied and a blackstart sequence is engineered.

ACKNOWLEDGEMENTS

It is my pleasure to thank all who have helped and inspired in the completion of my Master's degree. First and foremost, I sincerely thank my adviser Dr. Siddharth Suryanarayanan for his invaluable encouragement and guidance in the completion of this work. Dr. Sid's passion for research in *Smart Grids* is truly inspiring. I thank him for providing me the opportunity to be a part of his research group.

Thanks also to Dr. Rajopadhye, for his sound advice and guidance in the first part of my thesis.

I also thank Prof. Zimmerle for his support and advice in generator modeling. His friendly approach and cheerful attitude made my time at EECL a memorable learning experience.

Special thanks to Dr. Putkaradze for his tips and advice in my work.

This work was supported by Joint Institute for Strategic Energy Analysis (JISEA), CSU Energy Supercluster, National Renewable Energy Labs (NREL), US Navy and US Marine Corps. I would like to thank Ms. Julieta Giràldez for the help provided in this work. I also thank Jim Cale for providing me the opportunity for a part of this research.

I thank my family for their love and constant encouragement. I thank my parents, V A Natarajan and Poornima Natarajan, for always creating a positive learning environment at home, and constantly encouraging my brother and me to always strive for excellence. I thank my brother, Shiv Natarajan, for his invaluable guidance and reassurance in my capabilities. None of this work would have been possible without the unyielding support of my family.

I would like to thank the ECE dept. and Colorado State University for this opportunity. I have immensely enjoyed the experience.

Thanks to all members of the APEL lab for your tips. Special thanks to Manish Mohanpurkar and Robin Roche for your invaluable inputs and jovial company in the lab.

Lastly, a special thanks to Hrushikesh Kulkarni, Ishan Thakkar, Mihir Desai, and Pritam Shah. You have made my graduate life a truly memorable time.

TABLE OF CONTENTS

LIST OF TABLES

LIST OF FIGURES

NOMENCLATURE

3FDR	Three Feeder system
3-SAT	Length 3 clause satisfiability problem
ε	Radial distance of destination bus from slack bus on same feeder
ω	Radial distance of the source bus from the slack bus on the same feeder
β	Load step value
ψ	Conjunctive normal form expression
∂	Step size of a step load
Ω	Formal notation associated with Big-O notation
θ	Formal notation associated with Big-O notation
ΔT_β	Duration of load step β
λ	Wavelength
A	Known NP problem
AC	Alternating Current
ACO	Ant Colony Optimization
ASAI	Average System Availability Index
ASCR	Aluminum Conductor Steel Reinforced
B	Problem to be proved to be in NP
B_{ij}	Binary bus connection indicator
BEM	Building Energy Management
c_1, c_2, c	Constants
C	Set of clauses in a SAT problem
C_{DG}	Cost of distributed generation
CF_{CDG}	Capacity factor of conventional distributed generation resource
CF_{RE}	Capacity factor of renewable resource

C_i	Cost of possible connection i
C_i^{DG}	Cost of DG located at bus i.
CAIDI	Customer Average Interruption Duration Index
CDG	Conventional Distributed Generation
CERTS	US Centre for Energy Reliability Technology Solutions
CF	Capacity Factor
CHP	Combined Heat and Power
CNF	Conjunctive Normal Form
COM	Component Object Model
CPP	Critical Peak Pricing
d	Radial distance between feeders
D	Length of intertie
DA	Distribution Automation
DC	Direct Current
DER	Distributed Energy Resource
DG	Distributed Generation
DOE	US Department of Energy
DR	Demand Response
DRP	Demand Reduction Program
DS	Distributed Storage
EDLC	Electric Double Layer Capacitor
ENS	Energy Not Served
f_n	Maximization function
$F(x)$	Complete objective function matrix
$F_k(x)$	Objective function

$g(x)$	Inequality constraints
$g(n)$	Lower or upper bounding function in Big-O notation
G	Weighted graph in a TSP
G_n	n^{th} generator in the 3FDR system
GA	Genetic Algorithm
GB	Great Britain
GEP	Generation Expansion Planning
$h(x)$	Equality constraints
HQ	Hydro Québec
HVAC	High Voltage Alternating Current
i	Index to bus number in the feeder system Index to number of power overloaded lines Index to number of voltage overloaded buses having voltage under 1 p.u Index to number of variables in the SAT/3-SAT problem Index to number of buses that have a power generation source
I	Integer or integer matrix associated with the maximization function in a feeder reconfiguration problem
IEEE	The Institute of Electrical and Electronics Engineers
IPS	Integrated electric Power Systems
j	Index to bus number in the feeder system Index to number of inequality constraints in an optimization problem Index to number of voltage overloaded buses having voltage over 1 p.u
k	Number of objective functions
K_d	Gain of differential controller
K_c	Critical gain of system in second Zeigler Nicholas method
K_i	Gain of integral controller
K_p	Gain of proportional controller
l	Index to number of equality constraints in an optimization problem
L_i	Average load at bus *i* in the distribution network

	Length of an intertie *i*
L_{ij}	Length of a possible connection from bus *i* to bus *j*
$L_{i,Pload_{max}}$	Maximum load at bus *i* in the distribution network
L_n	n^{th} load in the 3FDR system
L_β	Load level β
$L_{\beta max}$	Annual maximum load level β (peak load)
$L_{\beta min}$	Annual minimum load level β (base load)
LV	Low Voltage
m	Number of inequality constrains
MAIFI	Momentary Average Interruption Frequency Index
MCFC	Molten Carbonate Fuel Cell
MOGA	Multi Objective Genetic Algorithm
MW	Mega Watt
n	Size of input to a function Number of radial feeders in the reconfiguration problem Number of loads in the 3FDR system Number of generators in the 3FDR system Number of transformers in the 3FDR system
n1	number of voltage overloaded buses having voltage under 1 p.u
n2	number of voltage overloaded buses having voltage over 1 p.u
N	Number of strings produced in each generation Number of pointers in the roulette wheel
N_β	Number of load levels
N_{branch}	Number of branch loading violations
N_{bus}	Number of bus loading violations
N_c	Number of bus loading violations
N_s	Number of buses that have a power source in the distribution network
NiMH	Nickel Metal Hydride

NG	Natural Gas
NP	Non-Deterministic Polynomial Time
NREL	National Renewable Energy Labs
O	Formal notation associated with Big-O notation
O_i	Power overload at branch *i*
$p(n)$	Polynomial function of input size *n*
P	Polynomial time problem
P_{CDG}	Power output of conventional DG resource
P_{DG}	Power output of DG resource
P_{DS}	Power output of DS resource
P_i^{DG}	Power output of DG located at bus *i*
P_{ij}	Power flow between two buses *i* and *j*
P_{out}	Total power
P_{power_flow}	Branch violation penalty
P_{renew}	Power output of renewable resource
P_s	Power output of power source located at bus *s* Period of oscillation in the second Zeigler Nicholas method
$P_{voltage}$	Bus voltage violation penalty
PID	Proportional Integral Differential controller
PMF	Probability Mass Function
PSCAD™	Power Systems Computer Aided Design
PSO	Particle Swarm Optimization
PUCT	Public Utility Commission of Texas
PV	Photovoltaic
R_{CDG}	Rated power output of conventional DG resource

R_{RE}	Rated value of renewable resource
r	Number of equality constraints
R	Resistance of line
RAM	Random Access Machine
RBTS	Roy Billinton Test System
RE	Renewable Energy
RES	Renewable Energy Source
RTP	Real-Time Pricing
S	Start/end node in a TSP problem
SAIDI	System Average Interruption Duration Index
SAIFI	System Average Interruption Frequency Index
SAT	Satisfiability problem
SCADA	Supervisory Control And Data Acquisition
SGI	Smart Grid Initiative
SPIDERS	Smart Power Infrastructure Demonstration for Energy Reliability and Security
T_n	n^{th} transformer in the 3FDR system
THD	Total Harmonic Distortion
TNEP	Transmission Network Expansion Planning
TSP	Travelling Salesman Problem
U	Average duration for which power is unavailable
UCSD	University of California, San Diego
V	Set of variables in a SAT problem
v_i	Boolean variable
V_i	Voltage at a bus i
w	Number of overloaded lines
x	Input to a general multi-objective problem

	Total number of buses in the feeder system
x^*	An input to the multi-objective problem
x_{ij}	Intertie from bus *i* to bus *j*
x_n	n^{th} feeder in the system Number of buses in the n^{th} feeder
X	Reactance of line
y_i	Integer equivalent variables of a SAT Boolean variable
$\overline{y_i}$	Integer equivalent variables of a SAT Boolean variable
Z_n	Clause of a SAT problem

Chapter 1
Introduction

1.1 Objective

The objective of this thesis is two-pronged. In the first part of the work, bounds on the numerical growth of the problem of redesign of the traditional radial distribution feeder system into a meshed network are developed. Also, the existing computational technique for redesign of the distribution system is accelerated by an order of magnitude. The second objective of this thesis is to analyze the sequence of blackstart operations for a notional mission-specific islanded distributed resource (microgrid).

1.2 Motivation

The US grid represents more than $1 trillion in assets and serves over 100 million customers [1]. But the grid is an aging system, and was built as central system architecture. Long-term construction and operation plans were developed on the availability of large power generation units and redundancy was present in the system to withstand short-term variation in demand and line outages.

The US Electrical Advisory Committee's report titled "Smart Grid: Enabler of the new energy economy," points out the various pressures on the current electric power system that encourage evolution of the power grid [2]. As reproduced from the document, these include:

- "Aging infrastructure and workforce
- Continuing national security concerns
- Increasing awareness of environmental issues including global warming
- Regulatory pressures
- Social pressures
- Calls for energy efficiency
- Growing demand for energy
- Rising consumer expectations
- Rapid innovations in technology" [2].

The Title XIII of the Energy Independence and Security Act of 2007 outlined the 'Smart Grid Initiative' (SGI) as an official policy for modernization of the United States electricity transmission and distribution system to improve reliability and upgrade infrastructure to meet the ever increasing demand in electricity [3]. Introduction of electronics, telecommunication, and information technology will enable utilities to achieve higher levels of efficiency in operation and better quality of service to consumers. Additional information about the conditions on the grid, including customer information allows utility services to become more reliable and efficient. Real-time pricing information permits customers to be better informed regarding the variability of the energy tariff and hence could lead to savings on electric bills [4]. An analysis by the Public Utility Commission of Texas (PUCT) indicated a savings of at least $1547 million at the end of the first year of restructured operation in Texas (2003) [4]. Most of the savings were in the residential sector with only $225 million due to the mandatory six percent rate reductions. In addition, studies showed that residents could have saved an additional $636 million, had they switched to the lowest offering in that area [4].

Aging infrastructure, reduced reliability and quality of supply are not a problem in the United States alone. Such problems are being identified in other countries such as United Kingdom [5], Germany [6], India [7] and, China [8]. For example, SmartGrid GB is the initiative adopted by Great Britain to transform the power grid into a futuristic grid which would be composed of integrated renewable energy sources and smart meters among other components to make a positive impact on the overall socio-economic and environmental benefits [9]. In the Britain initiative, 'smarter grid' is defined as an incremental process of applying information technology to the electric system, thus enabling dynamic real-time flows of information on the network. This helps operators monitor the network better, automatically control flow of power, manage and smooth out short-term fluctuations in demand and facilitate the interaction of all actors - including generators, network companies, suppliers and consumers – aimed at delivering sustainable economic and secure electricity supply [9]. Britain plans to achieve virtually all electric generation through clean energy sources by 2050 in order to achieve a target of 80 percent reduction in carbon emissions as stated in the Low Carbon Transition Plan [9]. Although the

challenges faced by southeast Asian countries are different, similar initiatives are being considered by those countries as well, in order to meet the future demand for electricity.

For the United States, a vision of the smart grid is presented by the U.S DOEs National Energy Technology Laboratory. The objectives include:

- Consumer participation encouraged through installation of smart meters: Active consumer participation can bring benefits such as reduced cost of electricity. Well informed consumers could also change their pattern of energy usage to balance their demands to the system's capability to meet those demands.
- Resist attack: Cyber threat poses a big challenge to the electric grid. The smart grid must be able to resist cyber vulnerabilities and must be able to recover rapidly from such attacks. This calls for the integration of better communication and information technology equipment which are designed to resist such attacks.
- Better quality of power: Introduction of new standards for quality of power will improve the quality of power received at the consumers end at reasonable prices. A special pricing structure could also be developed such that consumers pay based on the quality of power that they demand and receive.
- Ability to integrate all generation and storage options: The modern grid should be able to seamlessly integrate all forms of Distributed Energy Resources (DER) in a simplified plug-and-play form of interconnection. More importantly, the modern grid must be able to integrate renewable energy sources, such as wind and solar farms. To be able to connect to the grid at all points, including feed from a consumer, the grid should have the capability to connect and disconnect DER's at all voltage levels. DER's must have the capability to automatically start and shut down. For this, better sensors and communication infrastructure must be integrated to the modern grid.

- Storage options: Electricity as a commodity poses a special challenge as a large volume of electricity cannot be stored efficiently. The modern grid must have efficient distributed storage (DS) options that can be brought online quickly.
- Efficient component interaction: All components, new and old, must be able to interact and work efficiently. This will result in increase in overall functionality and reliability while reducing costs. Sensors must be able to detect requirement of maintenance, and hence a system that can report the requirement of time and condition based maintenance would help in extending the life of the grid.
- Self-Healing: Grid responses to events are presently retroactive in nature, and hence protection of assets in the event of a system fault is the main objective. The modern grid is expected to proactively respond by performing continuous self-assessment to detect, analyze, respond and restore grid components as required. Hence, the concept of self-healing will help maintain the overall grid reliability [10].

The distribution feeder is the final link between the generation units and the end user. Distribution networks were traditionally designed in a radial topology since such configurations resulted in simpler protective schemes. More recently, there has been a renewed focus on distribution feeder reconfiguration [11]. Reconfiguration at the distribution level can be achieved by the use of switches and sectionalizers. This enables portions of the distribution network to be reconfigured dynamically to improve reliability or to add distributed generation resources whenever required. Hence, the topological structure of the distribution feeder in that section is now controllable. Another important application of distribution feeder reconfiguration is loss minimization. Different feeders have different load compositions. Hence, the peak load on these feeders will occur at different times. If a particular feeder is reconfigured to minimize losses on the feeder at a particular hour of the day, load conditions are likely to change later that day. Distribution feeder reconfiguration can be classified under the larger concept of Distribution Automation (DA) [12]. An advanced distribution management system could be conceived for the management of various distribution level functions [13]. This system would be responsible for the following operations:

- Optimal network reconfiguration: Reconfiguration aids in controlling load on the system using switches to connect or disconnect load. Since the distribution feeder is typically radial, breakers or switches could be used to make interconnections between feeders. In cases where small generation units are present at the distribution level, a configuration can be chosen such that the load is evenly distributed between the feeders. And since consumer loads are inherently dynamic in nature, the frequent reconfiguration maybe required.
- Fault detection, isolation, and service restoration: Distribution feeder reconfiguration could greatly help in this function as the management system would now be able to identify the location of the fault and quickly reconfigure in order to isolate the fault and restore service to the other feeder sections. Acceleration of reconfiguration algorithms could greatly reduce the restoration time from several hours to a few minutes.
- Load balancing: This is a technique where the management system can classify loads according to their priority and hence, relieve the system of some of the low priority loads during periods of overload [13].

Distributed generation can be further realized/enhanced by the spread of microgrids. The Centre for Electricity Reliability Technology Solutions (CERTS) defines a microgrid as an aggregation of loads, microsources and associated controls providing heat and electricity to a localized region [14]. The IEEE 1547.4 Standard on 'The guide for design, operation and integration of DR island systems with electric power supply' defines a microgrid as an electric power system that has the following properties:

- a local distributed resource and load,
- the ability to disconnect from and parallel with the area electric power supply,
- ability to include the local electric power supply and portions of area electric power supply. During a disturbance, the microgrid separates from the main grid and can continue to maintain reliability of supply to the consumers who are connected to the microgrid [15].

The concept of a microgrid fits well into the notion of a smart grid since the microgrid can serve as a distributed source maintaining reliability of uninterrupted supply to critical loads. The microgrid also maintains quality of supply and most importantly, microgrids can be driven by clean sources of power. Traditionally, large power sources used to be located far away from the consumers, and long transmission and distribution lines were drawn to supply these loads. The centralized concept is not a viable option today for two reasons. Firstly, these power sources were mainly using sources of fuel whose burning caused high levels of pollution. With a large emphasis on green energy today, development of such plants in future will not be an option. Next problem is related to transmission lines. Drawing of a transmission line over an area of land virtually makes that piece of land unusable due to regulations. Hence, states today are not open to the idea of having such lines. These problems make distributed generation an attractive option. Distributed generation uses smaller microsources that run on clean fuel, and maintain reliability and quality of supply. Another big advantage of the microgrid is the ability to generate power closer to heat loads, such that the waste heat from the generator could be reused for the heat loads. This is known as a Combined Heat and Power (CHP) cycle. CHP essentially improves the efficiency of the entire system. Smaller generating units provide an option of locating microsources near heating loads, and hence improve the efficiency of the source. Centralized generation and distribution techniques are soon giving way to distributed generation due to loss of economies of scale [16]. The microgrid is viewed by the grid as a controllable load, consumers view the microgrid as a source of heat and electric power as well as a source of better quality power and voltage support. In future, micrigrids will have the option to intentionally isolate from the grid in want of better quality of power for the microgrid loads. Since microgrids drive smaller units of load as compared to central units, they have the option to derive their power from relatively smaller generators which can be run from cleaner sources of fuel [17].

Some of the options that are explored are natural gas plants, microturbines, fuel cells, PV and wind resources, battery storage and combined heat and plant (CHP). Natural gas in an attractive option due to its lower cost, greater availability and lower pollution [16]. Microturbines are a relatively new technology, well suited for microgrids due to compact size and ability to utilize waste fuels [18]. PV and

wind have been explored for a long time, and are important sources of green energy today. Problems with these sources include need for large expanses of land for setup of these units and the fact that they are a non-dispatchable resource [16]. The major source of loss in centralized generation plants is due to the heat generated in these plants. Heat generated in such plants is rarely reused, and is usually disposed off, potentially leading to environmental concerns. CHP units take the heat generated from the engines and reuse this recovered heat for other applications such as industrial heating, on-site space heating, local district heating, domestic hot water, sterilization, etc. [18]. The same cannot be adopted in current centralized setup because the generating units are usually located far away from any such heat load source. Moreover, transport and storage of heat is inefficient. A large portion of energy will be lost before the steam arrives at the desired location. Hence, microgrids make optimal use of this waste heat by co-locating the generating units near heat loads. Since microgrids typically use smaller generating units, in the order of 2-4 MW per unit, these can be easily located near heating loads [18]. The relatively small scale of heat generated in CHP units enables easy control and makes this heat energy ideal for several applications. As space cooling and refrigeration is a considerable source of power load in the US, the produced heat could be used for absorption cooling and desiccant dehumidification. Denmark, as of 1996, met 48% of its electric demand and 38% of its heat demand through CHP units [16]. Penetration in the US in comparison is a modest 12% as of 2008 [18]. The efficiency of the overall unit can be as high as 75-80% due to the re-use of heat. The main advantages of such a unit are:

- reduced fuel prices due to higher efficiency of system, and hence reduced dependence on fuel for heating purposes,
- reduced carbon emission, as the unit is working more efficiently,
- Reduced impact on environment, as the heat is reused and not disposed as waste into the environment [16].

Microgrids must essentially have peer-to-peer and plug-in capability [17]. A peer-to-peer capability ensures that there is no single unit in the system, whose loss could potentially bring down the entire microgrid. In other words, all units in the microgrid must complement and partially assume the

functionality of the other's in order to maintain an (N-1) reliability. Plug-in capability means that the generating unit and the associated control system can be moved to another location in the microgrid and can continue to work without extensive rework [17]. This capability will ensure that generating units can be located near heat loads, hence ensuring overall high efficiency of the system.

A microgrid operates in both grid-connected and in grid isolated mode [17]. A static switch is present at the point of common coupling. This switch is opened on the detection of a disturbance or fault on the grid. In a grid connected mode, the generators in the microgrid are turned off or are in standby mode. An option that is currently under study is whether a microgrid can export power to the main grid under favorable conditions. On observing a disturbance on the grid, the microgrid must be able to seamlessly isolate from the grid with little or no disruptions to the loads within the microgrid.

1.3 Scope

This section outlines the scope of this thesis. The first part of the thesis will establish bounds on the growth of the distribution feeder reconfiguration problem. The work further goes on to establish the computational complexity of the feeder reconfiguration problem. Such analyses provide justification for the use of non-conventional algorithms, and other heuristic algorithms over conventional search algorithms. Part of this thesis is an extension to the existing work on distribution feeder reconfiguration, given in [19], which involved modification of a radial feeder topology to a meshed network through the introduction of inter-ties in order to improve the reliability of supply in the network. This work was further extended in [20], where the author considered simultaneous co-location of DGs in addition to distribution feeder reconfiguration. But, solutions took long durations to converge even on simple systems [21]. The work in this thesis identified techniques to accelerate the convergence of solutions, whose implementation reduced the convergence time by an order of magnitude.

Work in the second part of this thesis involves the modeling of a notional mission-specific microgrid which consists of a mix of different types of generators. The work also involves arriving at a stable sequence of load and generator operations for blackstart operations. This work however does not cover the fault studies on the generators for the microgrid.

1.4 Literature Search

This section describes the current work in the area of distribution feeder engineering and microgrid operation. The four parts of this section cover the current trends of distribution feeder engineering, the evolution and current practices in microgrid planning and engineering, computational complexity of search algorithms and finally, the software tools and methods that were used in this work.

1.4.1 Distribution feeder engineering

Grid 2030 is the US DOEs long term vision for modernization of the power grid to meet the demands of 21st electric infrastructure [22]. In order to achieve this, intelligence needs to be incorporated in the current system through the integration of smart devices, meters, appliances, controls, communication and pathway sensors [23-28]. Hence, to achieve this true intelligence, a smart distribution system must be designed with the following properties:

- Identifying locations where increased intelligence of system would make most sense, and identifying the level of intelligence at each of these locations
- Distribution feeder reconfiguration from radial to partially meshed system
- Automation of controls through the strategic placement of sensors
- Identifying factors that will permit the seamless integration of renewable resources at distribution end [29].

1.4.1.1 Increased intelligence at consumer end through sensor deployment – Demand response

Recent trends point towards major changes in distribution power systems for improved efficiency and reliability [30]. Sensing and monitoring equipment will play an important role in this as real-time or near real-time updates to both user and distribution company will help in realizing goals such as demand response and self-healing capability respectively. Real-time monitoring of grid resources requires widespread deployment of sensing equipment. Based on the location of the sensing equipment the different parameters will be available, such as direction and amount of power flow, location and usage patterns of DER, notification in-case a DER is energizing the system, and the current system protection

settings [19]. Automation at the distribution level, such as smart meters, smart controls, and smart switches are a few of the resources whose benefits are currently being studied. In addition, customers in future will be able to choose the quality of power that they desire. Fixed tariffs for power will also be slowly phased out, ushering in attractive power structures to avoid peak loads and help in peak shaving [30]. Schemes will also be introduced to enable customers to voluntarily turn off high power consumption devices such as room heaters during peak loading, in order exchange for credits on their electric bills [30]. Through the use of sectionalizers and switches, utilities are able to restore power to some loads on faulty feeders. Feeder reconfiguration could also be used to reduce active losses of the network or to balance the load of the feeders. But, these reconfigurations need to be planned in advance, since the process of choosing the node or switch that needs to be connected or disconnected respectively must ensure that no loops are created in the system and no power or voltage constraints are violated in the process.

Despite a larger part of the investment that is made in the power grid being directed to distribution system engineering, distribution systems have not received the technological impact in the manner as the generation and transmission systems. Smart meters are an important step towards the realization of the objectives set forth by the Smart Grid Initiative. Smart meters act as a link between the distribution company and the customer by establishing a two-way communication link providing customer with real-time reads [29]. Other additional functionality could include automatic time synchronization, tamper detection alarms, current and voltage profiling and capability to download and store time-of-use schedules [29]. Real-time updates help customers adjust power usage patterns to avoid paying high prices during peak load periods. Since utilities need to generate power from low efficiency generators during these periods of peak loads, the utilities save due to this demand response by the customer. With the evolution of smart meters over 20 years, they now are approaching a life-cycle cost that is cheaper than that of electromechanical time-of-use meters [31]. By using a high frequency powerline carrier, the price of electricity can be transmitted to each user, and displayed on their power meters [31]. Economists argue that electric systems can achieve optimal efficiency only if the customers have the option to pay true minute-by-minute marginal cost [4]. Several techniques have been

experimented by utilities to engage the customer in responding to varying electricity prices. Some of these are the Critical Peak Pricing (CPP) that was tried in California [32], the Demand Reduction Program (DRP) [33] and the Interruptible Program [33]. As a part of research program conducted by the University of California Berkeley, Lawrence Berkeley National Lab and the California Energy Commission, a study was conducted to see the impact of CPP on customer response. The participating customers received high price signals dispatched by their local distribution company. On pricing the high price signals at three times the regular on-peak price, they found that several customers without automatic control technology reduced their consumption by upto 13% during the periods of high prices, and customers with advanced control equipment reduced their consumption by upto 25% [33]. Real Time Pricing (RTP) is another technique wherein the customer is charged different retail electricity price for different hours of the day for different days. RTP has not received good response among consumers. Advanced communication equipment and meters are essential for realizing CPP, RTP, or any other demand response program. Component-wise requirements maybe an interval meter that measures hourly energy consumption, automated communication equipment that can upload this data to a central repository, customer access to the uploaded data, and notification of RTP prices and alerts can be used to trigger load reduction behavior [33]. Interruptible load program, was a program initiated by the Taiwan Power Company, which serves load demand of Taiwan, R.O.C, in the year 1987 [34]. The program was an urgent need-of-the-hour strategy adopted by the company to reduce the peak load on the system. Customers who signed in for this would reduce their load, at times requested by the utility, through the use of demand limiters or control methods adopted by the utility in exchange for incentivized rates of electricity for those customers. The utility was able to achieve peak shavings upto required level since industries such as steel industries also signed up for this scheme and was able to reduce peak by a large extent.

1.4.1.2 Optimal resource utilization – Distribution feeder reconfiguration

One of the points outlined for the development of a smart grid is to dynamically optimize grid resources and operation. Distribution feeder reconfiguration is an important aspect, since reconfiguration optimizes the existing resources by simply opening/closing appropriate switches or sectionalizers. One of

the problems with this is the reconfigured system must not violate any of the line flows or bus voltage limits. Another potential problem is that these sectionalizers may not be present on old feeders that were designed with the idea to maintain radial nature among the feeders. In such cases, new interties need to be added among the feeders. These interties must be added at optimal locations in order to improve system reliability under an upper limit of cost set by the designer at the utility.

Although the authors in [19, 35, 36, 37] have identified that the large state space of the problem makes finding solutions through the use of conventional algorithms difficult, the problem's computational complexity has never been identified clearly, to the best of the knowledge of the author of this thesis. Growth and computational complexity are important problems that must be identified in a problem. Knowledge of these properties will help in identifying and justifying the use of an algorithm for the problem. Several non-conventional algorithms have been applied to find solutions for the feeder reconfiguration problem. Notable among these are the use of Genetic algorithm [19], Ant colony optimization [35], simulated annealing [36], and Tabu search [37]. Although these methods find good solutions, they take a long time, in the order of days for simple systems, to solve and hence cannot be used in real-time scenarios unless the load conditions on feeders are known much in advance [19, 20].

1.4.2 Integration of renewables – Distributed Energy Resource

With the emergence of new regulatory and operational conditions of power generation units, traditional generational techniques are soon giving way to new forms of generation and storage such as microgrids and pluggable hybrids. Due to its flexibility to use renewable sources such as wind and solar, distributed generation is an attractive option for power generation. Moreover, as the generating units can be located close to load centers, the waste heat from the generating units can be used to serve heating loads. Such plants are knows as CHP plants, and they improve the efficiency of the plant by a large percentage.

Microgrids have been deployed in at several locations in the world, under different modes of operation. While some are in research and testing stages, others have been deployed on field and are

operating in tandem with the main power grid. Microgrids are also deployed at some military bases in order to retain supply at the base in the event of loss of power on the main grid [38].

Several microgrids have been designed and tested in North America [39]. Among the popular microgrids in North America are:

- CERTS microgrid: The CERTS microgrid is located at American Electric Power (AEP) Walnut Chest facility in Columbus, Ohio. This microgrid functionality is provided by three advanced techniques:
    - "Seamless transition between grid-connected and islanded modes of operation
    - Special protection under islanded mode of operation. This is required since, under islanded mode of operation, the load is expected to experience larger fluctuations in frequency and voltage
    - Voltage and frequency stability without extensive communication infrastructure" [15].

    The CERTS microgrid is an innovative and new technique to integrate DER sources to the main grid. The grid views this microgrid as a single self-controlled entity despite microgrids, normally, being an integration of several sources. The microgrid is unique in its design as the microgrid can disconnect from the main grid during a disturbance on the grid, and yet maintain uninterrupted supply to all or most of all its loads [15]. This is achieved without extensive custom engineering.
- Santa Rita Microgrid: Santa Rita is a prison located approximately 40 miles east of San Francisco, CA. A project undertaken over the past ten years aims to transform this facility to a 'green' facility power primarily by green energy resources [40] has been realized through the integration of various renewable energy resources. Among these are a 1.2MW rooftop PV system, a 1MW molten carbonate fuel cell (MCFC) with CHP, and retrofits to lighting and HVAC systems to reduce peak loads [40]. MCFCs are suited for large scale power

generation, since they generate high temperatures that can be reused for on-site heating purposes. MCFC are different from regular fuel cells as they cannot use pure hydrogen alone as a source of fuel [41]. But MCFCs can use a range of other hydrocarbon fuels such as natural gas, biogas, synthesis gas, methane and propane. The Santa Rita facility uses natural gas as the source of fuel [40]. The efficiency of MCFCs can be as high as 85% when used as a cogeneration unit [41]. Frequent fuel cell outage, as a result of highly voltage sensitive nature of fuel cells, has led to considerable operating and maintenance expenses at the plant [40]. This also makes the fuel cell an unreliable dispatchable resource. Hence, plans are underway for the installation of a large scale battery storage source. The battery source will serve as the only truly dispatchable energy resource. Also, the battery source can be used to store power during off-peak hours and discharge the same during periods of expensive grid power. Future plans for the installation of a fast disconnect switch will transform this unit into a true microgrid [40]. The fast acting switch will quickly disconnect from the grid during instances of disturbance on the grid. Intentional islanding is also under consideration to disconnect when PV sources are generating optimal outputs. Also under consideration is the proposal to export power to the main grid [40].

- Hydro-Québec microgrid: The Hydro Québec (HQ) microgrid, located at Montreal, Canada, is one of the most important utilities in Canada, with an installed capacity of 35 GW [42]. HQ generates most of its power from a renewable resource viz. hydro resource. HQ also is known to have the most extensive transmission network in North America serving well over 3 million customers. With the introduction of Distribution Automation in the year 2005, plans were laid for the introduction of DERs connected to the distribution system through use of intelligent systems for planned islanding and microgrid operation [42]. HQs first planned islanding when a 120kV transmission line feeding a substation (Senneterre) required urgent maintenance. This substation was also interconnected by a privately owned thermal power plant (Boralex) [42]. In order to carry out the maintenance without interruption to the HQ

customers, plans were made to use Boralex power plant for islanding of HQ's Senneterre substation [42]. Due to the limited spinning reserve of Boralex (1-2MW), all substation and feeder automatic reclosures had to be deactivated during times of microgrid operation so that the plant would have sufficient time to pick-up load values higher than the spinning reserve. After several protection and stability studies, the first microgrid operation was attempted in October 2005, which persisted for 8 hours [42]. Analysis showed stable voltage and frequency for both load reduction and controlled load augmentation [42].

- University of San Diego microgrid: The University of San Diego (UCSD) has one of the largest fully functional on-campus university microgrid. The microgrid has a mix of resources such as cogeneration units, PVs, fuel cells and plans for an energy storage unit and a Sea Water Air Conditioning unit [43]. The 1.2MW installed capacity of PV and supplies about 1% of the campus demand [43]. The 3MW MCFC uses waste methane as its source of fuel [43]. Operating at a net efficiency of 66%, the CHP unit is the centerpiece of the UCSD microgrid [43]. The waste heat from the cogen plat is used to drive a compressor which drives chilled water that is cooled overnight. The water cooling is hence performed during off-peak hours. This cooled water is stored in a storage tower, and is released during the day for air conditioning at the campus buildings [43]. Cooling towers are used to release heat that is absorbed by the buildings. The cogen plant operates in a load following mode [43]. A load following unit is one that changes its output following the change in load. UCSD is able to realize 85% of its campus electricity supplies and 95% of heating and cooling thorough the cogen unit [43]. Fast acting switches, in case of an event on the grid, can disconnect the campus from the main grid. The campus is also in the process of installing a microgrid master controller that can schedule on-campus generation and storage based on the dynamic market prices.
- Mad River Microgrid: The Mad River microgrid is located at Mad River, Vermont. The microgrid has an array of mixed generation sources which are a propane genset (280 kW),

two biodiesel gensets (100kW each), PV arrays, and 30kW microturbines serving six commercial and industrial facilities and twelve residences. Future integration of distributed storage resource is also possible [44].

- FortZED RDSI microgrid: The FortZED (Zero Energy District) project is among the four projects of the DOE's Renewable and Distributed Systems Integration (RDSI) program. The project was a demonstration project implemented at Fort Collins, CO by Fort Collins utilities, in collaboration with Colorado State University and local businesses. The objective of the project were to 1) "Demonstrate a coordinated system of mixed distribution energy resources (DERs), 2) Demonstrate intentional islanding, and 3) Reduce peak load on selected distribution feeders by 20-30%" [45]. The system has a centralized control system which controlled dispatchable generation and demand response. The comprised of 17 distinct dispatchable generation units totaling 2.830 MW, consisting of nine diesel gensets, five natural gas and two biogas units. The biogas units were supplied from an anaerobic digester which obtained its raw materials from a neighboring micro-brewery. Due to a smaller diversity in the generation resources, the project posed unique challenges, such as:
    - "Emission restrictions,
    - Unavailability of grounding transformers, hence restricting operation of some generators in emergency circuits only,
    - Reduced output from older generators,
    - Problems due to utilization of research generation units" [45].

  During the final test, the project achieved 9-25% reduction in peak load through effective control of the distribution generation resources [45] and demand response.

A few microgrids in South America are located at Robinson Crusoe Island (Chile), Huatacondo's microgrid (Chile), and Chiloe Island (Chile). Microgrids have also been developed in Asian countries. In Southeast Asia, over 160 million people have no access to electricity [46]. Most of this population lives in remote locations and engages in agricultural activities. Microgrids could provide ideal power solutions to

in these cases. An example of this is the rural PV hybrid microgrid, located at West Bank, Palestine. Other Asian microgrids include:

- Hangzhou Dianzi University in Zhejiang, China: This university microgrid is designed to supply the power needs at the university. The microgrid can operate in both gird connected and islanded modes. The microgrid consists of a mix of 120kW of installed solar capacity, 120kW of diesel generation, and a battery resource [47]. The power output levels from PV and the expected load on the system is forecast until the day before, based on past data and weather pattern [47]. On the day of operation, load follow-up control of load functions occurring on that day is implemented and power generation revision based on extent of diversion from the forecasted pattern is monitored and controlled accordingly. The on-site battery resources are used to compensate for short period supply fluctuations at the breaker point in grid connected operation and short period voltage and frequency fluctuations in islanded mode [47]. The battery unit could take from a few seconds upto ten seconds to respond to such fluctuations. An Electric Double Layer Capacitor (EDLC) is used to provide for faster responses to fluctuation events in grid connected or islanded modes for fluctuations of under a few seconds in duration [47].
- Shimizu Microgrid: This is a pilot project to better understand the functionality of microgrids in Japan [39]. The microgrid consists of a mix of several DGs, run on conventional fuel resources, and DS units comprising NiMH batteries and ultracapacitors [39]. Shimizu also uses a PV array. Operating and testing on this microgrid led to two important findings: one that scheduling generators on a microgrid when the unit is lightly loaded is not straightforward, and second that if the power electronics interface is non-uniform, then responses of DGs and DSs are difficult to control [39].
- Sendai Project: This microgrid is a low output 1 MW microgrid located close to the customer. Sendai microgrid consists of PV resources and gas engines. The microgrid also consists of a dedicated circuit that supplies DC loads for critical telecommunication equipment, and

different quality of AC supply based on the load that the feeder serves. For example, the hospital load is served through a high quality supply line [48]. Due to its proximity to the end-user a CHP unit is also installed at the microgrid improving the overall efficiency of the system. This microgrid is used to serve a hospital and a small neighborhood, and was the only source that continued to supply power in Sendai city after the devastating earthquake of 2011 in Japan [49].

Several other microgrids are present in China (Zhengzhou City, Zuo'anmen, Foshan Island etc). Power generated by the Foshan island microgrid is used on-site for desalination of sea water [50].

Other microgrids are present in European nations (Demotec in Germany, Continuon Holiday park in Netherlands EDP feeder in Portugal, CESI at Spain to name a few).

- Agria microgrid: The Agria microgrid is a rural microgrid located in the Republic of Macedonia [51]. Farms were observed to be significant contributors to pollution due to the large amounts of waste they produce everyday. The Agria farm is a pig farm, and consists of a bio-digester and a waste collection system. Biogas is produced locally by the bio-digester and is used as fuel in an engine that runs a 25kVA generator [51]. Bio-gas production, by itself, requires to run two electric pumps: one for circulating the gas through heat exchange pipes when the ambient temperature is low, and the second for mixing the manure [51]. The heater is required during periods of low temperature in order to provide appropriate conditions for bio-gas usage. The Agria microgrid is designed to run in both grid connected and islanded modes of operation [51].

Blackstart operation is an important operation in microgrids. Although some microgrids have the capability to seamlessly disconnect from the main grid without interruptions to its load, many other microgrids may not have this capability. For these microgrids, planning the order in which various generation units will be brought online, and the order in which the various loads will be added, is an important consideration. This is known as blackstart operation and is a key to the stability of the microgrid.

1.4.3 Computational complexity

Search problems can be classified based on the computational complexity of the problem. If an optimal solution can be found to a problem in polynomial time, the problem is known to have polynomial time complexity i.e., for an input of size *'n'*, the solution can be found in the order of time *p(n)* where *p* is any polynomial function [52]. On the other hand, if there is no known algorithm in literature that can find an optimal solution to the problem in polynomial time, the problem is classified as a non-deterministic polynomial time or NP problem. The size for such NP problems grows exponentially for '*n*', and hence, conventional algorithms can only find solutions to these problems for small values of '*n*'. There are many known hard problems in literature, such as the Travelling Salesman Problem (TSP), Boolean satisfiability problem (SAT) and the vertex cover problem [53]. If we can prove that an NP-complete problem can be solved using a deterministic polynomial time algorithm, then this holds as proof that all NP problems can be solved in polynomial time, using a similar algorithm [54]. Since there is no NP complete problem that has a less than exponential time solution, proving a problem to be NP complete is equivalent to proving that the problem in question has no polynomial time algorithm.

To find an efficient algorithm to solve a search problem, classification of the computational complexity of the problem is important. This can be done through the process of reductions. Reduction is an important tool used to transform a known NP problem, such as the TSP or SAT, into another problem whose complexity is to be evaluated [53]. Finding bounds on growth of the state space of the problem could provide a good indicator regarding the computational complexity. Hence, finding bounds on the growth of the problem prior to applying reductions is sometimes useful [54].

The literature review briefly describes the current trends and research in the topics of distribution engineering and microgrids. This thesis advances some of this work, in terms of accelerating the convergence of solutions in distributed feeder reconfiguration, classifying the computational complexity of the problem, and microgrid modeling and simulation when a mix of various fuel sources are available. None of this work is currently present in literature, to the best of the knowledge of the author.

1.4.4 Software tools and methods

Various software tools were used in achieving the objectives related to different parts of this work.

1.4.4.1 Matlab™

Matlab™ was chosen as the preferred tool for running the GA, as Matlab™ provided an in-built genetic algorithm toolbox. A call to the GA function runs the all the steps of the genetic algorithm, other than penalty functions. Code, specific to the feeder reconfiguration problem, is written outside the toolbox.

1.4.4.2 PowerWorld™

PowerWorld™ was used to model and represent the microgrid power system, used in chapter 3, in a graphical user interface format. This software has an add-on, known as the Simulation Auto Server (SimAuto™) which was used to establish communication between Matlab™ and PowerWorld™. This add-on permitted modifying files that were created in PowerWorld™, from external software, which was Matlab™ in this case.

Hence, the system that was initially modeled in PowerWorld™, is modified in each step using Matlab™ to create new inputs. This modified topology is then verified for voltage or power deviations using the SimAuto™ link on PowerWorld™, and the results are read out using the same link. Voltage and power deviations are used to compute the penalty functions on Matlab™, in order to evaluate validity of a feeder configuration.

1.4.4.3 PSCAD™

PSCAD™ stands for Power Systems Computer Aided Design. This software was used for modeling the notional mission specific microgrid in chapter 4. PSCAD™ was chosen as the preferred tool as it provided easy machine modeling and control systems tools. Also, the author contends that PSCAD™ provides excellent transient and fault analysis capabilities.

1.5 Organization of the Thesis

Followed by introduction, chapter 2 of this thesis focuses on establishing the computational complexity of the feeder reconfiguration problem, and finding the bounds on the growth of the problem. Chapter 3 advances prior work [19] [20] to accelerate the convergence of solutions for the feeder reconfiguration problem. Chapter 4 describes the modeling of a notional mission-specific microgrid including analysis on the sequence for blackstart operations in the notional microgrid. Chapter 5 concludes with results and explores prospects for future work.

Chapter 2
Computational complexity of the distribution feeder reconfiguration problem

This chapter of the thesis focuses on the problem of distribution feeder reconfiguration. To ensure completeness the general reliability concepts are reviewed and an algorithm that is used by authors [19] [20] to find solutions to the problem is presented. The problem addressed in this work is: To find the bounds on the growth of redesign the conventional radial feeder design into a partially meshed design by the introduction of interties. As will also be discussed in this chapter, conventional algorithms will not be suitable for the feeder reconfiguration problem due to the computational complexity of the problem. This work justifies the use of Multi Objective Genetic algorithm (MOGA) for finding optimal solutions and also goes forward in finding a technique to accelerate the process.

2.1 Modeling radial distribution system

Power system distribution systems have traditionally always been modeled as radial distribution systems. This reason for this is mainly due to easier protection system configuration and simpler fault analysis. Lately, with the evolution of the concept of Smart Grids, much research has been focused on converting this to a partially meshed topology for two primary reasons:

- Improve reliability of the system
- Addition of DGs in the system

This new approach has already been implemented in the transmission realm, and hence this approach conceptually bears close resemblance to the Transmission Network Expansion planning (TNEP) and the Generation Expansion planning (GEP) problems [55][56]. Distribution systems have large variation is load based on the time of day. As mentioned in chapter 1, load varies in a cyclic pattern through the day. Load modeling is an important for power system stability studies due to the impact of load variation on voltage and transient stability studies [57]. In order to model load points on the system, two approaches of load modeling can be used [20].

- Average annual load: In this model, the average load for one year is computed at every load point on the system, and is kept fixed during load flow analysis. Hence, this scheme assumes that this average load will remain constant at the load points during all times of the year. Load at a point *i* in the system can be represented as

  L_i = Average load at bus *i* computed over 8760 hours.

- Step-load duration cure: Load duration curves are very effective in approximating loads and are often used in planning. Load profile obtained through either estimation or actual data is plotted for one period. This is then divided into intervals, and is plotted on a histogram. The probability mass functions (PMF) are then obtained by dividing each count by the total number of intervals. The PMF can be used to compute the probability of a load being within a range. Scaling of this curve over original time duration, gives us the step load duration curve [58]. In order to simplify calculations, as mentioned in [20], the step size is approximated as

$$\partial = \frac{\left(L_{\beta_{max}} - L_{\beta_{min}}\right)}{N_\beta - 1} \tag{2.1}$$

  Where,

  N_β is the number of load levels between annual peak demand seen by the system $L_{\beta_{max}}$ and annual peak base load $L_{\beta_{min}}$.

  Hence the demand at load point *i* is,

$$L_i = L_{i,PLoad_{max}} * L_\beta(\Delta T_\beta) \tag{2.2}$$

  Where,

  $L_\beta(\Delta T_\beta)$ is the power level occurring for ΔT_β hours.

2.2 DG Modeling

Renewable energy resources will play an important role as distributed energy resources in future. The main reason being attributed to them being non-polluting sources, they can be located near load sources. Up to 25% of the DGs in the system are expected to be from renewable resources [29]. The main

sources of renewable sources are PVs and wind. But, these being non-dispatchable sources, may always need to be supplemented by dispatchable sources such as storage batteries or conventional fuel driven engines. The power output from a PV source is proportional to the total solar radiation on the inclined surface, the efficiency of conversion of the cells which in-turn depends on the technology, and the area of the PV surface [59]. The output from a wind turbine is also dependent on various factors such as the wind speed at hub height and the speed characteristics of the turbine [59]. Close to the rated speed of the wind turbine, the output of the unit is proportional to the cube of the wind velocity at the hub. Below cut-in speed and above cut-out speed, the output from the turbine is zero. For simplicity of analysis, these factors are combined into a single unit known as capacity factor of the unit. The capacity factor of the generator can be represented as the ratio of the actual energy produced over a given period of time (usually, annual), to the power that the generator could have produced had the generator been operated at rated power during the entire period of consideration [60]. In [61] the author analyzes the wind units at several locations, and finds that the capacity factor for Boulder, CO is 30%. This capacity factor was used for analysis in [19] [20] and is reused in this work to maintain uniformity. Based on the generation mix identified by the survey conducted in [19], the total system DER power could be formulated as

$$P_{out} = P_{renew} + P_{DS} + P_{CDG} \tag{2.3}$$

Where,

P_{out} in the total power from distributed resource

P_{renew} is the Generation from renewable resources and equals ($R_{RE} * CF_{RE}$)

P_{DS} is the Contribution of renewable resource that is supported by DS

$= 0.15 * (1 - CF_{RE}) * L_i$

P_{CDG} is the Power output by the conventional DGs

$= R_{CDG} * CF_{CDG}$

Here, R_{RE} is the rated output of the renewable resource, and CF_{RE} is the capacity factor of the resource. As mentioned earlier, renewables being non-dispatchable resources need to be supported by a

distributed storage (DS) resource. Hence, the support from DS is set to be 15% of the total of the average installed load at the bus, L_i [29]. Further, the distributed resource is also supported by a conventional generation source, such as a diesel or natural gas setup, rated at R_{CDG} and having capacity factor of CF_{CDG}.

2.3 Review of reliability indices

The ability of the power system to adequately supply electrical energy to the load and maintain reasonable assurance of continuity and quality is known as reliability of the power system [60]. One measure of system reliability is the total electrical interruptions at the customer end. The measure of electrical interruption is only meant for measuring complete loss of voltage. The common reliability indices that are used to classify distribution systems are SAIFI (system average interruption frequency index), SAIDI (system average interruption duration index), CAIDI (customer average interruption duration index) and ASAI (average system availability index). Another term that is used to measure momentary interruptions is MAIFI (momentary average interruption frequency index). System reliability does not cover voltage sags, swells, impulses or harmonics which are classified under power quality issues and are measured using other indices such as THD (Total Harmonic Distortion), crest factor and flicker. The IEEE Std. 1366-2003 deals with SAIFI, SAIDI, CAIDI and MAIFI as these interruptions are over one minute in duration. These reliability indices measure both, the frequency and duration of power interruptions at the customer end [60].

$$SAIDI = (\text{total number of customer interruptions})/(\text{total number of customers served}) \tag{2.4}$$

$$SAIFI = \frac{(\text{sum of customer interruption duration})}{\text{total number of customers}} \tag{2.5}$$

$$ASAI = (\text{customer hours of available service})/(\text{customer hours demand}) \tag{2.6}$$

As in [19] and [20], the ASAI index is modified to compute the reliability index. The metric that is used in this thesis to evaluate reliability is termed as Energy Not Served (ENS). In order to maintain normal operating conditions, the power generated must at all times be equal to the load demand. The slack bus concept is used to find the ENS of the system. The slack bus is an infinite bus that is able to

absorb any excess supply in the system or supply the deficiency of power in the system. Hence, the readings from the slack bus are analyzed to get the actual load that is not served in the system.

The two methods of modeling load, mentioned above, are used [20]. In the first method, the un-served load is assumed to be a constant value, and this corresponds directly to the reading of the slack bus. This value multiplied by number of hours in a year (8760) gives the energy not served. The same cannot be performed on using the step load duration curve, since the load values are different during the entire year. Hence, for the step duration case, slack bus output is multiplied by the number of hours corresponding to each load step. This is directly reproduced from [20].

$$U = (1 - ASAI) \tag{2.7}$$

$$ENS \text{ (for constant load)} = U * 8760 * \sum_{i=1}^{N_s} P_s \tag{2.8}$$

$$ENS \text{ (for stepped load)} = U * \sum_{i,\beta=1}^{N_s,N_\beta} \Delta T_\beta * P_s(L_\beta) \tag{2.9}$$

Where,

U is the average duration for which the system is not available.

P_s is the power output by power source located at bus 'i'

N_s and N_β are the number of buses which have a power source and number of steps in the step duration curve respectively

ΔT_β is the duration of the step load β

and L_β is the power level at ΔT_β

Collocating DGs and adding interties to the network is an intertwined problem and cannot be solved in two different steps. First adding the DG to the network, followed by adding interties may not give the best solution. Adding DGs to the most loaded bus may give the optimal DG connection in the radial distribution system. But, on the other hand, adding interties between heavily loaded buses and buses that have DG sources may prove to be a cheaper option. In contrast, adding this intertie could

overload some line in the network and may not even be the most optimal connection. Also, geographical proximity of two feeders could serve as an advantage in this problem.

Hence, the problem addressed in this chapter is: to find the numerical bounds on the growth of the distribution feeder reconfiguration problem, and hence classify the computational complexity of the problem. In the next chapter, this thesis also addresses the problem of accelerating the process of finding solution to the feeder reconfiguration problem. This work is an extension to prior work in [19] and [20]. Although authors in [19] and [20] identified the need for a heuristic based algorithm due to the large state space of the feeder reconfiguration problem, the growth of the problem and hence the computational complexity of the problem was not identified.

The author in [19] used the multi objective genetic algorithm to solve the problem. Two different cases were identified in [19] to test the algorithm: the 3 feeder test case and the Roy Billinton Test system (RBTS) case. The author assumed the location of the DGs to be fixed in this analysis. Also, the loads were assumed to be aggregated and fixed during the entire period of the analysis. Although the analysis was able to build the Pareto front, the time taken for solutions to converge to the Pareto front was of the order of one hour for the three feeder test system and of the order of six hours for the RBTS system.

The author in [20] extended the work in [19], and found solutions to the two test cases. In this work, the author did not assume the locations of the DGs to be fixed and framed the problem to collocate DGs while finding optimal interties. In this work, the author also uses step load duration curves to represent loads. This increases the complexity of the feeder reconfiguration problem and also causes multifold increase in the state space of the problem. Due to this, the time taken to solve the problem also increases as compared to [19].

As a part of the work in this thesis is an extension to the prior work in [19] and [20], the assumptions made in [19] and [20] are maintained here too. These assumptions are:

- "The protection system allows bi-directional power flow
- All connections between feeders are permitted
- DGs can be placed on any bus in the system, other than the slack bus

- The reliability of the existing components will not change as a result of redesign of the given distribution system and also that the new configuration will have similar reliability as the existing components" [19] [20].

2.4 Genetic algorithm

Genetic algorithm (GA) is a non-conventional algorithm inspired from observation of natural process of evolution of species of plants and animals [62]. Conventional algorithms have a set of well-defined that they carry out in order to reach the solution. The main difference between a conventional and non-conventional algorithm is that conventional algorithms are time invariant systems. From a system point of view, this means, given a set of inputs the output of the system will remain the same at irrespective of the time. However, the same cannot be said of non-conventional algorithms. Since they have at least one step that involves randomization of the inputs fed to the algorithm, the output cannot be predicted to remain the same for every trial. These families of algorithms are used when the state space is of the exponential order of input [62].

2.4.1 Multi-objective Genetic algorithm

The general multi-objective optimization problem can be defined as follows:

Maximize $F(x) = [F_1(x), F_2(x), \dots, F_k(x)]^T$

subject to $g_j(x) \leq 0, j = 1,2, \dots m$

and $h_l(x) = 0, l = 1,2, \dots r$

Where,

k is the number of objective functions

m is the number of inequality constraints

r is the number of equality constraints

The problem explored in this thesis is a multi-objective problem with possibly conflicting objectives of improving reliability and reducing cost. Typically, multi-objective problems do not have a global solution that can be termed as the best solution. The solution consists of a set of points, all of

which qualify to be an optimum since they satisfy at least one predetermined definition for optimality [61]. The concept of optimality when the objectives are conflicting in nature can be best solved through the use of Pareto optimality [62]. Conventional algorithms are not suitable to this problem for two reasons,

- Large state space
- The desired output is not one optimal solution, but a family of non-dominated pseudo-optimal solutions. This could be because the utility that plans the reconfiguration may need an array of options to choose from, based on their investment plans. For example, one solution may provide the least value for ENS at a prohibitively high cost, while another solution may provide a value of ENS close to the first value, but at a cost that is much lower. Given a set of options, the utility now has the opportunity to choose the solution. Hence, a tool that can construct the Pareto front of possible solutions can aid in making the final decision.

A point x^*, where $x^*, x \in (state\ space)$, and $F_n(x^*) \leq F_n(x)$, $F_n \in set\ of\ objective\ functions$ is said to be Pareto optimal if and only if there exists no other objective function (F_k), such that $F_k(x^*) < F_k(x)$ [61].

Genetic algorithms can be tailored to solve multi-objective problems. The authors, in [63], compared the solutions of the H-frame transmission problem by running tests using both simulated annealing and genetic algorithms. The analysis showed that genetic algorithms perform superior to simulated annealing algorithm under the same test conditions. Hence, genetic algorithm is a good choice for solving multi-objective problems. Since genetic algorithms do not use gradient approach in their search, the solutions are independent of the nature (gradient) of the objective function. Genetic algorithm combines the adaptive nature of natural genetics with functional optimization [62]. Genetic algorithms are normally used for problems that are non-linear, which implies that there is expected to be some form of interaction between the parameters that cannot be ignored. This interaction is known as epistasis [64]. An important assumption that needs to be made for using genetic algorithms is that variables representing

parameters can be represented as bit strings. The general steps of the genetic algorithm are shown in Fig 2.1.

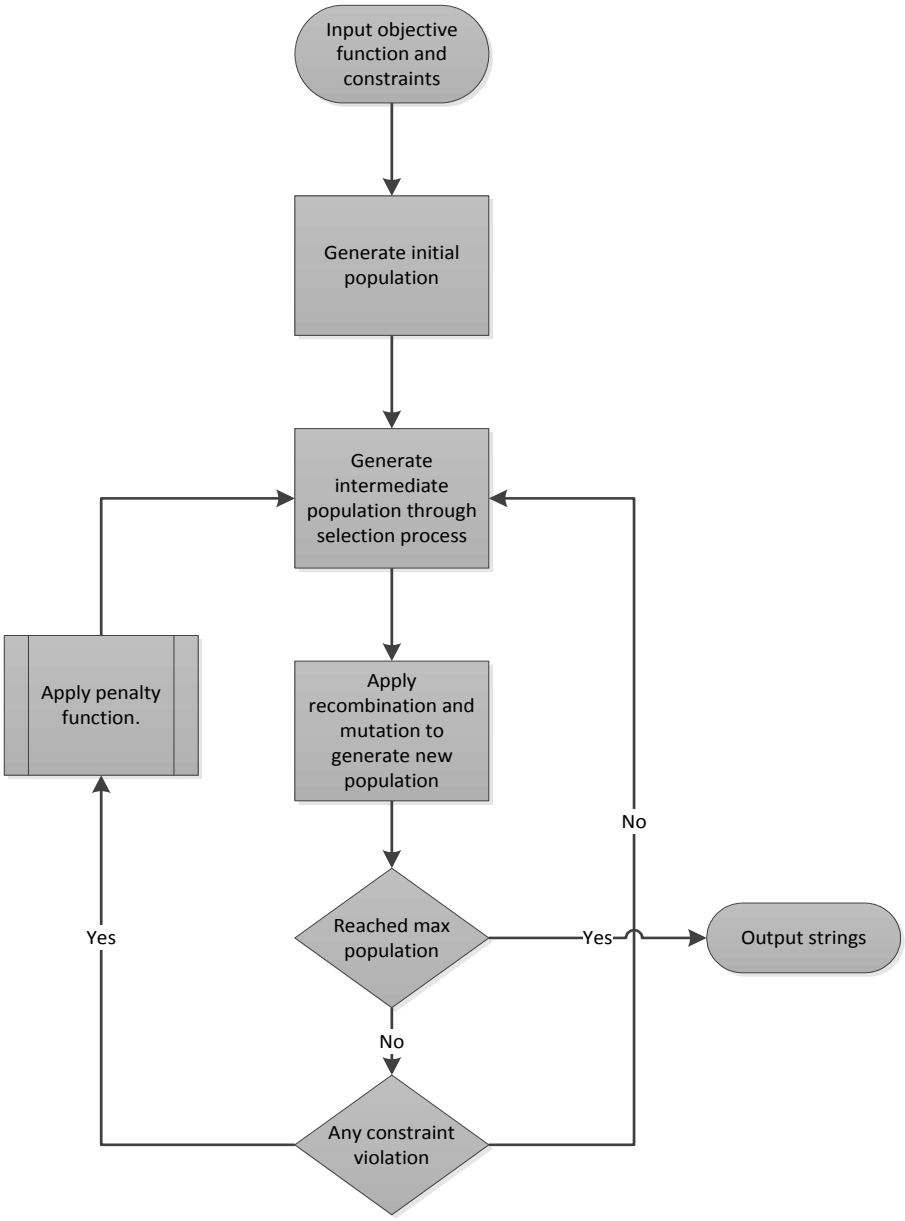

Fig 2.1 Flowchart depicting the steps involved in a general genetic algorithm solution.

The sequence that is generated at start and at the iteration of each generation is known as a chromosome string or string [64]. The system reads input data, objective function and the constraint equations in the input stage. The input data can be a random set of bits, as this will ensure that the solution does not converge at a local optimum in the first few steps.

After creation of an initial population each individual in the population (a string) is evaluated and assigned a fitness value. A fitness function transforms the measure of performance of the string into an allocation of reproductive opportunities [64]. A new generation is created from the current generation through a 2-step process. First an intermediate population is created through the selection process. Selection can be performed in a variety of ways. The roulette wheel selection is explored in [19] and is reused in this thesis. This technique maps the inputs on a pie chart, and each input occupies a percent of the pie chart directly corresponding to its output from the fitness function. A roulette wheel is placed on the exterior of the chart with *N* equally spaced pointers. Here, *N* represents the number of strings that is produced from each generation. A random rotation if the roulette wheel chooses populations for the next generation. Multiple rotations can also be done, based on implementation.

The intermediate population is now recombined, also known as crossover application, to produce a new population. Recombination point can be chosen at random. Next stage is the mutation operator. To avoid totally random sequences from being generated for the next generation, mutation is normally applied with a low probability (1% or lower). The output from this step hence generates a new population that can be used for the next generation.

The Genetic Algorithm Optimization Toolbox, available on Matlab, was used in [19] and [20], and is reused in this thesis. The distribution feeder reconfiguration problem has two objective functions, and two constrains.

- Cost objective function

$$\sum(C_i * L_{ij}) + \sum(C_{DG} * P_{DG}) \tag{2.10}$$

Where,

C_i is the cost of the interite (\$/km)

L_{ij} is the length of the line (km)

C_{DG} is the cost of the DG (\$/kW)

P_{DG} is the DG output rating (kW)

- ENS objective - This is calculated based on the method used for load modeling, as represented by (2.8) and (2.9).
- Power constraint function - In order to prevent overheating of power lines, the power that is transferred on a line must be maintained within rated limits. Overheating of power lines leads to increased sag on the line, which could eventually cause the line to contact a terrestrial object causing a fault to ground.

$$P_{ij} \leq 1.0\, p.u \tag{2.11}$$

- Voltage constraint - Over or under voltage causes the frequency of supply to drift, causing instability of supply.

$$0.95 \leq V_i \leq 1.05\, p.u \tag{2.12}$$

If a string in a population violated one or both of the constraints, a quadratic penalty function is used as a multiplier to penalize the solution proportional to the violation. Penalty functions are important, as they prevent strings that violate the constraints, from reaching the next generation. PowerWorld™ Simulator is used to evaluate the fitness of a particular string. In the implementation used in this thesis, the penalties are computed based on line overloads and voltage deviation on buses. (2.13), (2.14) and (2.15) are directly reproduced from [20]. The line overload penalty is given by

$$P_{power\_flow} = \prod_{i=1}^{w} O_i \tag{2.13}$$

Where,

w is the number of lines overloaded

O_i is the overload percentage on line i

And the voltage overload penalty is given by

$$P_{voltage} = \begin{cases} \prod_{i=1}^{n1} (2 - V_k)^2 \\ \prod_{j=1}^{n2} {V_k}^2 \end{cases} \quad (2.14)$$

Where,

$n1$ is the number of buses having voltage under 1 p.u,

$n2$ is the number of buses having voltage over 1 p.u

Combining both the penalties, the total penalty for a string is

$$P_{total} = P_{power\_flow} * P_{voltage} \quad (2.15)$$

2.5 Growth of the function

Algorithms are normally viewed from the perspective of a computer, since most practical problems are solved using computers. There are two models available for the analysis of algorithms 1) the RAM model and 2) the asymptotic analysis of worst case complexity [52].

- The RAM model: This model is designed based on a theoretical machine that is the Random Access Machine (RAM) that makes the following assumptions
    - Arithmetic operations addition, subtraction, multiplication, and division take only one step.
    - Time taken to execute loops is directly proportional to the number of iterations in the loop.
    - Each memory access can be completed in one time step.

Under the RAM model, an algorithm can be classified based on the best-case, average-case and worst-case operating times. The best-case operating time is the function that is formed when the number of steps taken by the algorithm is smallest for an input of size *n*. For example, the time taken by a sorting algorithm if the input is already sorted. The worst-case time is a function defined when the computation time is the longest for an input of size *n*. For example, if the input to the same sorting algorithm is exactly in the reverse form of how the result is to be sorted. The average-running time is the function that lies in

between the two extremes. Average running time is the average that is obtained when the algorithm is run several times with known input of size *n*.

- Big-O notation: Although the RAM model gives a good approximation of the algorithm, the model becomes very complicated to compute for complex algorithms. Also, there may not be any requirement for precise cycle information for such algorithms. Hence, in such cases the Big-O notation is used. Big-O simplifies the analysis by ignoring the cycle-to-cycle run duration of algorithms. The formal notation associated with Big-O notation is as follows [53]:
    - $f(n) = O(g(n))$ implies that $c * g(n)$ is an upper bound on $f(n)$.
    - $f(n) = \Omega(g(n))$ implies that $c * g(n)$is a lower bound on $f(n)$.
    - $f(n) = \theta(g(n))$ meaning $c_1 * g(n)$ is an upper bound on $f(n)$, and $c_2 * g(n)$ is a lower bound on $f(n)$. This implies that the function $f(n)$ has tight upper and lower bounds.

In order to develop an efficient algorithm to solve a problem, an understanding of certain characteristics of the problem is important. Useful among these are the growth rate of the problem and the computational complexity of the problem [52]. Conventional algorithms work efficiently when the state space of the problem grows as a polynomial function of the size of input. But sometimes, the time required to solve, grows as an exponential function of the size of input. In such cases, conventional algorithms fail to find the optimal solution, since the state space grows exponentially [65].

2.5.1 Growth of feeder reconfiguration problem

As mentioned earlier, an understanding of the growth of the problem is required to design an efficient algorithm. This section finds the growth of the distribution feeder reconfiguration problem. Consider the 3-feeder 9-bus system shown in Fig. 2.2. Potentially, an intertie can be added between any two buses excluding the slack buses; e.g., an intertie can be added between buses 1 and 6, or between buses 2 and 11 etc. In a generalized case,

Let number of radial feeders in system = n

And number of buses on the n^{th} feeder = x_n

Hence, total buses in the system (excluding slack buses) = $x = \sum x_n$

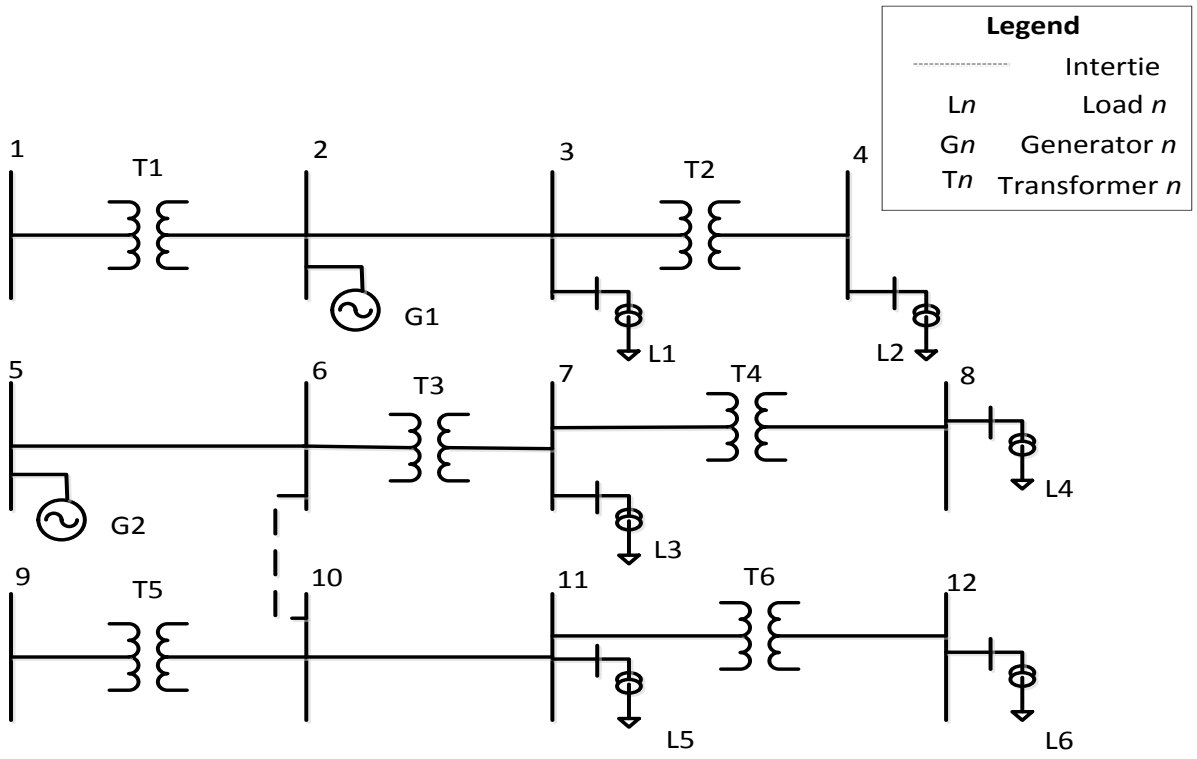

Fig. 2.2 A simple 3 feeder distribution system.

This can be expressed in the form of a two dimensional matrix, consisting of '*from*' and '*to*' connections.

$$\begin{bmatrix} x_{11} & x_{ij} & x_{1n} \\ \vdots & \ddots & \vdots \\ x_{n1} & \cdots & x_{nn} \end{bmatrix} \tag{2.16}$$

This matrix is a symmetric about the leading diagonal since an intertie from bus *j* to *i* equivalent to an intertie from bus *i* to *j*. This matrix has values of 1 and 0 only, representing if a connection is present or absent. For e.g. $x_{ij} = 1$ implies that a connection is present between bus *i* and bus *j*. Now, the x_{n-1} buses on feeder $(n-1)$ can potentially have interties to all the buses not present on bus $(n-1)$. Since, the presence or absence of a bus is a 1/0, or mod 2 operation, the total topologies of connections from bus $(n-1)$ is $2^{x_{n-1}(x-x_{n-1})}$. Therefore, the total possible topologies in the system are

$$2^{x_1(x-x_1)} * 2^{x_2(x-(x_1+x_2)} * \ldots * 2^{x_{n-1}(x-(x_1+x_2+\cdots+x_{n-2}+x_{n-1}))} \quad (2.17)$$

Consider only the exponent terms.

$$x_1(x - x_1) + x_2\big(x - (x_1 + x_2)\big) + \cdots x_{n-1}(x - (x_1 + x_2 + \cdots + x_{n-2} + x_{n-1})) \quad (2.18)$$

On the distribution end, the numbers of buses on each feeder are approximately equal. Hence,

$$x_1 = x_2 = x_3 = \cdots = x_n \quad (2.19)$$

Plugging this in (2.18) gives

$$x_n(x - x_n) + x_n\big(x - (x_n + x_n)\big) + \cdots x_n(x - (x_n + x_n + \cdots + x_n + x_n)) \quad (2.20)$$

Reducing and ignoring lower order terms,

$$\frac{1}{2}x_n^2 * n^2 \quad (2.21)$$

Hence, the growth of the feeder reconfiguration problem is

$$2^{\frac{1}{2}x_n^2 n^2} \quad (2.22)$$

This proves that the *growth of the problem is exponential*.

This work further establishes the minimum and maximum bounds on the growth of the problem. Bounds on the growth of a problem help understand if an algorithm is appropriate to be used to solve the problem. Case 1, below, establishes the lower bound on the problem and case 2 finds the upper bound.

Case 1: To find the lower bound, only two feeders are assumed to be present in the system, and of the n buses, $(n-1)$ buses are present on a single feeder and only one bus, the n^{th} bus, is present on the second feeder. In this case, only one intertie is possible from each bus on the first feeder to the bus on the second feeder. Hence, total possible topologies are

$$2^{(x-1)} \quad (2.23)$$

Case 2: A maximum number of interties will be possible *if* every bus is present on a different feeder. Maximum interties will directly correspond to maximum possible topologies. If each feeder has only one bus,

$$n = x; \text{and } x_n = 1 \quad (2.24)$$

Plugging this in (2.20) gives

$$2^{x(x-1)/2} \tag{2.25}$$

From case1 and case 2, growth of the problem can be established as

$$2^{(x-1)} \quad \leq \ Growth\ of\ Feeder\ Addition\ problem \quad \leq \quad 2^{x(x-1)/2} \tag{2.26}$$

This establishes that the distribution feeder reconfiguration problem has *atleast* an exponential growth. Table 2.1 shows the lower and upper bounds on the growth of two notional test systems, and the RBTS system. One bus on each feeder is assumed to be a slack bus, and is hence not a part of the analysis. Three slack buses are modeled in this system since the slack bus on a particular feeder can only provide information on the buses connected to that particular feeder. Hence, each feeder is provided a separate slack bus.

Table 2.1 Bounds on the growth of feeder reconfiguration problem for some distribution systems

Topology	Lower bound	Upper bound
3 feeder 9 bus	32	2^{15}
6 feeder 18 bus	2^{11}	2^{66}
6 feeder 33 bus	2^{32}	2^{351}

2.6 Computational Complexity

Computational problems can be broadly classified into two groups based on the complexity of the algorithm to solve the problem: $P\ and\ NP$. All problems that can be solved in time that is a polynomial function of the size of input ($n,\ n^2,\ n^3$), can be classified as polynomial time or '***P'*** problems. Problems that have an exponential growth function (2^n) or worse are useless to be tried through conventional algorithms [54]. Such problems are classified as non-deterministic polynomial time or '***NP'*** problems. There is no known algorithm that can be used to solve these problems in polynomial time. Examples of these problems include the 3-SAT (satisfiability) problem, the travelling salesman problem, vertex cover etc.

The satisfiability problem is an absolutely certified *hard* problem [52]. The satisfiability problem has a set of Boolean variables *V* and a set of clauses *C* over *V* [52]. Clauses are a function of the variables

and are represented in conjunctive normal form (CNF). In a CNF expression, the variables of each clause are in disjunctive normal form (OR) and each clause in the expression is in a conjunctive normal form (AND). Example, the variables

$$v_1, v_2, v_3 \, , and \; v_4 \quad v_i \in V, \tag{2.27}$$

can form the clauses

$$\begin{gathered} Z_1 = \{v_1 \vee v_2 \vee \overline{v_3}\} \\ Z_2 = \{v_2 \vee v_3\} \\ Z_3 = \{v_1 \vee v_2 \vee \overline{v_3} \vee \overline{v_4}\} \\ Z_4 = \{\overline{v_2}\} \end{gathered} \tag{2.28}$$

and form the expression

$$\psi = \{Z_1 \bigwedge Z_2 \bigwedge Z_3 \bigwedge Z_4\} \tag{2.29}$$

The objective is to find a satisfying assignment of *1's* and *0's* to the variables, such that all the clauses are satisfied. A 3-SAT is a special form of the SAT problem, where each clause has exactly three variables in regular or complemented form.

Another documented *hard* problem is the travelling salesman problem (TSP). Given a weighted graph *G*, the objective is to find a tour such that each vertex on the graph is covered, and the path minimizes the *cost* of the tour. Examples, given a weighted graph G in Fig. 2.3, find the optimal path such that the start and the end nodes are node *S*, and every node in the graph is covered.

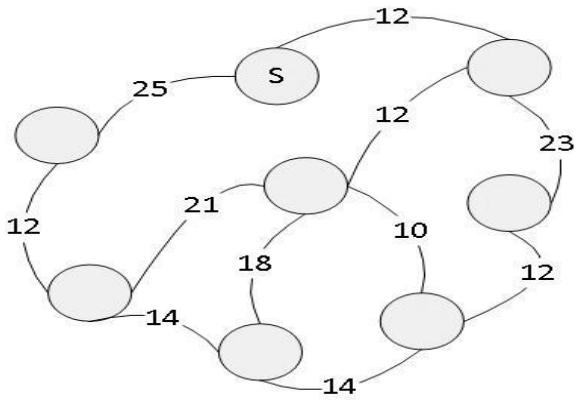

Fig. 2.3 Graph of a travelling salesman problem.

Such problems are required to be classified for two reasons. One, classification enables an algorithm designer to focus efforts in trying to find clever means to solve the problem, rather than trying conventional algorithms that are doomed to fail. Secondly, properties that make the problem *hard* can be clearly understood.

NP problems are approached using three techniques:

- Use of algorithms that solve in polynomial time for the average case of the problem. An assumption is made that the toughness of the problem is distributed as a Gaussian function, and hence the probability of a problem being on either extreme is expected to be lower. Example of this algorithm is the backtracking algorithm. Backtracking is a systematic technique for searching through the entire search space of the problem [52]. The backtracking algorithm starts with a single variable, and finds a partial solution of the problem with just that variable. At each proceeding step, the next partial solution is found by adding another variable. Proceeding with this until the last variable, the algorithm constructs a tree of partial solutions.
- Use of heuristic algorithm. All heuristic algorithms work on a similar concept. At the start of the algorithm, the algorithm behaves almost as a random search algorithm, to avoid converging on local minima. Once the algorithm finds a set of good candidate solution points, more informed decisions can be made. Most heuristic algorithms atleast have one step that adds a random nature to the algorithm. This is important to avoid local optima.
- Another approach could be to avoid looking for an optimal solution, and settle for pseudo-optimal solutions. This is widely popular since such relaxations can transform a problem from '***NP'*** **to** '***P'***. Approximation algorithms guarantee that the optimal solution can never be 'much' better than the currently available solution [52].

Even though an ***NP*** problem cannot be solved in polynomial time, it can be *verified* in polynomial time [52]. To prove that a problem is in ***NP,*** the concept of reductions is used. Reductions help transform one problem into another, to prove that both problems are equally '*hard'*. If a '*fast*'

algorithm can be found for one of the problems, the same can ideally be used for solving the other problem. To prove that the given problem at hand is in ***NP,*** a known ***NP*** problem must be reduced into the given problem. This should be possible in polynomial time. Hence, if the problem at hand can be solved in polynomial time, the known ***NP*** problem can also be solved in polynomial time. Accepting that $P \neq NP$ [53], if a known ***NP*** problem *A* can be reduced to problem *B*, then problem *B* is as hard as problem *A*. Reduction is used to prove that the distribution feeder reconfiguration problem is in ***NP***. The distribution feeder reconfiguration problem can be defined as follows:

Input:

- A set of 0/1 variables (x_{ij}), depicting the absence or presence of an intertie
- Maximization function (f_n): This is the multi-objective function comprising ENS and cost
- An integer or an integer matrix **I,** such that $f_n \geq \mathbf{I}$
- Constraints (voltage and power).

Note that any minimization function can be converted to a maximization function by negating the function.

Problem definition:

Is there a satisfying assignment to the variables x_{ij}*, such that* $f_n \geq I$.

To prove that the feeder reconfiguration problem is hard, a 3-SAT problem is reduced to the feeder reconfiguration problem. The 3-SAT is a proven ***NP*** problem that cannot be solved in polynomial time using any conventional algorithm. 3-SAT consists of Boolean variables as inputs, and 3 variable clauses (which are a function of the inputs) that must be satisfied.

Proof:

Step 1: The 3-SAT problem has Boolean variables and clauses. The Boolean variables are transformed into integer variables by representing each Boolean variable in the SAT, as two variables in the feeder reconfiguration problem. Each variable in the SAT is represented as two variables in the feeder

reconfiguration problem such that, each variable x_i in the SAT problem has two integer variables $y_i \; and \; \overline{y_i}$ in the feeder problem with constraints,

$$0 \leq y_i \; and \; \overline{y_i} \leq 1 \tag{2.30}$$

$$1 \leq y_i + \overline{y_i} \leq 1 \tag{2.31}$$

Step 2: Each clause of the SAT is converted to a constraint of the feeder problem. For example, A clause $\{x_1, \overline{x_3}, x_5\}$, is transformed as $y_1 + \overline{y_3} + y_5 \geq 1$, under the constraints mentioned in step 1. Also, just as every clause of the 3-SAT problem must be satisfied, every clause of the feeder reconfiguration problem must also be satisfied.

Hence, the transformation gives a set of variables and constraints. Even, without the maximization function, the SAT problem has been completely transformed to a feeder reconfiguration problem. As the constant ***I*** is associated with the maximization function, ***I*** can also be trivialized.

Inferences:

- Finding a solution to the transformed problem is equivalent to finding a solution to the SAT problem.
- A solution to the SAT problem is a solution to the transformed problem.
- The transformation can be performed in polynomial time.
- It is also noted that the *hardness* of the problem is not due to the number of variables, but due to the constraints that need to be satisfied.
- Finally, supposing there is a known hypothetical algorithm (black-box) that can solve the 3-SAT problem in polynomial time, the algorithm can be used to find the optimal solution to the feeder reconfiguration problem. It is assumed that the most optimal ENS and associated cost for the feeder reconfiguration problem are available. The black-box used for solving the 3-SAT can now be used to find the set of interties that must be introduced in the system to obtain the known ENS and cost.

Therefore, an efficient (*fast*) algorithm to solve the feeder problem will imply that SAT is not in ***NP***. But 3-SAT being a proven ***NP*** problem, implies that *distribution feeder reconfiguration problem is in NP*. Although this formulation of the feeder reconfiguration problem is proven to be in ***NP,*** it does not imply that all formulations of the feeder reconfiguration problems are equally hard. There could be some other formulation of the feeder reconfiguration problem that may not belong in ***NP***. Such formulations do not exist to the best of the knowledge of the author.

Chapter 2 provides an understanding of the complexity of the distribution feeder reconfiguration problem and proves why it is not possible to use conventional algorithms. It also explains why heuristic algorithms are a better choice of algorithms to solve the distribution feeder reconfiguration problem. Chapter 3 explores an existing algorithm that is used to solve the feeder reconfiguration problem, and provides a method to accelerate the process of building the Pareto front.

Chapter 3

Accelerating the process of Distributed Feeder Reconfiguration

The genetic algorithm described in chapter 2 is applied to a 3FDR test system and the Roy Billinton Test System (RBTS) in this chapter to test and compare results of the accelerated genetic algorithm. The RBTS was developed by the Power Systems Research Group at the University of Saskatchewan to conduct studies on distribution feeder electric systems [66, 67]. The time taken for the solutions to converge to a Pareto front took upto 40 hours on a non-devoted Intel® Core™ 2 Duo™ CPU at 2.66 GHz when the algorithm was applied to the RBTS [20]. Such long convergence durations may be unacceptable in distribution systems where the reconfiguration planning engineer may not have sufficient information regarding the loads on the system at various buses, two days in advance. Hence, the convergence to the Pareto front requires to be accelerated.

Several studies using time-stamps and data dumps were run on the 3FDR and the RBTS systems to find the sources of delay that contributed to high execution time of the code. It was found that the main component of delay was due to the communication between Matlab™ and PowerWorld™. As shown in Fig. 3.1, Matlab™ generates new strings of population in every generation, which are then used to re-configure the network on PowerWorld. Load flow analysis is run on the re-configured network, and the results are sent back to Matlab. Fitness of individual strings are computed based on the results of the load flow analysis. PowerWorld™ can be supplemented with an add-on software known as SimAuto™. SimAuto™ provides the ability to access the functions of PowerWorld™ from external software, which is Matlab™ in this case [code in Appendix A]. SimAuto™ acts as a Component Object Model (COM) object that is accessed from Matlab™ [68].

This connection was required to be made each time an individual string in a population was checked. The time to make each of these connections was approximately 5 seconds on a non-devoted Intel® Core™ 2 Duo™ CPU at 2.66 GHz. Hence, time to make each connection for all strings of each generation quickly propagated into long duration runs. Two solutions were planned for this problem: the

first was to create only one connection per generation, and to submit all jobs in that generation as a batch job, and second to create only one connection irrespective of the number of generations and maintain this connection until end of simulation.

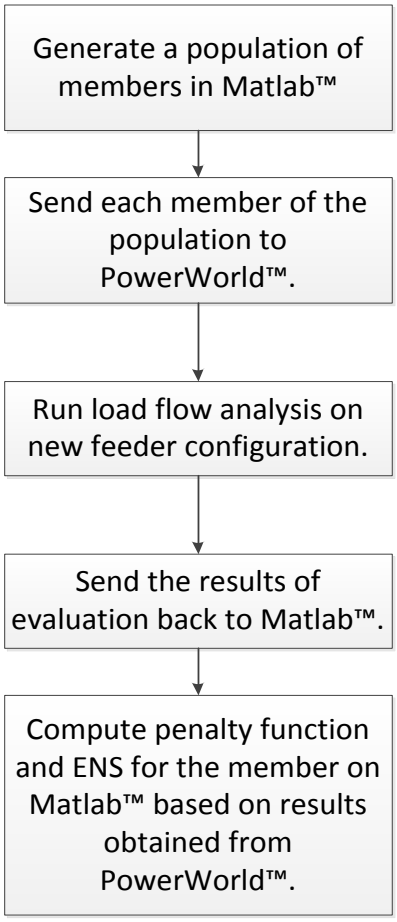

Fig. 3.1 Matlab™ and PowerWorld™ communication.

This required that the jobs be written to an external text file in a format that was specified by PowerWorld™, and PowerWorld™ read that file once for every generation [code in Appendix A]. Two problems were encountered in the external file technique. One, Matlab™ had to wait while PowerWorld™ read the text file, and the load flow analysis for each string of a generation. This led to simulation time being wasted, since the Matlab™ code had to wait for PowerWorld™ to get the penalty functions before the code could proceed to the next generation. The other problem was that Matlab™ had to poll to check if the output file was available at the end of simulation on PowerWorld™. In order to avoid this, the second method was chosen as a favorable method. In this case, only one connection was

made at the start of simulation, and was maintained until the end of simulations. In order to make this work, the contents of the register required to be flushed each time after testing a string. This was found to be more efficient than the file writing technique. Hence, the method of maintaining a single connection was chosen. Gains of an order of magnitude were observed, with no major change in the Pareto front of the output. All testing was performed on an Intel® Core™ 2 Duo™ non-dedicated PC with processor speed at 2.64 GHz. Every accelerated code was run three times, and the average of the run times is reported.

3.1 3-Feeder 9-Bus test system (3FDR)

The 3FDR system is a simplified system developed to test various reconfiguration algorithms [19, 69]. The 3FDR system used in this study is shown in Fig. 3.2.

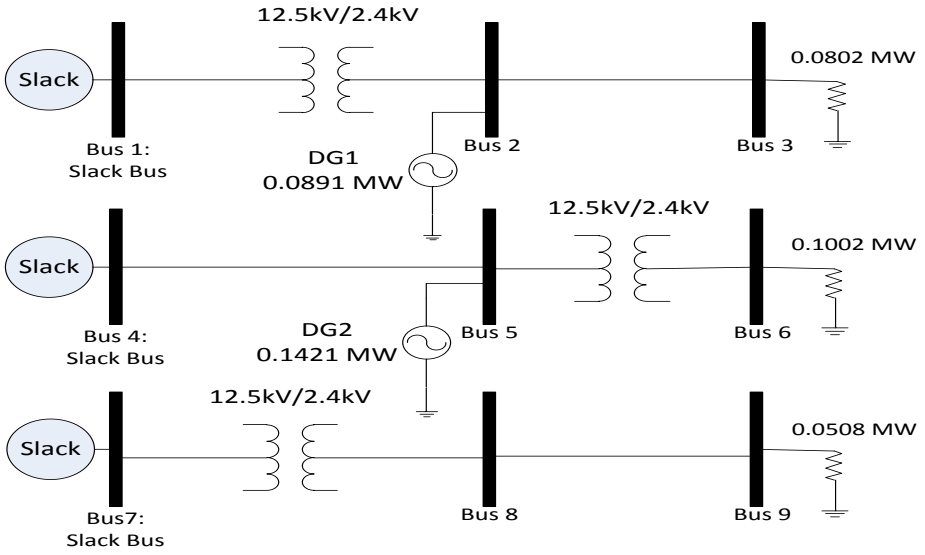

Fig. 3.2 3-Feeder 9-Bus test system.

The system consists of three feeders, ten buses, and two voltage levels, V_1 *and* V_2, and V_1 is greater than V_2 (V_1 = 12.5kV and V_2 = 2.4kV). Loads are present at buses 3, 6, and 9. Buses 1, 4, and 7 are the slack buses in the system. The slack bus is an important tool in load flow analysis. The output of a slack bus helps in determining the deficit or excess real and reactive power in the system. As mentioned in chapter 2, three slack buses are modeled in this system since the slack bus on a particular feeder can only provide information on the buses connected to that particular feeder. Hence, each feeder is provided

a separate slack bus. When two feeders are connected by an intertie, the corresponding slack buses will read equal values, and either one of the values can be used to calculate the ENS. The system is modeled as an islanded microgrid, and hence grid ties are absent in the representation. The loads on feeders 1 and 2 are assumed to be lower than the RE DG sources [19, 69].

RE DG sources are modeled using the wind and solar capacity factors, 0.25 and 0.30 respectively [19, 70]. The capacity factor of a wind resource depends on the wind profile in the region. The power produced by a wind turbine largely depends on the speed of wind [69]. Due to wide variations in wind speed as a function of time-of-day or season-of-year, 0.25 is a safe capacity factor for wind turbines. The capacity factor of 0.30 for the PV resource represents the actual capacity factor of a South-facing fixed tilt collector at Boulder, CO.

On connecting an intertie between two buses at different voltages, a transformer is assumed to be present with $(0.01 + 0.06i)\ p.u$ impedance on the base of the transformer. All other system data required for simulation is presented in table 3.1, which was directly reproduced from [19, 20].

Table 3.1 System data for 3FDR and RBTS simulations.

System Data:
Power output of the DG resource at bus *i* (P_i^{DG}) (data taken directly from [18])

i	**2**	**3**	**5**	**6**	**8**	**9**
Wind (P_i^{DG}) [kW]	0.0891	0.0891	0.1421	0.1421	0.1231	0.1231
PV (P_i^{DG}) [kW]	0.1069	0.0891	0.1705	0.1705	0.1477	0.1477

RE DG Costs (C_i^{DG})(taken directly from [71]):

Cost of setting up wind plant at bus *i*: 1.6 $/kW of installed capacity.
Cost of setting up PV units at bus *i*: 5.5 $/kW of installed capacity.

Intertie costs (C_i):
Cost of transformer [$] – 400000
Cost of 2.4kV line [$/ft] – 50
Cost of 12.47kV line [$/ft] – 100
Fixed line cost [$] – 100000

Length of intertie (L_i)

Intertie (from bus – to bus)	Length [miles]	Intertie (from bus – to bus)	Length [miles]
1 – 4	0.1894	3 – 6	0.4214
1 – 5	0.3788	3 – 7	1.0432
1 – 6	1.1364	3 – 8	0.9996
1 – 7	0.3206	3 – 9	1.4330
1 – 8	0.3909	4 – 7	0.1376
1 – 9	0.5666	4 – 8	0.1701
2 – 4	0.261	4 – 9	0.4543
2 – 5	0.2841	5 – 7	0.3588
2 – 6	0.3267	5 – 8	0.3933
2 – 7	0.3262	5 – 9	0.5764
2 – 8	0.3551	6 – 7	0.5687
2 – 9	0.5926	6 – 8	0.4136
3 – 4	0.8996	6 – 9	0.3855
3 – 5	0.7576		

The ASAI on the system is maintained as in [19, 61] = 0.999375
Annual outage time calculated based on this = (1 – 0.999375) = 0.000625 hours.

3.2 RBTS Test System

The Roy Billinton Test System, is a basic transmission and distribution reliability test system. The basic transmission reliability data was developed in [66] and extended in [67] for distribution systems. The 11kV circuits off Bus 3 were chosen for simulation in [19, 20], and the same is maintained in this work. The bus 3 distribution circuit has 6 feeders and 32 buses including the slack buses. A snapshot of the RBTS system as modeled on PowerWorld is shown in Fig. 3.3. Topological information regarding the buses were not available, the lengths of the interties are calculated using (3.1) [19].

$$D = \begin{cases} \sqrt{d^2 + (\varepsilon - \omega)^2} & when\ \varepsilon \neq \omega \\ d & when\ \epsilon = \omega \end{cases} \quad (3.1)$$

Where,

d is the distance between the feeders

ε is the radial distance of the destination bus from slack bus on the same feeder

ω is the radial distance of the source bus from the slack bus on the same feeder

A total of 302 interties are possible in the system. The lines for all connections were chosen to be ACSR Flamingo conductors. The data for the conductors is the same as used in [19], and is reproduced in table 3.2 for completeness.

Table 3.2 Line ratings of ACSR Flamingo line.

Diameter of line	666600 cmils
Current rating	800 A
Resistance	0.141 Ω/mi
Impedance	0.412 Ω/mi
Assumed cost	200000 $/mile

As per [67], 20% of the load on Bus 3 can be curtailed under emergency conditions. Since no specific information is available regarding which specific buses can curtail their loads, the total sum of the slack buses is multiplied by 0.8 to compensate for this requirement [19]. The transformers for the system are assumed as 11kV/480V with 0.06*j* p.u impedance, on a base of 1MW. The average loading of the line at the various buses is directly used from [19] and is shown in table 3.3.

Table 3.3 Distribution of load in the RBTS system.

Customer type	**Peak load (MW)**	**Avg. load (MW)**	**Load points**
Residential	0.8367	0.4684	1, 4-7, 20-24, 32-36
Residential	0.8500	0.4758	11-13, 18, 25
Residential	0.7750	0.4339	2, 15, 26, 30
Small industry	1.0167	0.8472	8 – 10
Commercial	0.5222	0.2886	3, 16, 17, 19, 28, 29, 31, 37, 38
Office buildings	0.9520	0.5680	14, 27

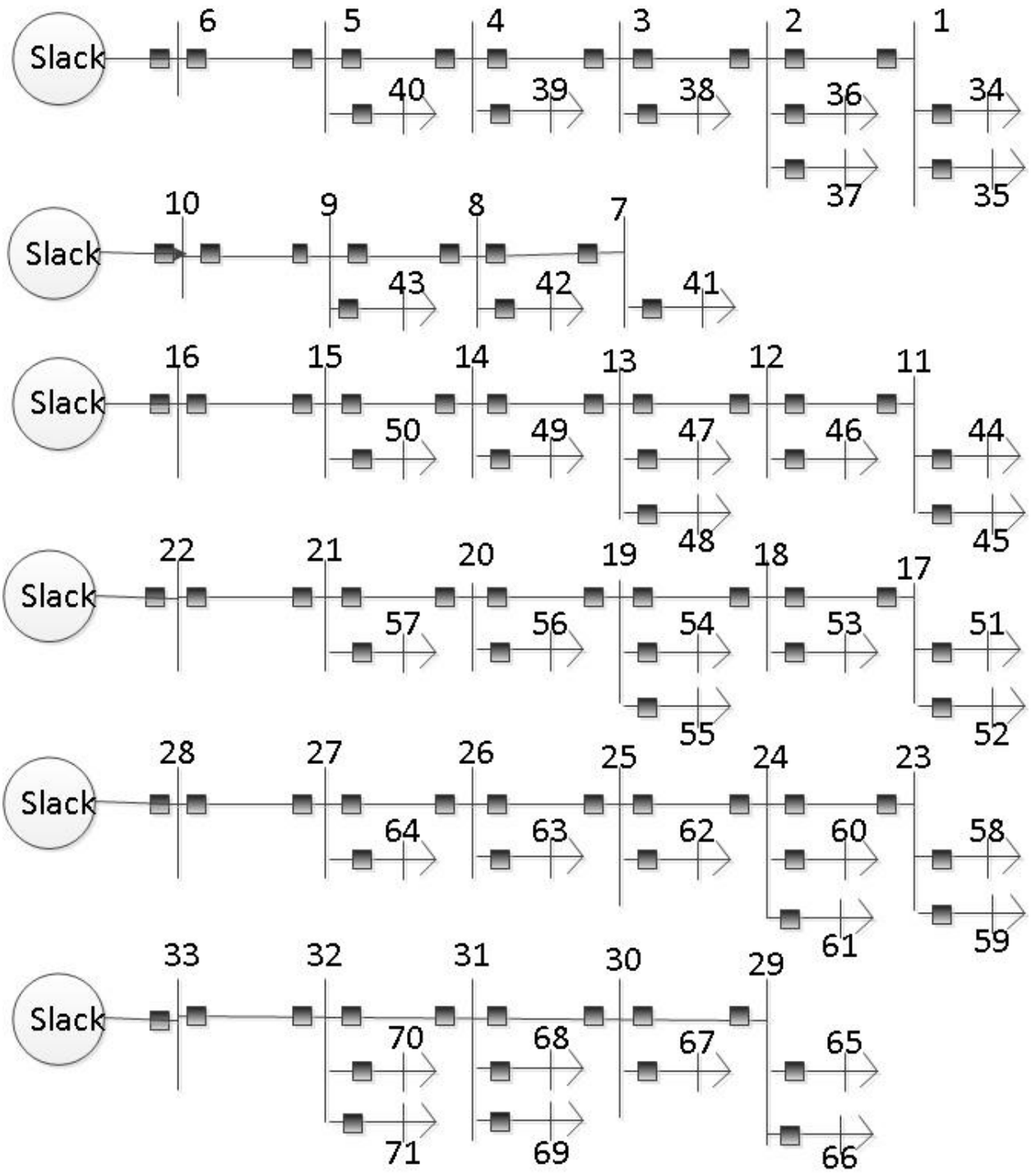

Fig. 3.3 6-feeder RBTS system.

The RE DG resources in this analysis are also assumed to be wind and PV with capacity factors of 0.25 and 0.3 respectively [19, 70]. In addition the total RE DG resource is assumed to be comprised of 40% wind resources and 60% solar resources.

3.3 Comparison of Results

This section of the thesis compares results of the accelerated code and the unaccelerated code when applied to 3 feeder problem and the RBTS problem [Code in electronic appendix]. The unaccelerated code is directly obtained from [19, 20]. The accelerated code, developed as a part of this thesis, is modified in each case to match the assumptions made in the prior work for the unaccelerated code.

3.3.1 Comparison of results for 3FDR system

In [19], to simplify analysis, the author assumes that the location of the DGs are fixed. Location of the DGs are assumed to be at bus 2 (PV array) and bus 4 (wind turbine). As mentioned earlier, the capacity factor of wind is modeled to be 0.25 and that of solar is modeled to 0.30. Load buses are composed of critical and non-critical load components [19]. Critical loads cannot be interrupted. The 3FDR system topology is modeled as a sparse adjacency matrix [19]. The binary bus connection matrix B_{ij}, as described in [69], is reproduced for ease of reference.

$$B_{ij} = \begin{cases} 1 \text{ if bus i is connected to bus } j \\ 0 \text{ if bus i not connected to bus } j \\ 1 \text{ if } i = j \end{cases} \tag{3.2}$$

The 3FDR test system is built on PowerWorld™, with interties being represented as open lines. Line and transformer capacities are oversized in this analysis [19]. Each string in the genetic algorithm represents all possible interties. Hence, the length of the string in each generation is 27 for the 3FDR problem. The objective of the analysis is to reduce cost and ENS. The equations of cost and ENS were discussed in chapter 2. Table 3.4 shows the possible interties with associated costs of the unaccelerated code. The table has been sorted in ascending order of costs. The Pareto front obtained is shown in Fig. 3.4. The number of generations in a genetic algorithm decides how much of the state space the algorithm

is allowed to explore. A very low value leads to sub-optimal solutions. On the other hand, a very large number of generations may not improve the solution significantly, if at all, and results in increased computational time. Through repeated executions, 25 generations was found sufficient for the 3FDR system, and increasing the number of generations did not yield any better solutions. The duration of execution is approximately 54.19 minutes for running 25 generations of the unaccelerated code. .

Table 3.4 Solutions obtained for the 3FDR unaccelerated code.

Solution #	Interties	Cost (thousand $)	ENS (MWh)
1	4 – 7	172.65	0.048733
2	2 – 6, 4 – 7	358.9	0.000005
3	2 – 8, 4 – 7	366.4	0.0

This duration of execution is high for a test system with 3 feeders and 9 buses. Hence, the code required to be accelerated. The results from the accelerated code for 25 generations of MOGA are shown in table 3.5 and the Pareto front obtained is shown in Fig. 3.5. The accelerated code executes in 83 seconds. This is an order faster than the unaccelerated code and is acceptable execution duration for a test system.

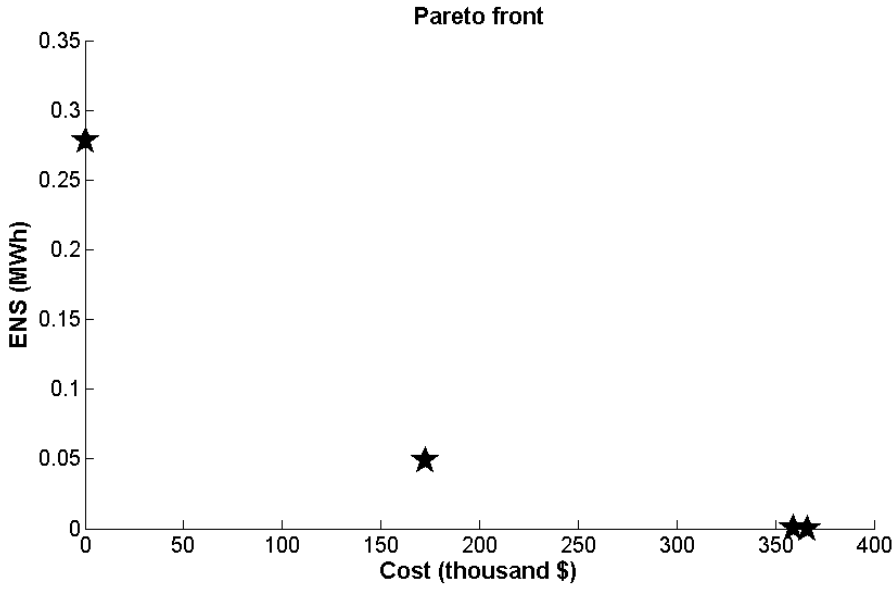

Fig. 3.4 Pareto front of the 3FDR unaccelerated code.

It can be observed that the converged solution points of the accelerated code are exactly the same as the unaccelerated code. The reason for the similarity can be attributed to the relatively smaller state space of the problem. Hence, even though the two methods may differ in the search path due to the roulette wheel selection stage, the final solution points are the same.

Table 3.5 Solutions obtained for 3FDR accelerated code.

Solution #	Interties	Cost (thousand $)	ENS (MWh)
1	4 – 7	172.65	0.048733
2	2 – 6, 4 – 7	358.9	0.000005
3	2 – 8, 4 – 7	366.4	0.0

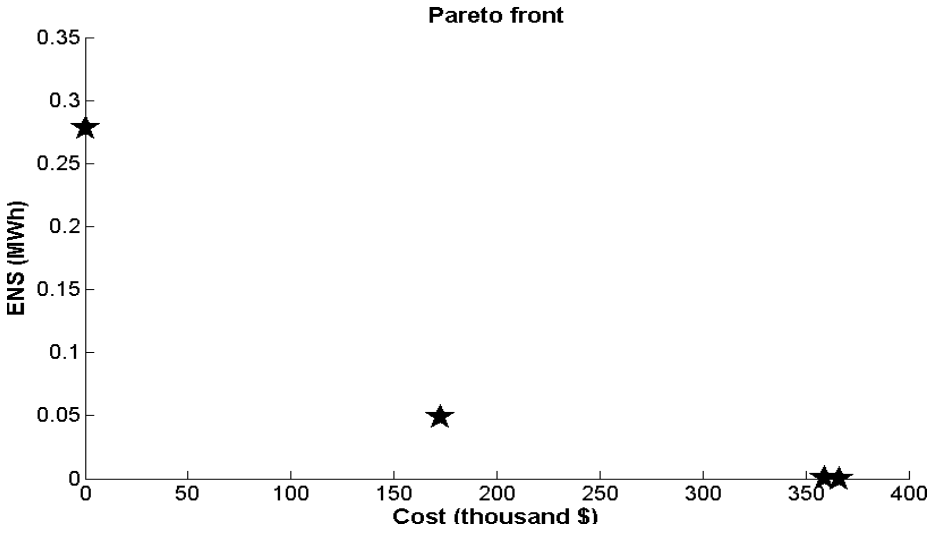

Fig. 3.5 Pareto front obtained for 3FDR accelerated code.

3.3.2 Comparison of results for RBTS case

In the RBTS analysis, the author in [19] again assumes that the DG locations are fixed. The DG locations are assumed to be at buses 23, 8, and 2. These buses were selected at random [19]. Three different cases, each having a different number of generators in the system were tested for the RBTS case. In each case the length of the each string in the genetic algorithm is equal to the total number of possible interties, i.e. 302. As the string size is higher as compared to the 3FDR case, time taken to converge to the Pareto front is higher. The DG locations and values are reproduced directly from [19] for completeness in analysis and shown in table 3.6.

Table 3.6 RBTS testcases

DG	Case I	Case II	Case III
A	9.5236 MW	4.8109 MW	3.2400 MW
B	0	4.8042 MW	3.2333 MW
C	0	0	3.2235 MW
Total	9.5236 MW	9.6151 MW	9.6968 MW

Case I

In this analysis, one RE DG is assumed to be present in the system, and the location of the DG is at bus 23 on feeder 5. As can be seen, the time taken to converge to the Pareto front for a 15 generation MOGA execution is around 6 hours (5.89 hours.) for the unaccelerated code. Close resemblance from an execution of the unaccelerated code and multiple (3) executions of the accelerated code suggests that increasing the number of generations would not yield results that are much better than the currently obtained solutions. Also it was found from the executions that the solution points lying at the extremities of the objective function did not change much. Hence, 15 generation execution was considered sufficient for this case. Results from the execution, and the associated Pareto front are shown in table 3.7 and Fig. 3.6. Variation in the solutions can be solely attributed to the randomness that is introduced in the roulette selection step in the genetic algorithm.

Table 3.7 Solutions for Case I RBTS unaccelerated code.

Solution #	Interties	Cost (thousand $)	ENS (MWh)
1	11 – 17, 18 – 24, 23 – 29	201.0	34.5421
2	15 – 20, 18 – 23, 23 – 29	516.0	34.5398
3	5 – 20, 17 – 24, 23 – 29	868.0	34.5394
4	5 – 20, 18 – 26, 23 – 29	909.2	34.5393

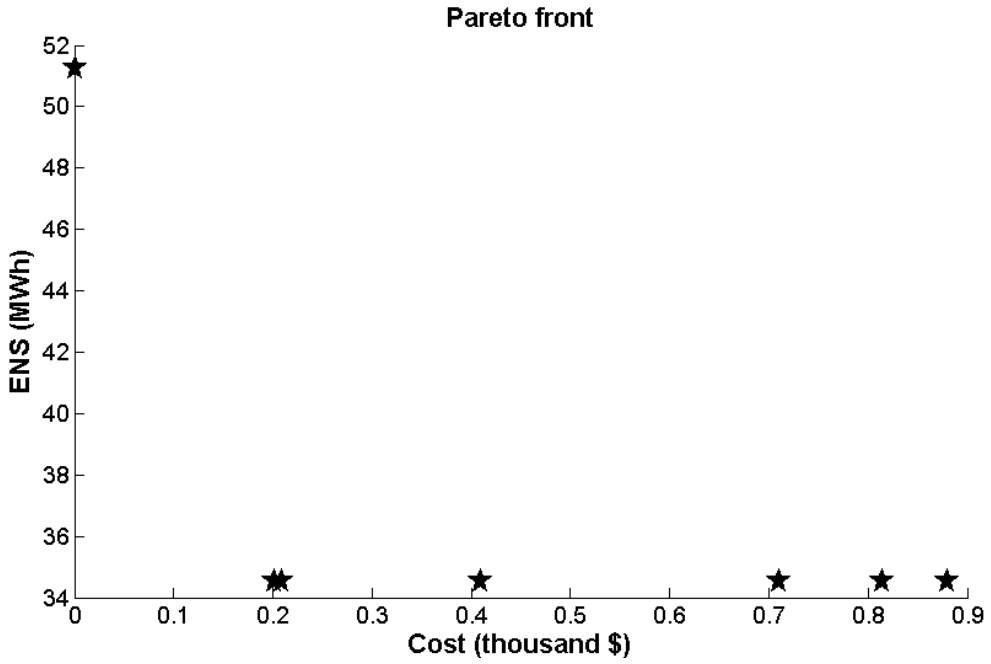

Fig. 3.6 Pareto Front for Case I RBTS unaccelerated code.

The code acceleration is then applied and, with all other conditions remaining unchanged, the code is executed for 15 generations. The code is now observed to execution in under half an hour (29.65 minutes). As can be observed from the plot in Fig 3.7 the Pareto front is nearly the same. Solutions obtained are tabulated in table 3.8.

Table 3.8 Solutions for Case I RBTS accelerated code.

Solution #	Interties	Cost (thousand $)	ENS (MWh)
1	11 – 17, 18 – 24, 23 – 29	201.0	34.5421
2	11 – 17, 20 – 27, 23 – 29	208.8	34.5406
3	15 – 20, 18 – 23, 23 – 29	516.0	34.5398
4	5 – 24, 19 – 24, 23 - 29	1202.1	34.5397

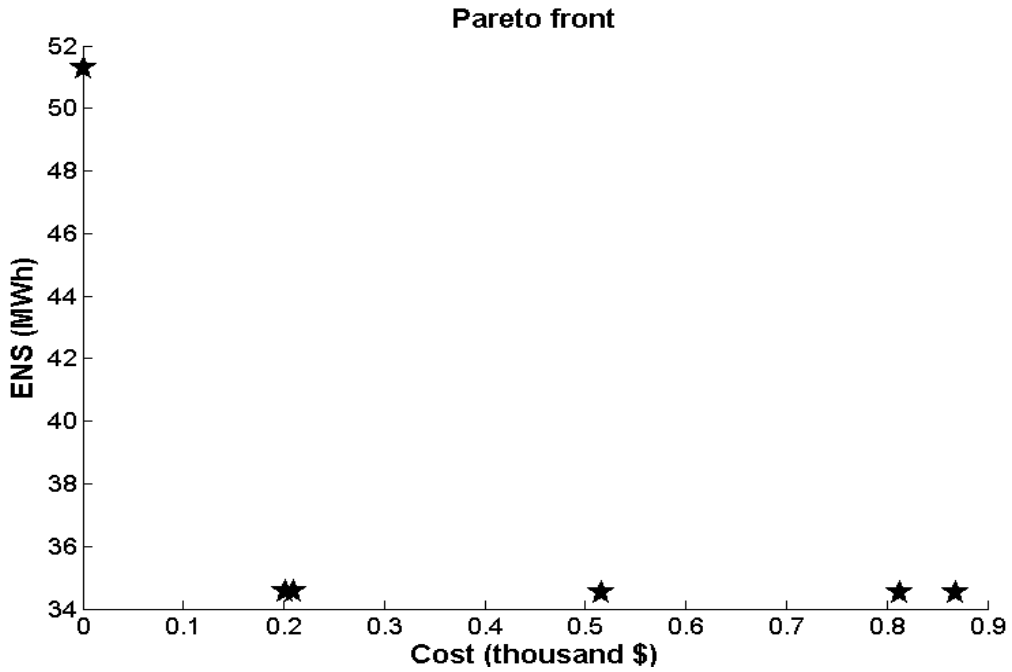

Fig. 3.7 Pareto Front for Case I RBTS accelerated code.

Case II

In this case, two generators are assumed to be located at buses 23 and 8 [18]. All other conditions remain unchanged. Results and the Pareto front from executing the unaccelerated code are shown in Table 3.9 and Fig. 3.8 respectively. Since the conditions for the GA are unchanged, the duration of execution for the unaccelerated code remains at 6 hours. With all other conditions remaining unchanged, the accelerated code is executed for this case, and table 3.10 represents the results obtained and Fig. 3.9 shows the Pareto front. The accelerated code executes in 28 minutes.

Table 3.9 Solutions for Case II RBTS unaccelerated code (15 generation).

Solution #	Interties	Cost (thousand $)	ENS (MWh)
1	1 – 7, 23 – 29	0.0	34.1468
2	1 – 7, 18 – 24	201.0	34.1436
3	5 – 9, 21 – 26	521.2	34.142
4	1 – 7, 21 – 26	312.4	34.1417

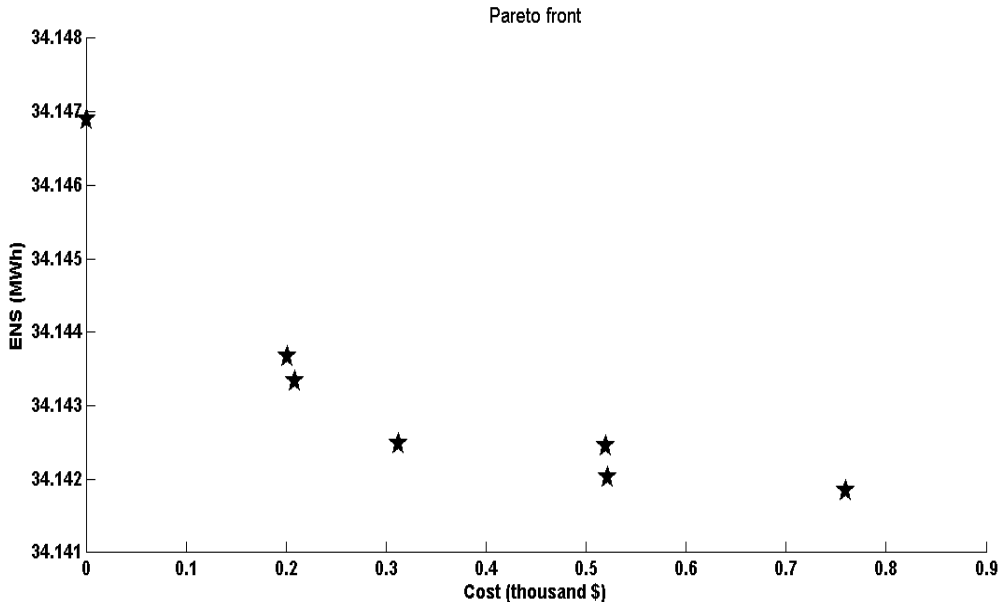

Fig. 3.8 Pareto Front for Case II RBTS unaccelerated code (15 generation).

Table 3.10 Solutions for Case II RBTS accelerated code (15 generation).

Solution #	Interties	Cost (thousand $)	ENS (MWh)
1	1 – 7, 23 – 29	0.0	34.1468
2	1 – 7, 18 – 24	201.0	34.1436
3	5 – 11, 9 – 15, 14 – 27	1381.1	34.1396
4	5 – 11, 9 – 15, 9 – 24	169.5	34.139

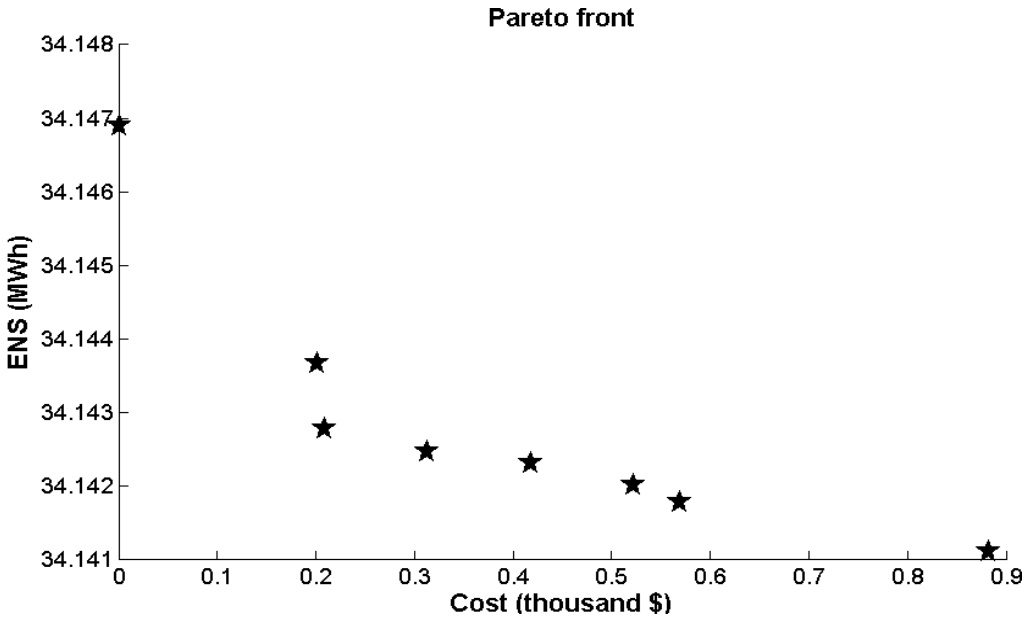

Fig. 3.9 Pareto Front for Case II RBTS accelerated code (15 generation).

At first sight, Pareto front from the accelerated code seems to have performed better than the unaccelerated code. But this would be a flawed assumption. As the accelerated code has so far been proven to converge to the same solutions as the unaccelerated code, a difference in the Pareto front suggests that the number of generations is insufficient for the code to explore the state space. This is then tested by executing the unaccelerated and accelerated codes for 30 generations. The results of the unaccelerated code and the associated Pareto front are shown in table 3.11 and Fig. 3.10 respectively. Also, the table and Fig. of accelerated code are presented in table 3.12 and Fig. 3.11 respectively. Comparing Fig. 3.10 and 3.11 shows that the Pareto front generated are similar. This provides justification for the reasoning that the Pareto front generated for 15 generation looked dissimilar because 15 generations were insufficient for the algorithm to explore a larger portion of the state space.

Table 3.11 Solutions for Case II RBTS unaccelerated code (30 generation).

Solution #	Interties	Cost (thousand $)	ENS (MWh)
1	1 – 7, 23 – 29	0.0	34.1468
2	1 – 7, 18 – 24	201.0	34.1436
3	1 – 7, 20 – 26	233.2	34.1430
4	5 – 11, 9 – 15, 9 – 24	169.5	34.139

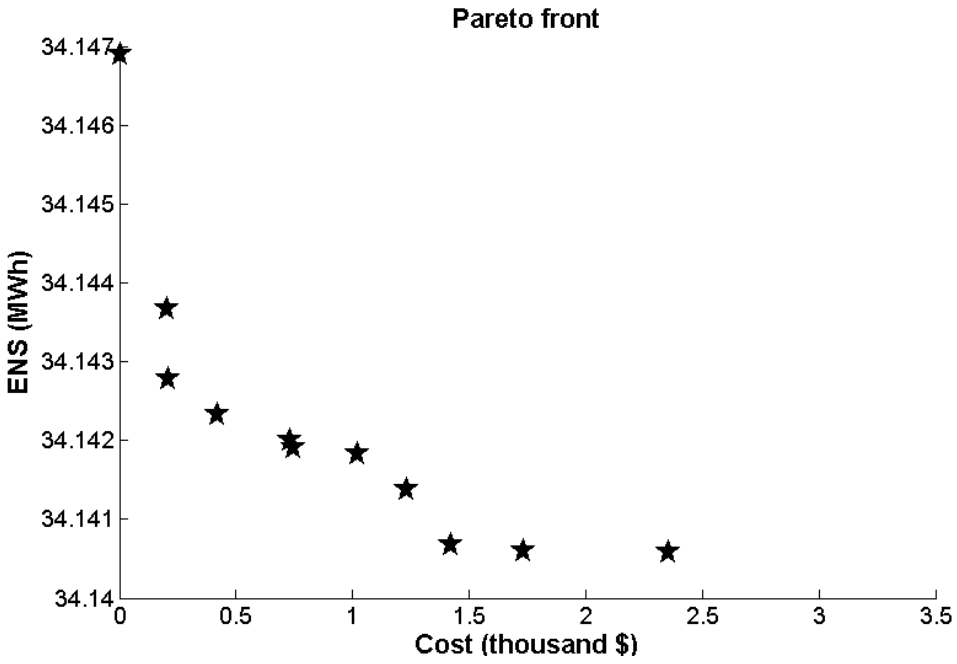

Fig. 3.10 Pareto Front for Case II RBTS unaccelerated code (30 generation).

Table 3.12 Solutions for Case II RBTS accelerated code (30 generation).

Solution #	Interties	Cost (thousand $)	ENS (MWh)
1	1 – 7, 23 – 29	0.0	34.1468
2	1 – 7, 18 – 24	201.0	34.1436
3	5 – 9, 21 – 24	728.8	34.142
4	5 – 11, 9 – 15, 9 – 24	169.5	34.139

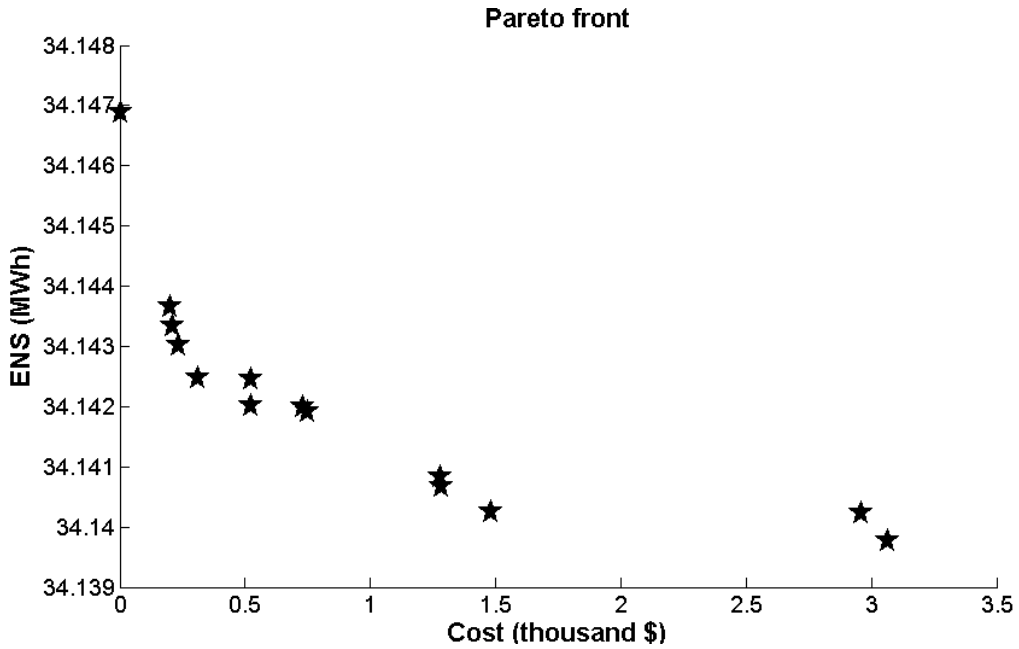

Fig. 3.11 Pareto Front for Case II RBTS accelerated code (30 generation).

Case III

This is the final case in the series of test-cases evaluated by the author in [19]. All three generators are connected in this case, and the test case is executed for 15 generations. Table 3.13 and Fig. 3.12 show respectively the results and Pareto front obtained. Solutions are obtained in approximately 6 hours. The acceleration technique is then applied to the problem, and the results and Pareto front are obtained as shown in table 3.14 and Fig. 3.13. The accelerated code executes in approximately 30 minutes. As can be observed from table 3.13 and table 3.14, the accelerated and the unaccelerated code converge to similar solutions. The difference in solution points can be attributed to the random nature of selection at the roulette wheel step of the genetic algorithm.

Table 3.13 Solutions for Case III RBTS unaccelerated code.

Solution #	Interties	Cost (thousand $)	ENS (MWh)
1	23 – 29	0.0	37.5213
2	8 – 14, 23 – 29	204.0	34.5204
3	1 – 7, 9 – 14, 23 – 29	233.2	33.8045
4	4 – 9, 8 – 14, 20 – 27	646.0	33.7956

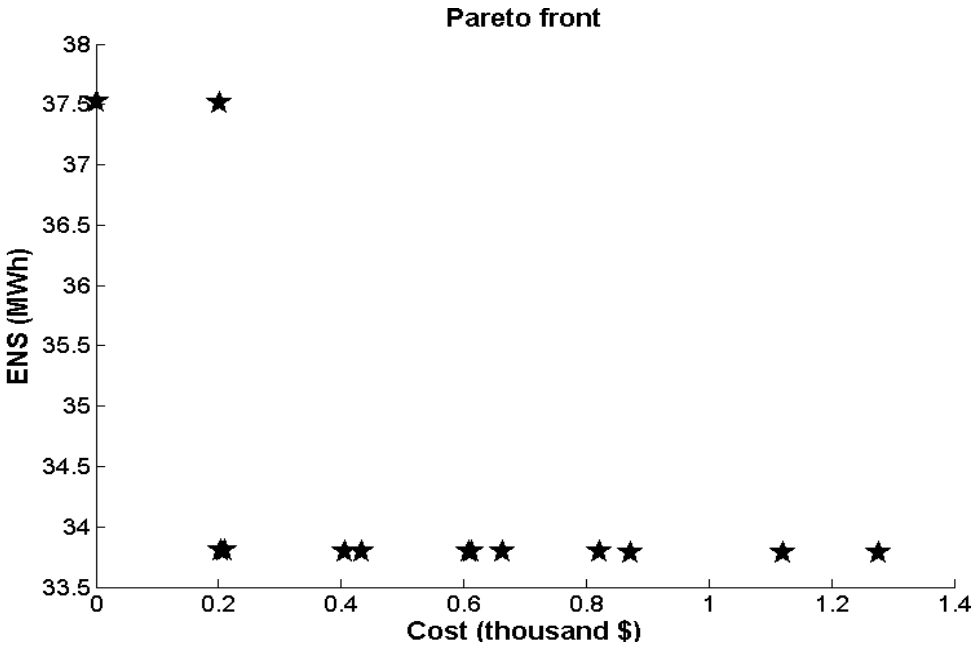

Fig. 3.12 Pareto Front for Case III RBTS unaccelerated code.

Table 3.14 Solutions for Case III RBTS accelerated code.

Solution #	Interties	Cost (thousand $)	ENS (MWh)
1	23 - 29	201.0	37.5134
2	8 – 14, 23 – 29	204.0	34.5204
3	1 – 7, 9 – 14, 23 – 29	233.2	33.8045
4	1 – 7, 8 – 14, 18 – 24	405.0	33.7966

Fig. 3.14 summarizes the code execution durations of accelerated and unaccelerated codes for all the test cases in sections 3.3.1 and 3.3.2. As can be clearly seen, the accelerated code executes an order of magnitude faster than the unaccelerated code. Also, as shown in sections 3.3.1 and 3.3.2, the solutions obtained from the accelerated and unaccelerated codes closely resemble each other.

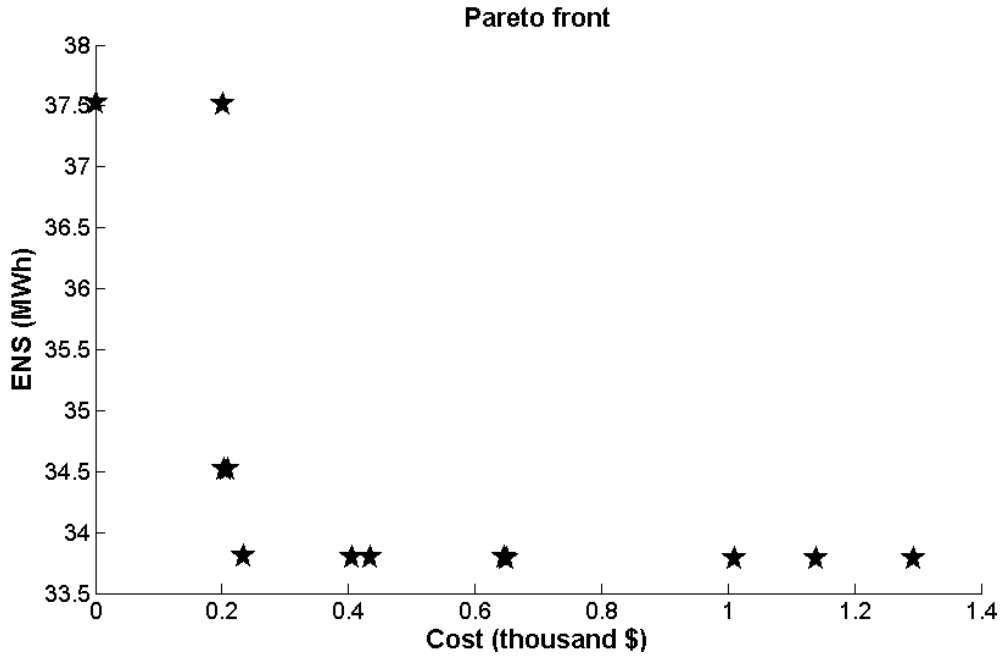

Fig. 3.13 Pareto Front for Case III RBTS accelerated code.

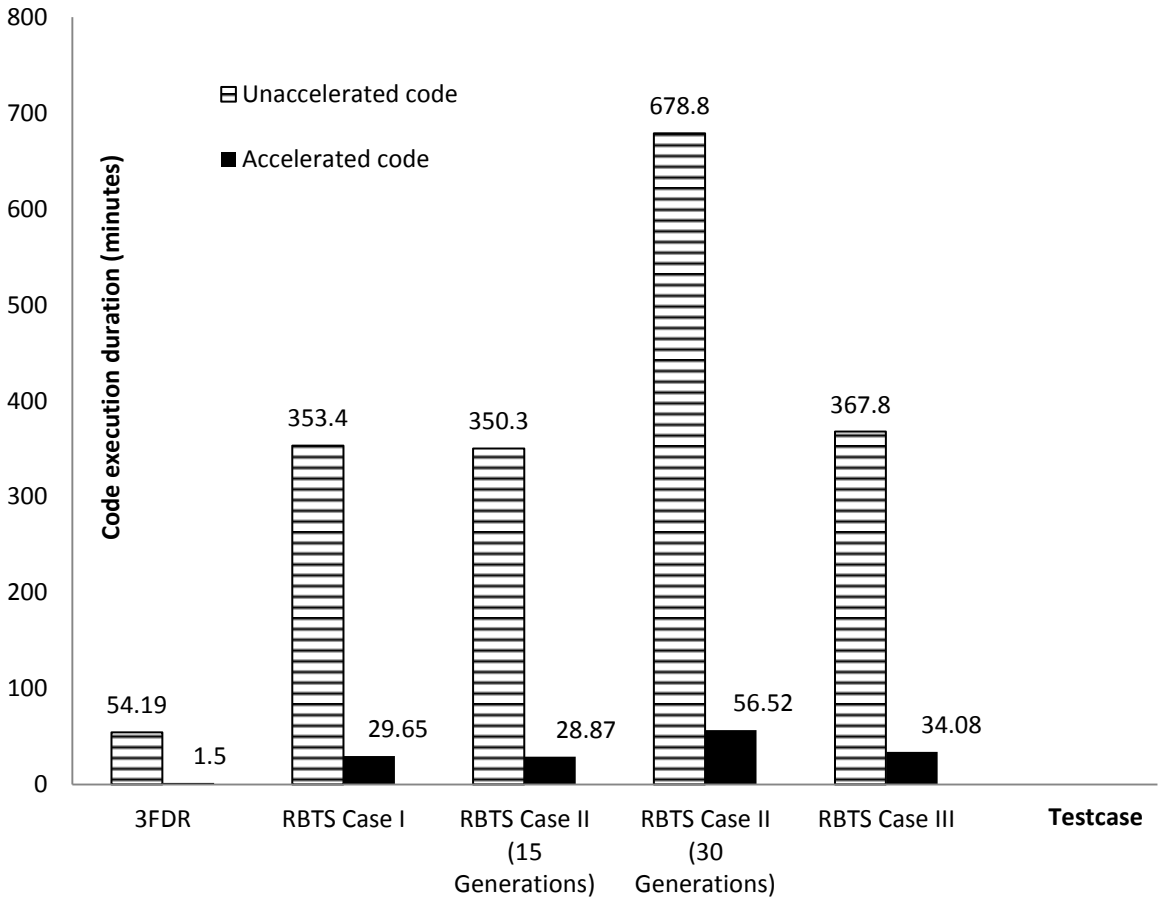

Fig. 3.14 Code execution duration comparison for testcases with fixed DG.

In [19] the author assumes the locations of DGs to be fixed for ease of analysis. In [20], the author finds Pareto solutions for the problem by finding optimal interties and collocating DGs simultaneously. DGs are not assumed to be fixed at the start of the analysis. The problem now poses two new challenges, due to which the solution time is expected to increase: the state space of the problem is now much larger, and the string length of population of each generation of genetic algorithm is also longer.

3.3.3 Comparison of RBTS system with DG collocation

In section 3.3.2, the locations of the DGs were assumed to be fixed. In this analysis, the locations for DGs are solved as a part of the MOGA to optimize the solution of the feeder reconfiguration problem. RE DGs are assumed to be wind and PV. The capacity factors of wind and solar are assumed to be 0.25 and 0.30 respectively [20]. Also, this section analyzes the effect of fixed load versus stepped load on the solution and verifies how the duration of execution of the code changes in the two cases. All test cases were executed for 15 generations of the MOGA. The average duration of execution calculated from three executions is presented.

Case I Comparison of RBTS system with DG collocation and fixed load

As compared to section 3.3.2, the string size for the genetic algorithm is longer in this case. Each string is now composed of two portions. As shown in Fig. 3.15, the string is of 329 bits in length as opposed to 302 bits in section 3.3.2.

Potential interties (302 bits)	*Potential DG location (27 bits)*

Fig. 3.15 Structure of GA string for RBTS with generator allocation case.

With increased string length, the duration of execution is expected to increase. Output from executing the unaccelerated code and Pareto front generated are shown in table 3.15 and Fig. 3.16 respectively.

Table 3.15 Solutions for RBTS with DG collocation and fixed load unaccelerated code.

Solution #	DG location	Interties	Cost (million $)	ENS (MWh)
1	3	1 – 7	18.0	32.801
2	4	1 – 7	18.0	32.801
3	5, 25	1 – 7, 23 – 29	18.06	26.513
4	11, 17, 20	1 – 7	18.36	22.381

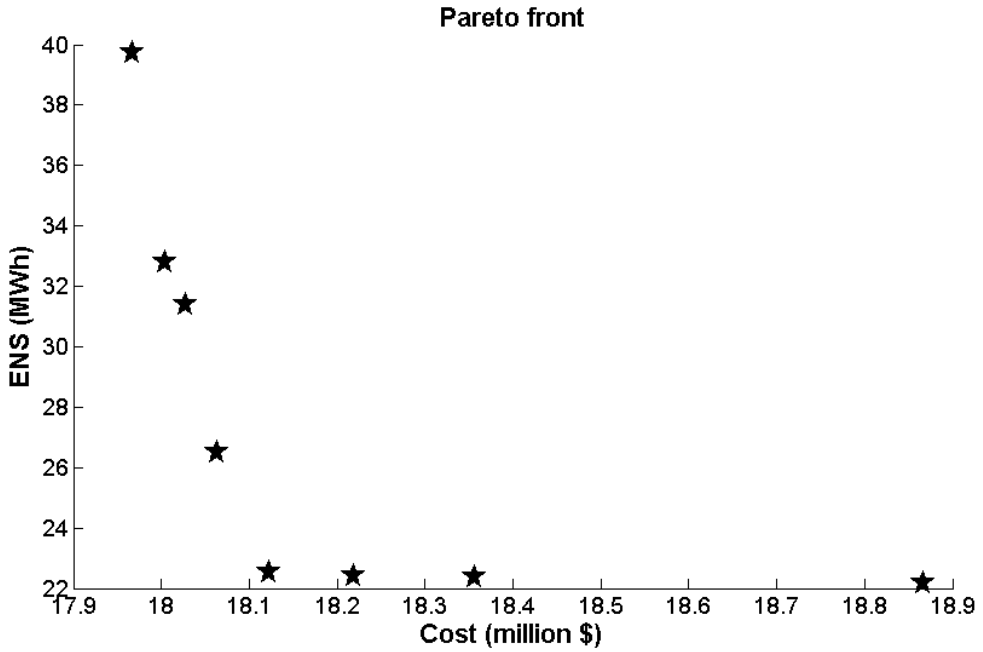

Fig. 3.16 Pareto Front for RBTS system with DG collocation and fixed load unaccelerated code.

The duration of execution of the code is approximately 153.19 minutes. This is a long convergence time for a test system. Hence, the code must be accelerated. The code is accelerated using the same technique as mentioned in section 3.1. The results and Pareto front generated by the accelerated code is shown in table 3.16 and Fig. 3.17. The time duration of execution for the accelerated code is on an average 13.67 minutes. Hence, the gain observed by executing the accelerated code is approximately 140 minutes (over 2 hours). Also, on comparing the solutions obtained, it can be noticed that the two codes converge on similar solution points of cost and ENS. The differences can be attributed to the random step in genetic algorithm.

Table 3.16 Solutions for RBTS with DG collocation and fixed load accelerated code.

Solution #	DG location	Interties	Cost (million $)	ENS (MWh)
1	25	23 – 29	17.97	39.75
2	15, 25	23 – 29	18.03	31.40
3	4, 25	1 – 7	18.06	31.24
4	3, 15, 20	3 – 19	18.76	22.43

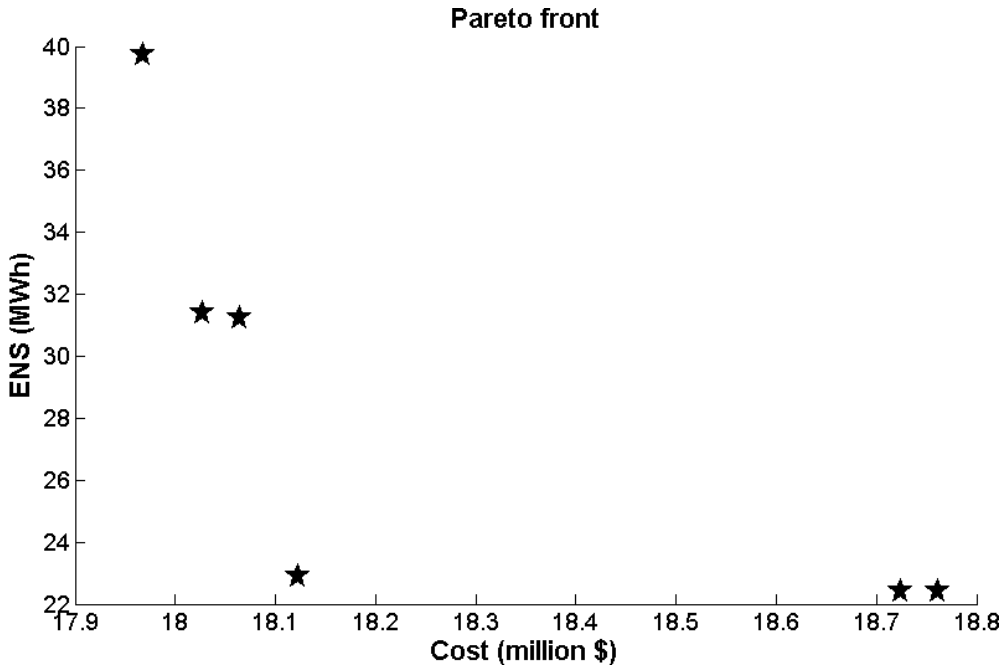

Fig. 3.17 Pareto Front for RBTS system with DG collocation and fixed load accelerated code.

Case II Comparison of RBTS system with DG collocation and stepped load

In this case, the stepped load is modeled on the RBTS system. As explained in chapter 3, the stepped load condition is a more realistic assumption of actual load modeling in distribution systems. This is a more accurate representation of the distribution system since loads almost never remain constant. Results obtained from executing the unaccelerated code are shown in table 3.17 and the Pareto front generated is shown in Fig. 3.18. The code execution duration is longer for the stepped load case, since the data is now changed on every step of execution. This change must be communicated to PowerWorld™ and updated before running the load flow analysis. The code execution duration is approximately 402.67 minutes.

Table 3.17 Solutions for RBTS with DG collocation and stepped load unaccelerated code.

Solution #	DG location	Interties	Cost (million $)	ENS (MWh)
1	-	23 – 29	0	45.87
2	14	-	17.60	37.36
3	5, 13, 20 ,24	7 – 13, 23 – 31	18.81	21.37
4	7, 15, 21	2 – 15, 5 – 17, 8 – 29, 12 – 29	20.87	20.56

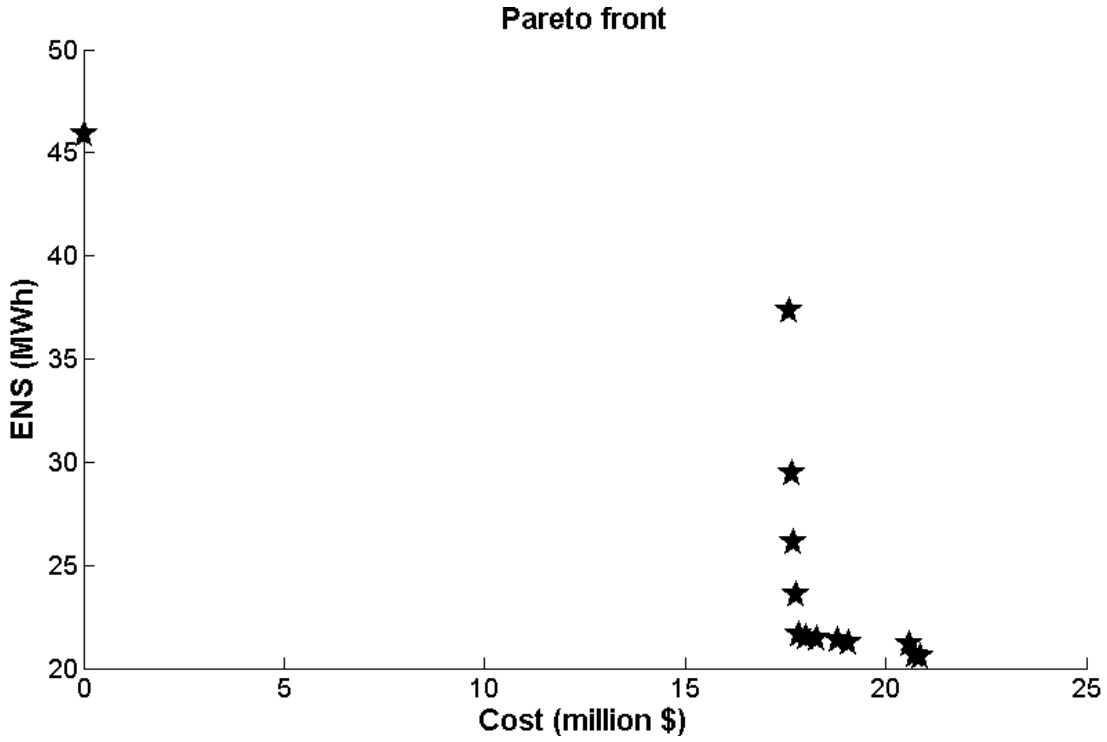

Fig. 3.18 Pareto Front for RBTS system with DG collocation and stepped load unaccelerated code.

Maintaining all other parameters the same, the accelerated code is now executed for this condition. The results and associated Pareto front is shown in table 3.18 and Fig. 3.19. The code execution duration for the accelerated run is approximately 55.71 minutes. Hence, the accelerated code saves approximately 6 hours of code execution duration and yields similar results.

Table 3.18 Solutions for RBTS with DG collocation and stepped load accelerated code.

Solution #	DG location	Interties	Cost (million $)	ENS (MWh)
1	-	23 – 29	0	45.87
2	14	-	17.60	37.36
3	1, 13, 17	2 – 14, 5 – 14	19.06	21.20
4	7, 15, 21	2 – 15, 5 – 17, 8 – 29, 12 – 29	20.87	20.56

In order to confirm that 15 generations is sufficient to converge at the correct Pareto front, the accelerated code is re-run for 25 generations. The Pareto front observed in shown in Fig. 3.20. The close resemblance between the 15 generation and 25 generation execution confirm that 15 generations is sufficient to converge correctly.

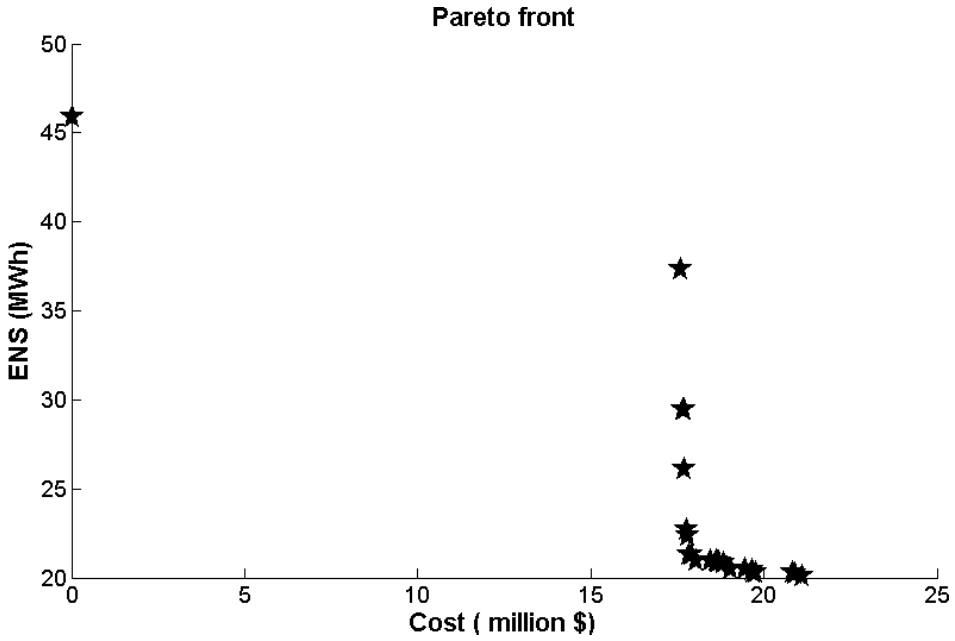

Fig. 3.19 Pareto Front for RBTS system with DG collocation and stepped load accelerated code.

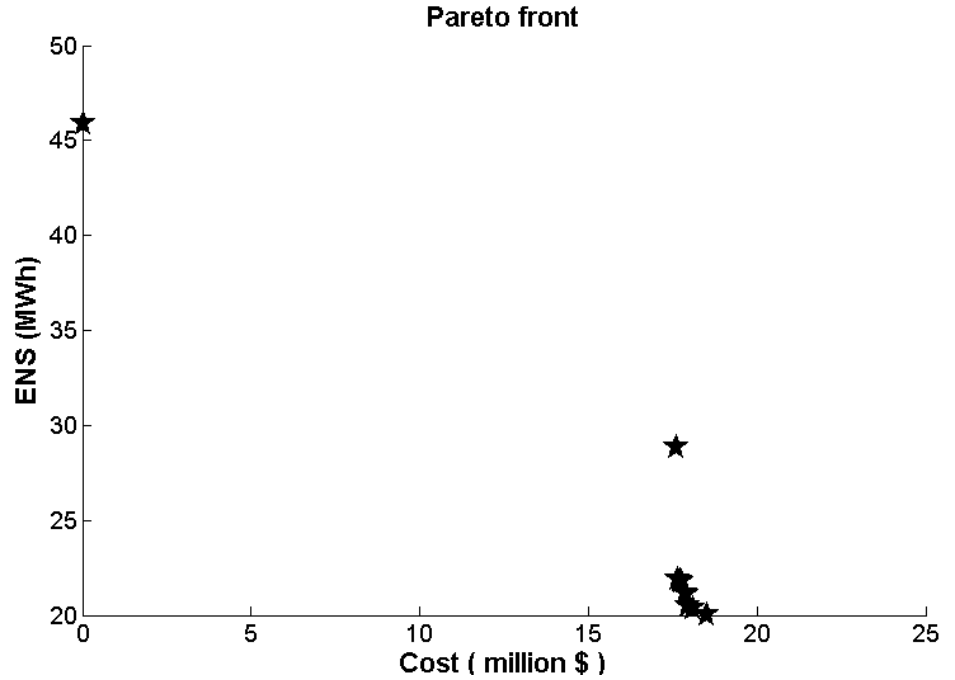

Fig. 3.20 Pareto Front for RBTS system with DG collocation and stepped load accelerated code (25 generation MOGA).

Fig. 3.21 summarizes the code execution durations of the various testcases with feeder reconfiguration with DG collocation. As can be seen, the gains due to code acceleration are of an order of magnitude.

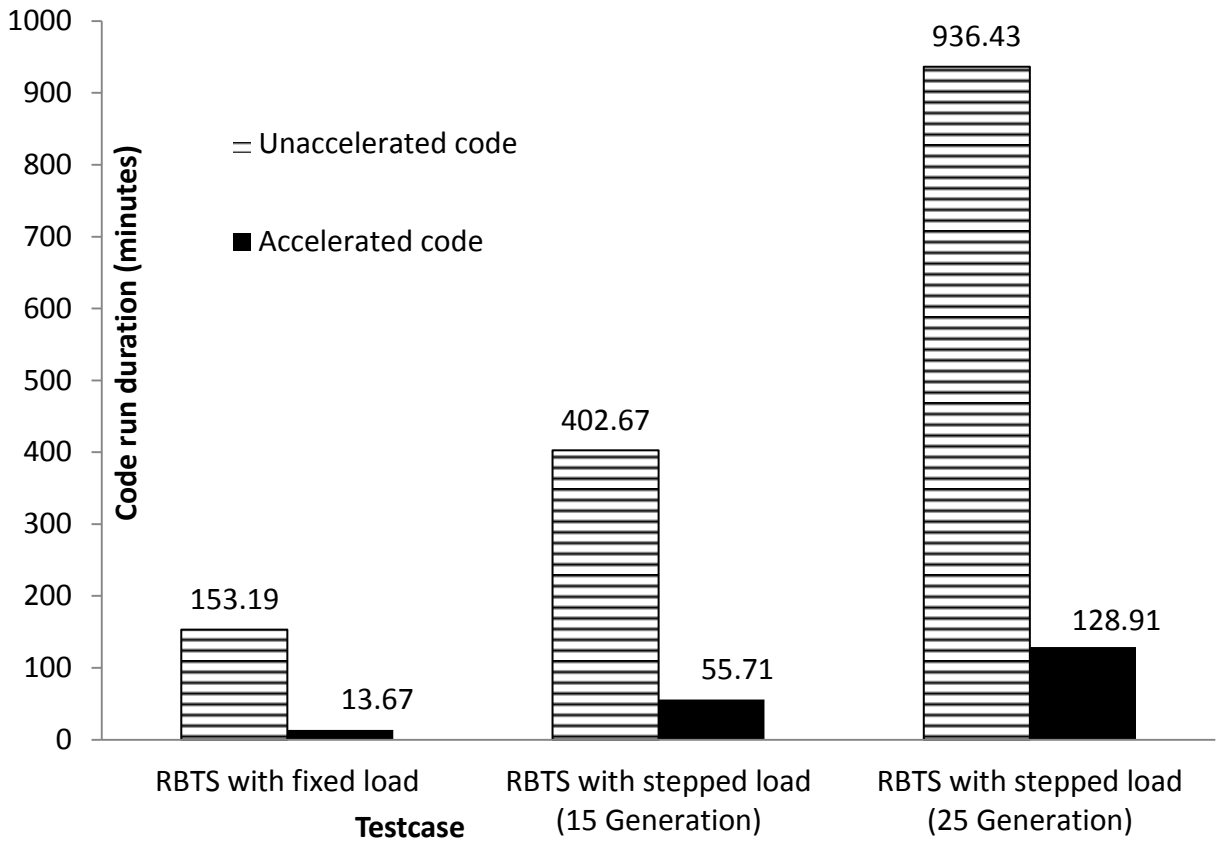

Fig. 3.21 Code execution duration comparison for testcases with collocated DG.

From the analysis we can see that an order of magnitude savings in execution time can be achieved through the use of the accelerated feeder reconfiguration technique. Also, as observed, the accelerated and the unaccelerated code converge on similar solutions. Any difference in solutions were minor in nature, and were attributed to the random nature of the search algorithm. Seeding the random number generator of the GA may have produced reproducible results, and better comparison between accelerated and unaccelerated code. But, since the GA toolbox of Matlab was used, modifications to the files owned in the toolbox were not permitted. Hence, random number seeding was not possible.

Chapter 3 concludes discussion of the distribution feeder reconfiguration and acceleration techniques. Chapter 4 introduces the concept of microgrids, and provides details on the implementation, considerations, and potential problems in the notional microgrid.

Chapter 4
Microgrids and Blackstart operations

This chapter explains the implementation of a computer simulated model of a mission-specific notional microgrid and simulation of blackstart operations. As explained in chapter 1, a microgrid is an aggregation of loads and generation sources which has the capability to isolate from the main grid either when a disturbance is detected on the main grid or if the cost of purchasing power from the main grid is higher than the cost of generating power locally. The proximity of generating resources to loads in a microgrid permits creative selection of generators based on the most abundant resources of fuel in the vicinity. This allows renewable energy resources to be integrated in the mix of generating resources. Most microgrids in the United States, integrate at least one form of renewable resource [15], [29], [39], [40], [43], [44]. Another important advantage of a microgrid is the ability to re-use the waste heat produced as a by-product of power generation. Such CHP units improve the overall efficiency of the microgrid's conventional generation to as high as 80 – 85% [16]. The notional microgrid in this work is modeled with a specific mission to serve the critical resources on a military base. Two specific missions are identified for the microgrid: 1) to supply critical loads in the microgrid in the event of loss of supply from the main grid, and 2) to aid the main grid in peak shaving during periods of peak loads, by supplying power back to the main grid.

An important application of microgrids is to improve the energy security at military bases. Smart Power Infrastructure Demonstration for Energy Reliability and Security (SPIDERS) is a joint initiative between Department of Energy and Department of Defense in applying Energy Surety Microgrids™ concept to military bases to keep mission critical facilities running despite a loss of connection to the main grid [71]. An Energy Surety Microgrid™ is a concept developed at Sandia National Laboratories for defense applications that is used to characterize energy systems [72]. The main requisites identified for the energy surety model are:

- "To reduce the number of single point failures

- Generating energy as close as possible to the load
- Running generators full-time in order to ensure no interruption in supply, on transitioning from grid connected to islanded modes of operation
- Using proven technologies
- Decreased dependence on fossil fuels by introduction of mix in generation, especially through the introduction of renewables
- Securing fuel supply
- Inclusion of sufficient an appropriate on-site fuel and energy storage" [72].

The dependence of the military on the main grid is of concern due to the vulnerability of the main grid to natural and man-made disasters. The Energy Surety Microgrid™ provides effective solutions to reduce the military's dependence on the main grid.

The SPIDERS project addresses four critical requirements to enhance the surety for national security:

- "Protect defense critical infrastructure from power loss due to physical disruptions or cyber-attack to the bulk-grid
- Integration of renewables and other DS options
- Sustain critical operations during sustained power outage on the bulk-grid
- Reduce carbon footprint by integration of renewables" [71].

Another military application of microgrids is on-board a notional US Navy destroyer class ship [73]. An integrated electric power system (IPS) aboard the ship provides advantages to the Navy in areas of improved maneuverability, capability to operate future generation weapons such as electromagnetic guns and electromagnetic aircraft launchers [73]. The propulsion system forms the bulk of the load for the ship. The IPS is different from a terrestrial power system for the following reasons:

- "Absence of a slack bus, i.e., a finite inertia system
- Tight coupling among various components on the system
- DC isolation between load and generator zones

- Different grounding philosophy" [73].

The all-electric ship, now called the Zumwalt class, is also equipped with the ability to reconfigure the integrated power system, in order to improve reliability during combat, in the face of battle damage [73].

An important operation in a microgrid is the ability of the microgrid to blackstart. Blackstart operation is required when the microgrid isolates from the main grid and sheds all local loads. Although some microgrids may have the ability to continue almost uninterrupted supply to the local loads despite isolation from the grid (CERTS microgrid) [15], most microgrids rely on blackstart capability [74]. The ability of the microgrid to continue uninterrupted supply to loads on isolation from the grid requires a storage resource managed by a control system which can engage the storage immediately on detection of isolation from main grid. Blackstart operation defines the steps that must be followed to bring up the generating resources and local loads in a microgrid, upon isolation from the main grid.

In this chapter, the blackstart operation of a notional, mission specific microgrid will be presented in detail. The structure of the notional microgrid is shown in Fig. 4.1.

4.1 PSCAD™

Power System Computer Aided Design (PSCAD™) is the tool used to study the notional microgrid. The tool provides flexible resources to model the different generators that were included in this study. PSCAD™ also provides resources to model the control systems for the generators. PSCAD™ is capable of communicating with other software tools. Although templates for these communication blocks are not available by default, the blocks can easily be created and commanded using script files. These blocks can then be used to communicate with modules on other tools such as Matlab™. In an extension to the work proposed in this thesis, PSCAD™ communicates with Woodward® Netsim™ software for generator control.

4.2 Generators

This work included the study of several types of generators which were available, or planned to be, on-site at the microgrid. While all loads were rated at 480 V, the site voltage of the notional microgrid is 12.5 kV. Table 4.1 depicts the generators and their ratings that were available at the notional microgrid

studied in this work. Fig. 4.1 depicts the structure and table 4.2 shows the load and generation distribution in the notional microgrid.

Diesel and natural gas are fossil fuels. A diesel plant is present in most generation configurations proposed for the microgrid, due to the quick startup, ramping and disturbance response of diesel generators. Since diesel fuel has a high energy density and is directly injected into the engine cylinders, diesel engines can respond quickly to changes of fuel command.

Use of natural gas to produce electricity has been popular since the early 1990s, due to the lower atmospheric emissions of natural gas, low fuel cost and readily available supplies. Power generation from natural gas is expected to grow from 23 percent in 2009 to 25 percent in 2035. [75]. While most utility-scale natural gas plants utilize simple- or combined-cycle gas turbines, the availability of high-efficiency internal combustion engines makes natural gas attractive as a distributed generation resource for microgrids.

Table 4.1 Mix of generators available at the notional microgrid.

Generator Type	Number of generators	Rating
Diesel	3	2.050 MW
Natural gas	3	2.055 MW
Biomass gas	2	1.60 MW

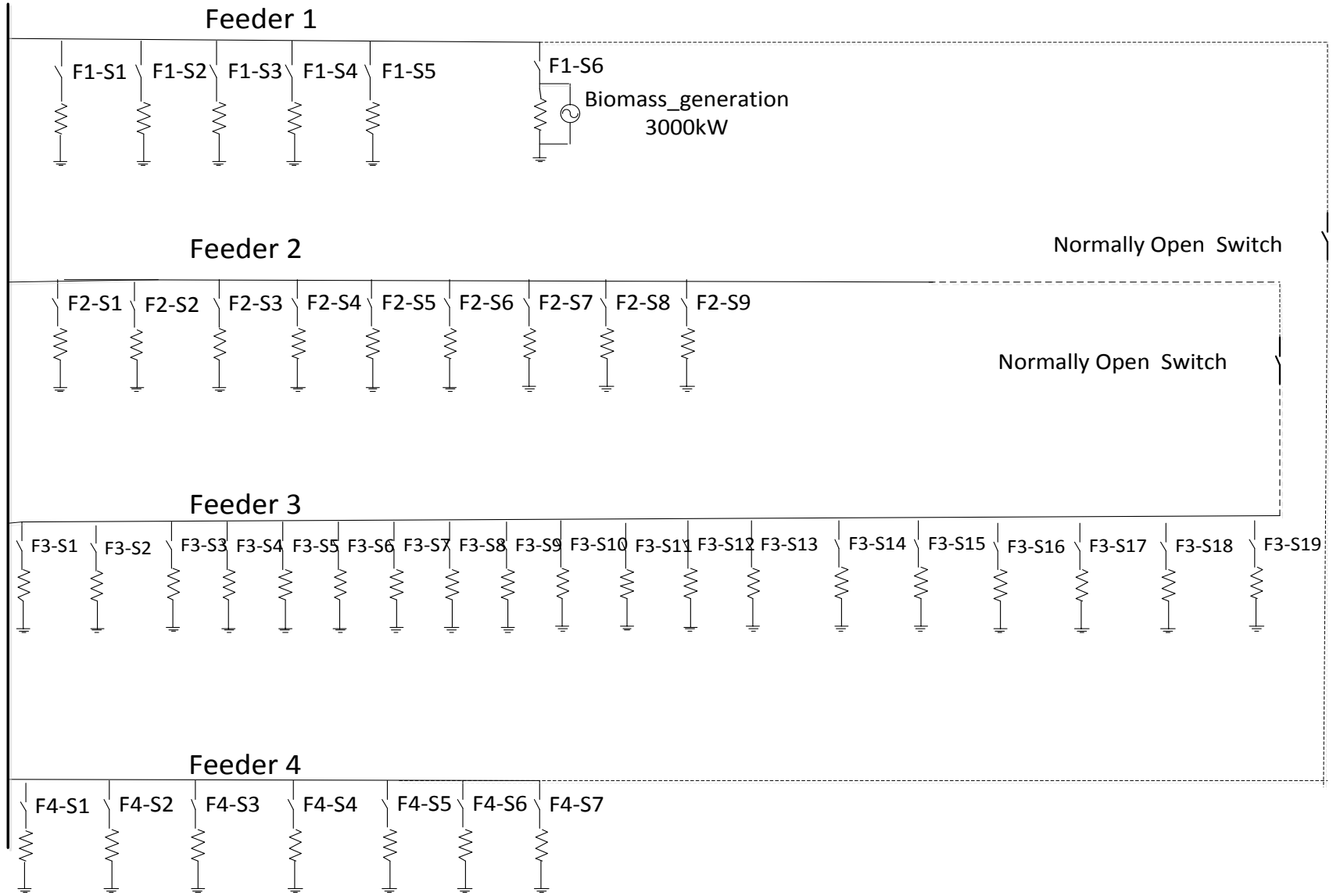

Fig. 4.1 One-line diagram of notional microgrid

Table 4.2 Load and generator distribution in the notional microgrid.

Switch	Components	Switch	Components
F1-S1	777.68 kW load (100% Building Energy Management (BEM))	F3-S7	226.08 kW (80% BEM)
F1-S2	280.88 kW load (100% BEM)	F3-S8	384.8 kW (100% BEM)
F1-S3	721.92 kW load (50% BEM), 400 kW backup generation	F3-S9	471.48 (100% BEM)
F1-S4	7.44 MW (100% BEM), 60 kW backup generation	F3-S10	224.2 kW (90% BEM)
F1-S5	9.92 MW load (100% BEM), 100 kW PV	F3-S11	335.64 kW (BEM)
F1-S6	278.24 kW (100% BEM), 60 kW backup generation	F3-S12	122.04 kW
F2-S1	124.44 kW	F3-S13	47.72 kW (30% BEM)
F2-S2	4.88 MW	F3-S14	67.56 kW (70% BEM), 50 kW backup generation
F2-S3	155.36 kW	F3-S15	181.24 kW (60% BEM), 40 kW backup generation
F2-S4	177.80 kW (80% BEM)	F3-S16	10.72 kW (90% BEM)
F2-S5	204.0 kW	F3-S17	241.2 kW (80% BEM), 25 kW backup generation
F2-S6	95.24 kW	F3-S18	169.44 kW (50% BEM), 45 kW backup
F2-S7	270.32 kW (70% BEM), 50 kW backup generation	F3-S19	184.36 kW (70% BEM), 110 backup generation
F2-S8	125.24 kW (40% BEM)	F4-S1	172.04 kW (80% BEM)
F2-S9	195.76 kW (100% BEM), 60 kW backup generation	F4-S2	318.76 kW, 60 kW backup generation
F3-S1	47.72 kW	F4-S3	221.08 kW (100% BEM)
F3-S2	18.56 kW	F4-S4	285.56 kW (30% BEM), 400 kW backup generation
F3-S3	222.56 kW (50% BEM)	F4-S5	358.56 kW
F3-S4	107.12 kW (80% BEM)	F4-S6	40.56 kW (80% BEM)
F3-S5	154.96 kW	F4-S7	184.36 kW
F3-S6	64.8 kW		

The oldest form of producing energy from biomass is by directly burning it to produce steam which turns a turbine to produce electricity. But, this is an inefficient form, and also results in higher air pollution. Also, steam cycle plants are difficult to operate and maintain as compared to internal combustion engines. Internal combustion engines provide an easier technique to convert biomass to energy. For this, the biomass must be processed through an anaerobic digester [78] or another gasification technology. Anaerobic conversion involves breaking down of biomass by micro-organisms to produce methane, carbon dioxide and other trace gasses. The gas mixture is then combusted in an engine to produce electricity. Such methane capture also helps prevent release of the greenhouse gas methane into the atmosphere. The notional microgrid modeled in this work uses methane gas produced by a bio-digester as a source of fuel for the biomass generator.

All gensets modeled in this study consist of the following components:

- Governor: A governor is a device which controls the fuel input to an engine, and thus its power output. In the model shown in Fig. 4.2, the governor controls the fuel based on the speed error. The speed error, calculated by the speed control component, is used to control the fuel demand to the engine and hence controls the power output of the engine. In this study, the engine is assumed to be directly coupled to the generator and the output torque of electrical machine applies load directly to the engine without any loss, neglecting any friction or coupling losses. Engines can also be coupled to the generator through a gearbox.

  The speed control unit in Fig. 4.2 has 2 inputs; the actual speed of the generator and the speed bias. The expected speed of the generator is 1 p.u ± speed bias. The speed bias setting is a small offset (< 2%) from the 1 p.u speed setting of the machine. The speed bias is set by an outer control loop shown in Fig. 4.3. This bias is normally required when the speed of the machine is to be controlled based on the output power of the generator. The proportional-integral-differential control (PID) loop in the speed control model generates an output signal based on the error signal. PID controllers are explained in detail in the next section.

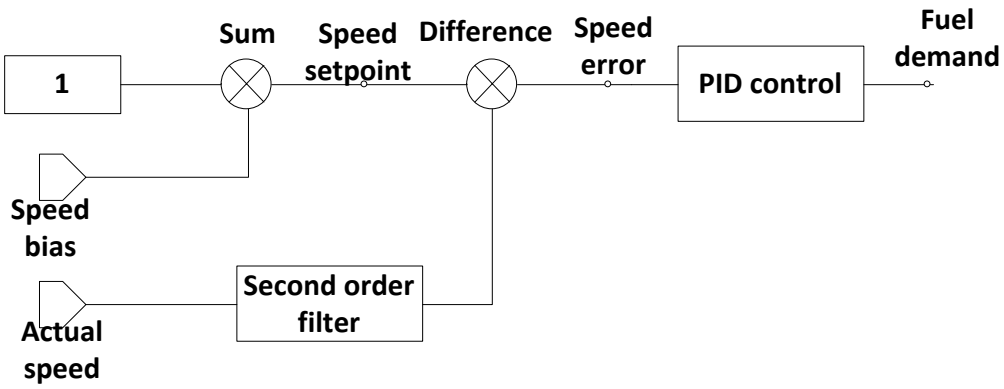

Fig. 4.2 Diesel governor modeled in PSCAD.

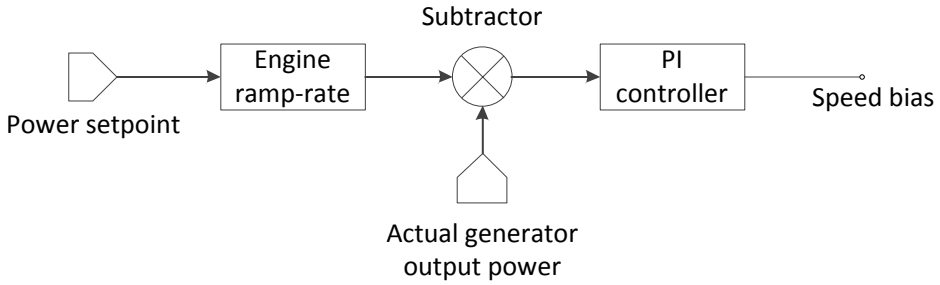

Fig. 4.3 Generator speed controller modeled in PSCAD.

- Turbocharger: The turbocharger increases the mass of air entering the engine, allowing more fuel to be combusted within the fixed displacement of the engine. The turbocharger's turbine stage is a centrifugal turbine powered from the exhaust of the engine. The turbine is coupled to a compressor at the air inlet passage. A simple turbocharger was modeled for all the engines. Fig. 4.4 shows the model of the turbocharger modeled in this work.

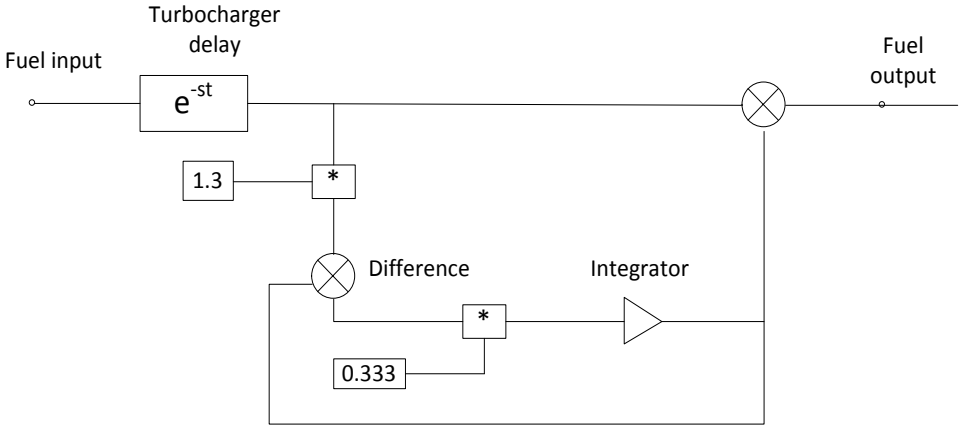

Fig. 4.4 Turbocharger model.

For microgrid applications, generators, in principle, can be operated in two modes:

- Base load operation, and
- Swing operation.

A base load machine reacts slowly to frequency disturbances – i.e. is operated with a low governor gain – and managed to maintain a power setpoint. The amount of load carried by the machine depends on the speed bias of the machine. The response of a typical base load machine is shown in Fig. 4.4. An isochronous machine, also known as a swing machine, reacts quickly to frequency disturbances – i.e. it is operated with a high governor gain. The swing machine changes its output to follow the load variations in order to maintain its speed and hence the frequency of the microgrid. To minimize frequency excursions, swing machines must be fast acting machines, and must be operated at a load level that provides sufficient capacity to react to a sudden load addition or loss in the system. The typical response of an isochronous is shown in Fig. 4.4.

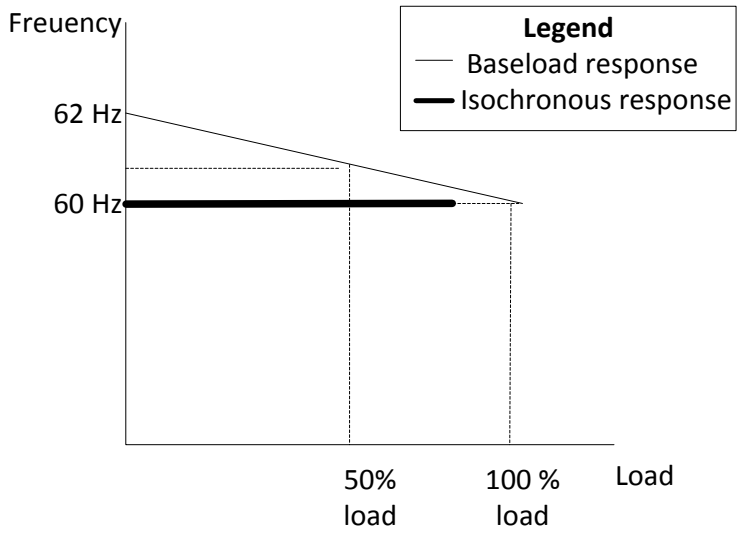

Fig. 4.5 Load-frequency characteristics of a base load and isochronous machine [79].

4.3 Loads

The local loads of the notional microgrid were ranked based on critical and non-critical operation. Critical loads are those that have the highest priority and must be powered as soon as possible following a loss of grid supply. Non-critical loads are defined as lower-priority loads that can be powered after the

critical loads are serviced. Non-critical loads may remain turned off in islanded operation of the microgrid if there is insufficient generation to supply these loads. As shown in Fig. 4.1, loads in the microgrid are distributed. Some portions of the load are controllable through the use of Building Energy Management (BEM) systems. BEM systems are normally used to control building mechanical and electrical systems. Controls in the building adjust the temperature and lighting based on current measurements, user preferences and historical energy usage patterns. Loads on feeder 1 have the highest priority, followed by loads on feeder 2, 3 and 4 in the order of decreasing priority. In this work, critical and non-critical loads are identified based on the feeder in which the load is connected. Loads in the microgrid studied in this work are modeled as lumped loads. A lumped load model means that all the loads on a particular feeder are lumped together without considering the effects of individual loads. Loads can be modeled as distributed loads or lumped loads based on the length of the line, ratio of the inductive line impedance of the line to the resistance of the line (also known as the X/R ratio), and the wavelength of the signal on the line. The microgrid under study had power lines of length under 2 km. Transmission lines are classified as short, medium or long based on the length of the line. Short transmission lines have length less than 80 km, medium transmission lines have length between 80 and 240 km and long transmission lines have length above 240 km. The effect of shunt capacitance and conductance are neglected for short transmission lines. Hence, the signal (power) does not undergo much change when travelling from source to load on short lines. Conclusions can be drawn based on the above arguments that the system consists of short transmission lines with loads that can be modeled as lumped loads.

4.4 Transformers

The notional microgrid studied in this thesis consisted of a distribution system that connected the generators to the loads. Transformers were used to step up and step down voltages at the generators and loads respectively. The presence of transformers complicates the blackstart operation. A transformer must be one of the first devices that must be turned on during a blackstart operation [71]. This is because the transformer provides the ground reference that is required to turn on other loads or generators in the microgrid. Transformers are highly inductive devices and have low resistance. Such a design is required

since transformers are widely present in transmission and distribution systems, and must not dissipate excessive power due to heat losses as a result of high resistance. Larger transformers have lower resistances. This creates a problem on inrush current when the transformer is turned on from a de-energized state. When the transformer is supplied from a de-energized state, as is the case during a blackstart operation, a very high current, known as inrush current, flows from the generator. This current value is very large as the only resistance encountered by the current is that of the coil resistance of the transformer, which is very low. In island operation, the inrush current must be serviced by the local generators, which have a much smaller current-carrying capacity than the grid. As a result, the inrush current is typically smaller and more sustained than in grid-connected operation, and may cause a larger voltage or frequency transients. Since this behavior is significantly different in island, versus grid-connected, operation, some protection devices will classify the inrush as a fault and could trip one or more breakers during black start operation. Hence, the protection system must be adjusted during startup operations [80].

Another problem is associated with the transformers in microgrids. As mentioned, transformers must be one of the first devices that must be turned on in the blackstart sequence of operations. Rotating machines, such as diesel engines, are capable of sustaining the large inrush currents associated with initial excitation of a transformer. But, power sources that do not have rotating parts, such as PVs and battery storage, have no inertia to ride through the large inrush currents. Hence, a transformer that is initially excited using a static power source may cause permanent damage to the power electronics interface that couples the power source to the system. Since the robust construction and larger inertia make them capable of riding through inrush currents, rotating generators would be an ideal fit for this purpose, in microgrids.

4.5 PID controller

The PID controller is one of the most widely used controllers in industrial control systems [81]. The main characteristics that make PID the most preferred controller are:

- General applicability to most control systems, even when the mathematical model of the controller is not known,
- The values of the controller gains can be tuned on-site based on the environment in which the controller is placed, and
- Some PID controllers can be tuned automatically using on-line tuning capabilities [81].

As shown in Fig. 4.5, the PID loop consists of three components: the proportional controller, the integral controller, and the differential controller with $K_p, K_i, and\ K_d$ as the respective gains.

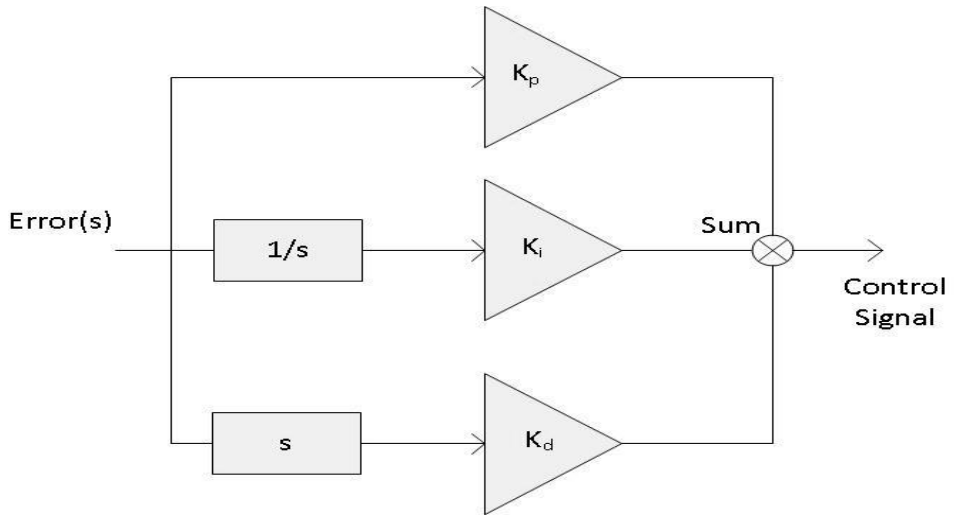

Fig. 4.6 A general PID control system.

The output of the proportional controller is only dependent on the value of the error signal. The speed of response of the system can be increased by increasing the value of the proportional multiplier [81]. But increasing the value of the proportional controller can cause the system to oscillate and become unstable.

The output of the integral controller is the sum of error term over a time period [81]. Hence, the output of the integral controller will continue to increase, unless the error term equals zero. This forces the steady state error of the system to zero. The output of the integral control could saturate, causing a steady state error to persist in the system for long periods [81]. Therefore, practical PID controllers contain additional elements to prevent saturation and over-shoot of the integral control term.

The output of the differential controller depends on the rate of change of the error term. A large derivative term results in a sharp increase in the output of the derivative controller for a small, but rapid, change in the error term. Most control systems have a very small or no derivative controller, since a mismatched output of the derivative controller could easily cause the system to slip into instability and oscillate [81]. A very sensitive derivative controller will also be unsuitable in a noisy environment, as derivatives tend to amplify high-frequency noise components. The proportional (K_p), integral (K_i) and differential (K_d) gains can be obtained using the one of the two Zeigler-Nicholas techniques [81].

4.5.1 First method

In this technique, the unit-step response of the system is first obtained. The presence of an integrator in the system causes an S-shaped system response as shown in Fig. 4.6. The delay time *L*, and the time constant *T* are determined by drawing a tangent at the inflection point as shown in Fig. 4.7. The values of K_p, K_i, and K_d can be obtained using table 4.3. Table 4.3 is directly reproduced from [81].

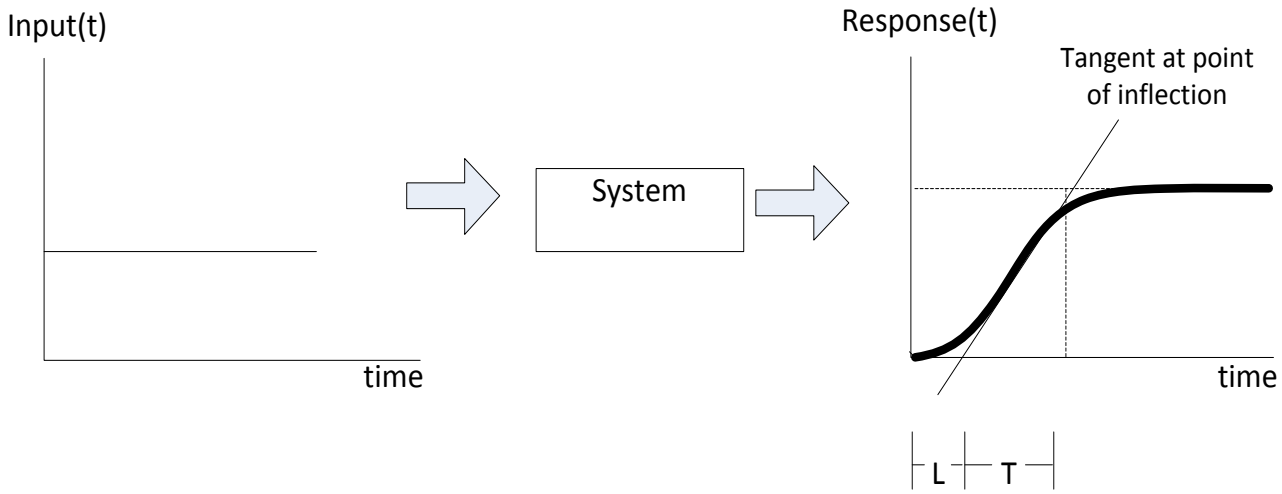

Fig. 4.7 First Ziegler-Nicholas method.

Table 4.3 PID values based on step response of system.

Proportional gain (K_p)	**Integral gain (K_i)**	**Differential gain (K_d)**
$0.5 * T/L$	$2 * L$	$0.5 * L$

4.5.2 Second method

In the second Zeigler-Nicholas method the integral and differential gains are initially set to zero and the proportional gain is increased until the system begins to oscillate. This gain value at which the system beings to oscillate is known as the critical gain (K_c) and the period of oscillation is (P_c) [81]. This is shown in Fig. 4.7. The values of proportional gain (K_p), integral gain (K_i), and differential gain (K_d) are then obtained directly using the table 4.4. Table 4.4 is directly reproduced from [81].

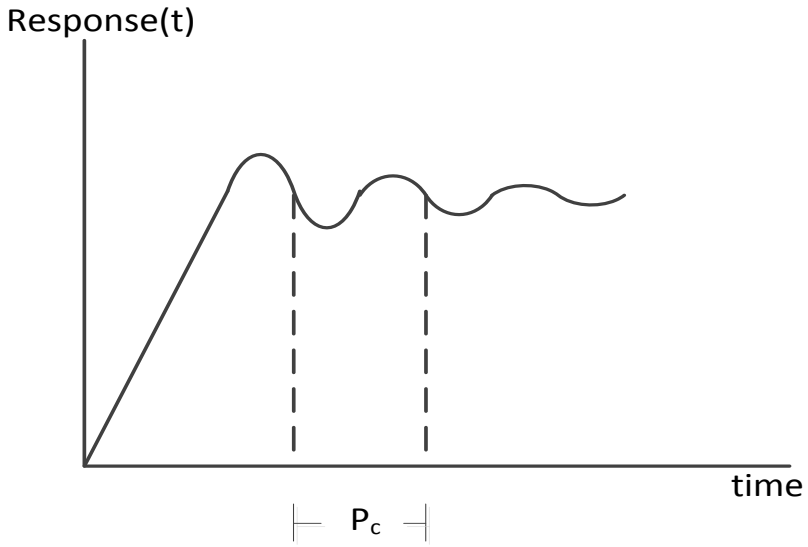

Fig. 4.8 Second Ziegler-Nicholas method.

Table 4.4 Second Ziegler-Nicholas method for obtaining PID gains.

Proportional gain (K_p)	**Integral gain (K_i)**	**Differential gain (K_d)**
0.6*K_c	0.5*P_c	P_c/8

In this thesis work, the second Zeigler-Nicholas method is used. The method is supplemented by a trial-and-error technique to tune the gain values of the controller. Table 4.5 presents the observed values of P_c and, derived values of K_p, K_i, and K_d for the governor blocks of the diesel and NG generator after tuning the values.

Table 4.5 PID gains of diesel and NG governor.

Generator	Observed P_c	Proportional gain (K_p)	Integral gain (K_i)	Differential gain (K_d)
Diesel	7.768	5.0	0.4	1
NG	5.69	1	0.5	0.7

4.6 Blackstart sequence

In the notional microgrid studied here, the largest disturbances are encountered as breakers are closed during blackstart, and during certain fault conditions which are similar in magnitude to the blackstart events, such as loss of a generation unit or a loaded feeder. It is of interest to microgrid designers and operators to understand and minimize the disturbances caused by these major events. In particular, an understanding of transients and disturbances is required to program protection devices for operation in island mode. These devices are typically programmed to sense voltage, current and frequency excursions, and programmed protection compare both the magnitude and duration of disturbances to expected values to identify fault conditions.

In this work the microgrid is assumed to have separated from the grid due to loss of grid supply or a sufficiently large disturbance on the grid. At this point the microgrid is islanded by opening all ties to the grid and all internal feeder breakers. It is assumed that all generators are disconnected and power down as well, either because they were not currently operational or because they tripped off during the islanding operation.

The following generator configurations were studied to find the blackstart sequence with the highest reliability, as defined above. These configurations were chosen considering both load and maximum deviations in voltage and frequency for the machines.

Case 1: 3 diesel generators

Case 2: 2 diesel, 1 natural gas (NG) generator

Case 3: 2 diesel, 2 biomass generators

Case 4: 3 natural gas generators

Case 1 is the most common case utilized for standby generation, and is included here as the benchmark for all other studies. Diesel engines are typically favored for standby generation, due to low installation and maintenance costs and their ability to quickly respond to disturbances. Diesel fuel is typically more expensive on a per-unit output basis than natural gas or biogas. All other test cases will be compared against the performance of Case 1.

Case 2 considers the case where a natural gas CHP plant is present in the microgrid and microgrid is operated by running the gas engine in combination with the diesel engines. For this case, we assume all engines are similarly sized at ~ 2MW. Therefore, all load in the microgrid can be carried by three machines.

Case 3 studies the possibility of utilizing biogas engines producing approximately the same output as the natural gas engine in Case 2. Since biogas as a lower volumetric energy density than natural gas, output per engine is reduced from 2 MW to approximately 1.6 MW. Therefore, four machines are required to service the entire microgrid load.

Case 1-3 include the same diesel configuration, which always configured as in isochronous load sharing as the swing machine on the microgrid. Deviations in performance between these cases are therefore attributable to the 3rd (Cases 1 & 2) or the 3rd and 4th (Case 3) machine added to the generation mix.

Case 4 checks the feasibility of operating the microgrid utilizing only natural gas gensets, operating in isochronous load sharing as the swing machine. Since natural gas gensets have significantly different operational characteristics than diesels, as noted above, this test case provides a reality check on whether gas gensets are sufficient for island operation. While biogas gensets and natural gas gensets have similar performance characteristics operating under baseload control, biogas machines are typically restricted to narrow operating ranges and cannot vary load sufficiently support the necessary load swings seen in island operation. Therefore, while the response characteristics of natural gas and biogas machines may be similar, only natural gas machines can typically be operated as swing machines – and then only

with special considerations to prevent unstable combustion (e.g. knock), increased emissions or other problems.

The blackstart sequence described in [74] was modified and engineered for this microgrid. Fig. 4.8 describes the sequence of steps that are followed in the blackstart operation in the notional microgrid.

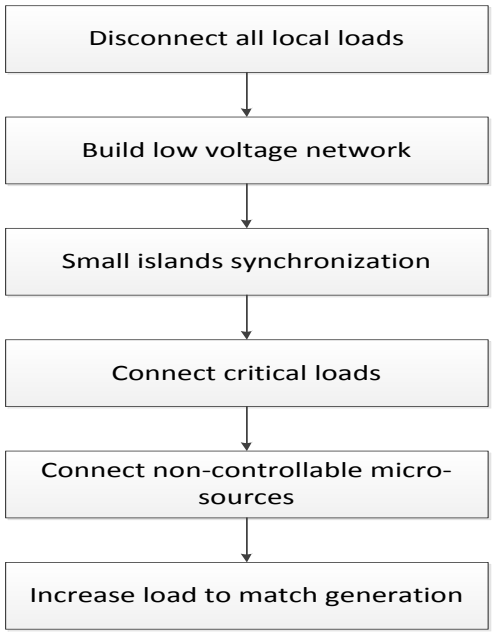

Fig. 4.9 Sequence of steps followed in blackstart operation.

While governors and voltage regulators on gensets respond directly to disturbances, overall operation of the microgrid are managed by a control system known as a supervisory control system. Supervisory controls include an array of sensors and actuators that feed information regarding the health of the main grid, the health of the various generators in the microgrid, load profile in the microgrid, breaker information for loads and generators, information on non-controllable micro-sources (PV and wind) etc. The health of a generator unit can generally be assessed based on the fuel availability, current status of the generator in-case it was taken offline for maintenance, engine temperature etc. Uncontrolled micro-sources were not separately tracked for this study, and are considered – in effect – as negative loads which modify load profiles extracted from historical data.

Information inputs to the supervisor are updated continuously, often in real time, but more typically with delays of milliseconds to seconds. Supervisory control systems are generally not fully

autonomous and, in reality, provide an assisted human interface for human control. Some systems are also capable of getting real-time electricity pricing of the main grid and the microgrid [82]. If real-time pricing information is available, the supervisor is capable of deciding if the economic benefit of purchasing power from the grid for supplying local loads or running generators in the microgrid to supply the local loads. If the supervisor calculates it is less expensive to produce power from local resources, the system will provide the operator an option to offset local loads within the microgrid. The supervisory control system assists the operator in performing the following steps to initiate a blackstart on this microgrid:

- Disconnect all loads: In response to sensing a disturbance on the main grid, the supervisory control system sends a command to open the 13.6 kV breaker that connects the microgrid to the main grid. Simultaneously, the system also sends commands to open all feeder breakers. The microgrid is now in a black state with no generation or load connected. All simulations in this work start from this state.
- Reconfigure protection devices: Once the loads are disconnected and the microgrid is islanded, the protection devices must be reconfigured to handle potentially the larger and longer voltage and frequency disturbances described above. This step is required for small microgrids that have tightly coupled devices due to the low generation inertia relative to the size of expected load steps. In larger microgrids with larger relative generation inertia, this step may not be required.
- Built low voltage (LV) network: Next, the supervisory control system starts the swing machine – in reality a group of gensets operating in isochronous load sharing mode. The isochronous load controller manages the start of the machines, inter-machine synchronization, and closes the generation stations' breaker to connect the machines to the microgrid circuits. A full load controller was not implemented for this study. To emulate this behavior, the all generators in the swing machine group are started at 0.5 seconds after start of simulation, and are connected to the microgrid ciruits 5 seconds after the start of the simulation.

- Connect Loads: Loads are added to the system in an order based on the priority of the load. Since loads are lumped on a feeder based on the priority of the feeder, load feeders are closed in an order based on the priority of the feeder. Load feeders are added in a sequence that ensures that the generators, currently online, are not overloaded.
- Systematically add generators and load: Once the system frequency and voltage stabilize, the supervisory control adds loads and base load machines as required.

The following sections discuss each of the test cases included in this study, including step loading and unloading tests.

4.6.1 3 Diesel generators

In this configuration, all three diesel generators are brought online in a isochronous load-sharing group as the swing machine, and the loads are added in order of priority. Since the most critical loads of the notional microgrid are on the highest priority feeder, this feeder also has the largest load. Fig. 4.9, 4.10 and 4.11 show the step response of the generator configuration.

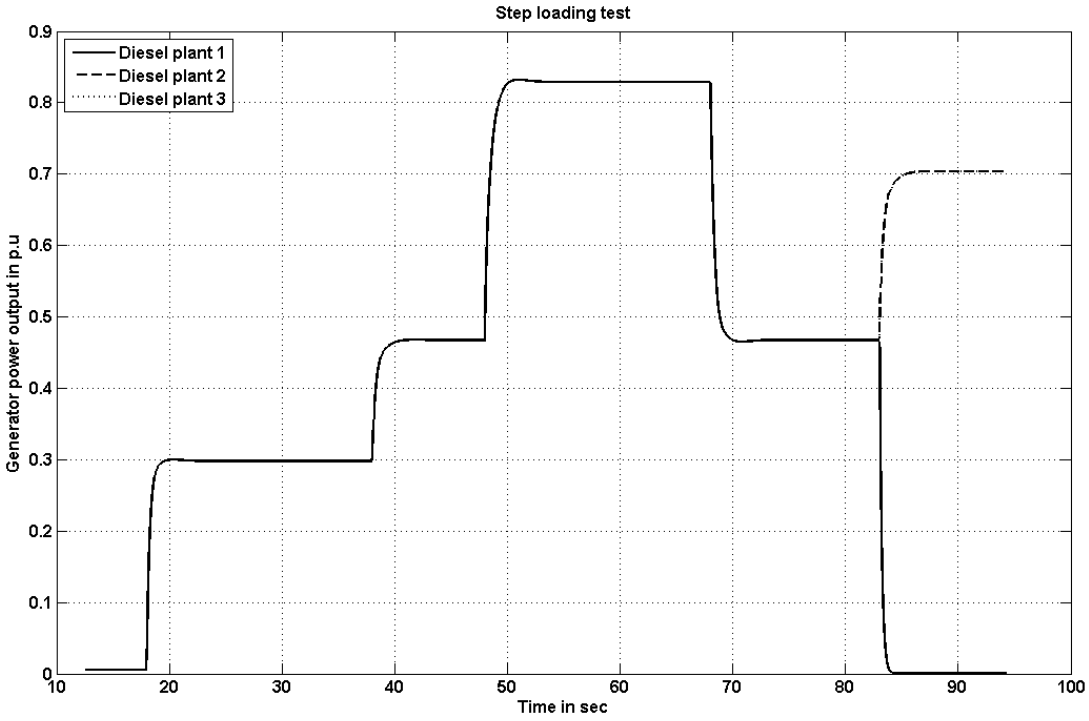

Fig. 4.10 Output power of generators for step loading test.

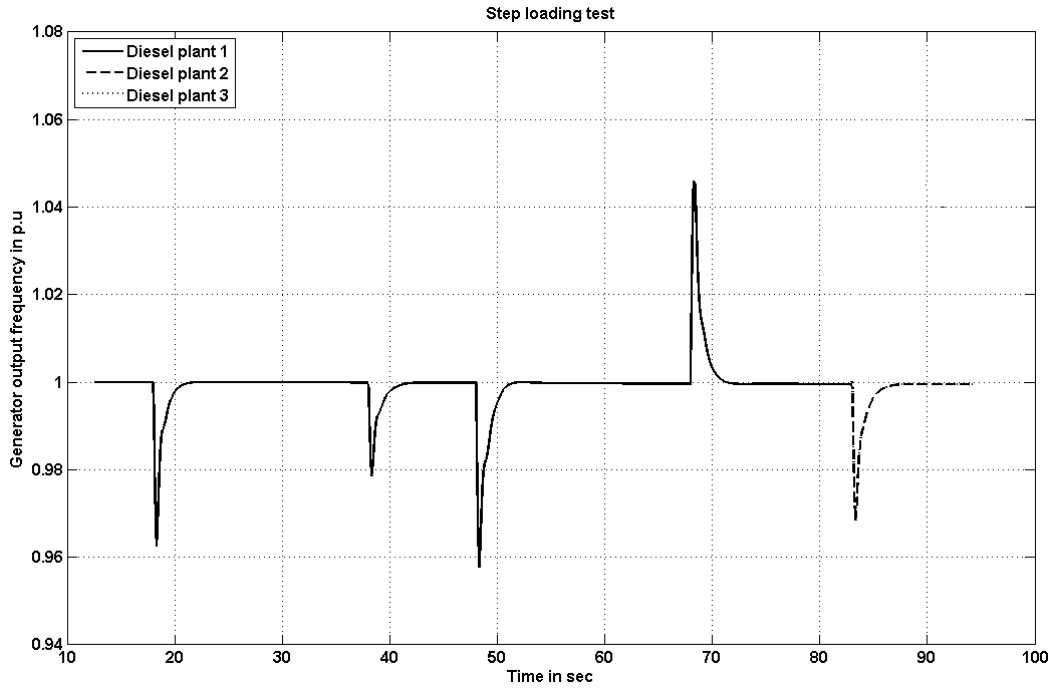

Fig. 4.11 Output frequency response of 3Diesel generator step load test.

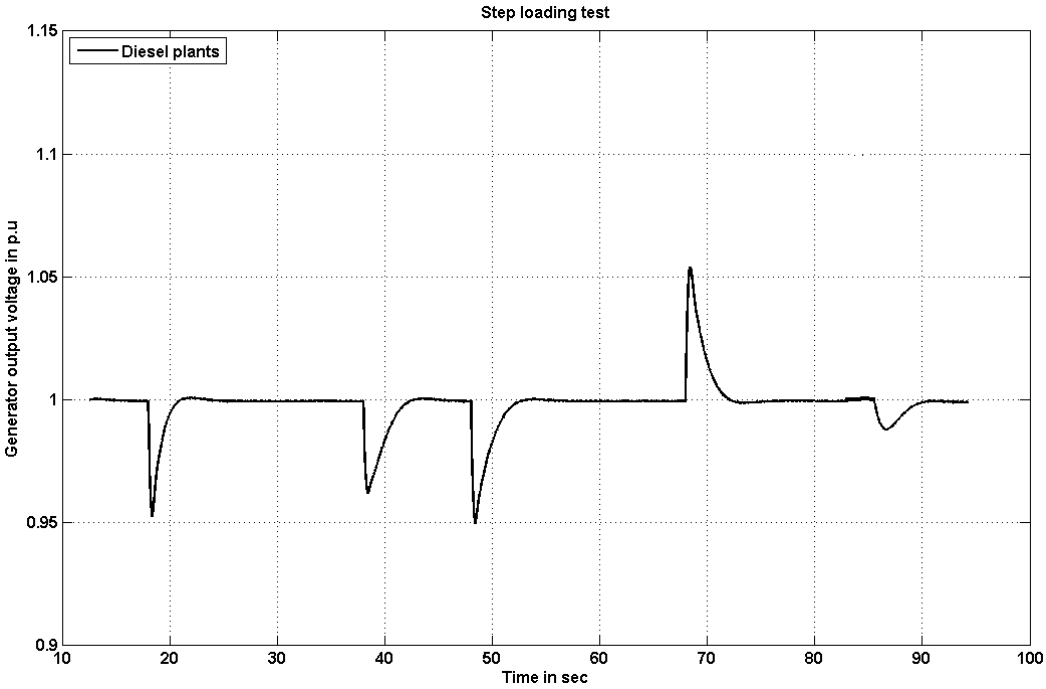

Fig. 4.12 Output voltage response of 3Diesel generator step load test.

- All diesel generators are turned on at 0.5 seconds, and are in idle state.
- At t = 5 sec, the generators are connected to the generator bus, and service a small parasitic plant load.

- At t = 18 sec, feeder 1 is connected to the load bus, to connect the highest priority load.
- Feeders 2 and 3 are added at t = 40 sec and t = 50 sec respectively. The frequency and voltage deviations due to addition of these loads can be observed in Fig. 4.10 and 4.11 respectively. Frequency and voltage depict a negative deviation on addition of load, since the system experiences a condition where generation is less than load for the brief period before the generators react to the deviation. As observed in Fig. 4.10, the machines are now running at over 85% of the maximum capacity of the machines. Hence, feeder 4 is not brought online in-order to prevent overloading of machines. Sustained overloading can cause overheating of machine components, and reduced life of the machine.
- At t = 70 sec, the largest feeder in the system is opened, to simulate loss of the largest load that is likely with a single-point failure – i.e. unexpected opening of the feeder 1 breaker. Analogous to the load addition case, the system now experiences a condition where generation is in excess to the load. Hence, the frequency and voltage of the system increase as shown in Fig. 4.10 and 4.11 respectively. The frequency swell is observed as an error by the governor of the machines, which quickly reduce the torque output of the engines, in order to reduce the speed of rotation of the generators, and match the new load.
- At t = 85 sec, a generator breaker is opened to simulate loss of generation. This again results in a condition where the load is in excess as compared to the generation, and hence, the governors of the engines react accordingly. The load is now shared by only two machines, and hence the output powers of the machines increase, as observed in Fig. 4.9.

In this discussion, it is important to note that the gensets are clustered into groups equipped with load controllers that cause the individual machines to react together, as if they were a single generation unit. Behavior of the load controllers was not modeled in detail, but is based upon the response characteristics of Woodward™ load controllers such as the DSLC™, EasyGen™ and EGCP3™ controllers.

4.6.2 2 Diesel 1 NG machine

In this test case, a natural gas genset replaces one diesel. Gas machines have a slower response than diesels, due to a longer fuel flow path that results in a significant delay between a change in fuel input and power output. For the engines modeled, the fuel-air mixture travels approximately 2 meters between the fuel inlet and engine cylinder [82] resulting in a command-to-power delay of 175-225 ms, compared to a similar delay in a diesel engine of 17-20 ms. Due to these delays, a gas engine will react significantly slower than a diesel engine. Therefore, in the presence of a mixed diesel-gas system, the diesel engines are typically operated in isochronous load sharing as the swing machine, while the gas engine is operated in baseload machine, with its real and reactive power setpoints determined by the supervisory control system.

As in Case 1, the system is loaded in steps, starting from the highest priority feeder. Fig. 4.12, 4.13 and 4.14 describe the system response to a step loading test.

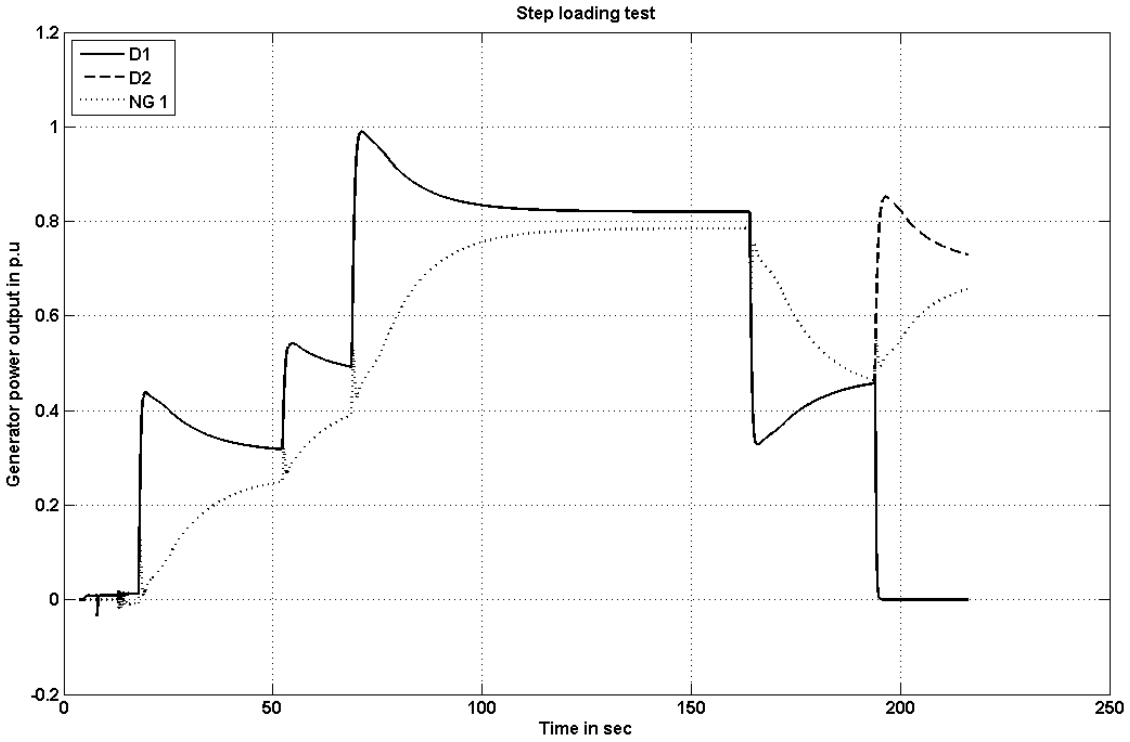

Fig. 4.13 Output power response of 2 Diesel 1 NG generator step load test.

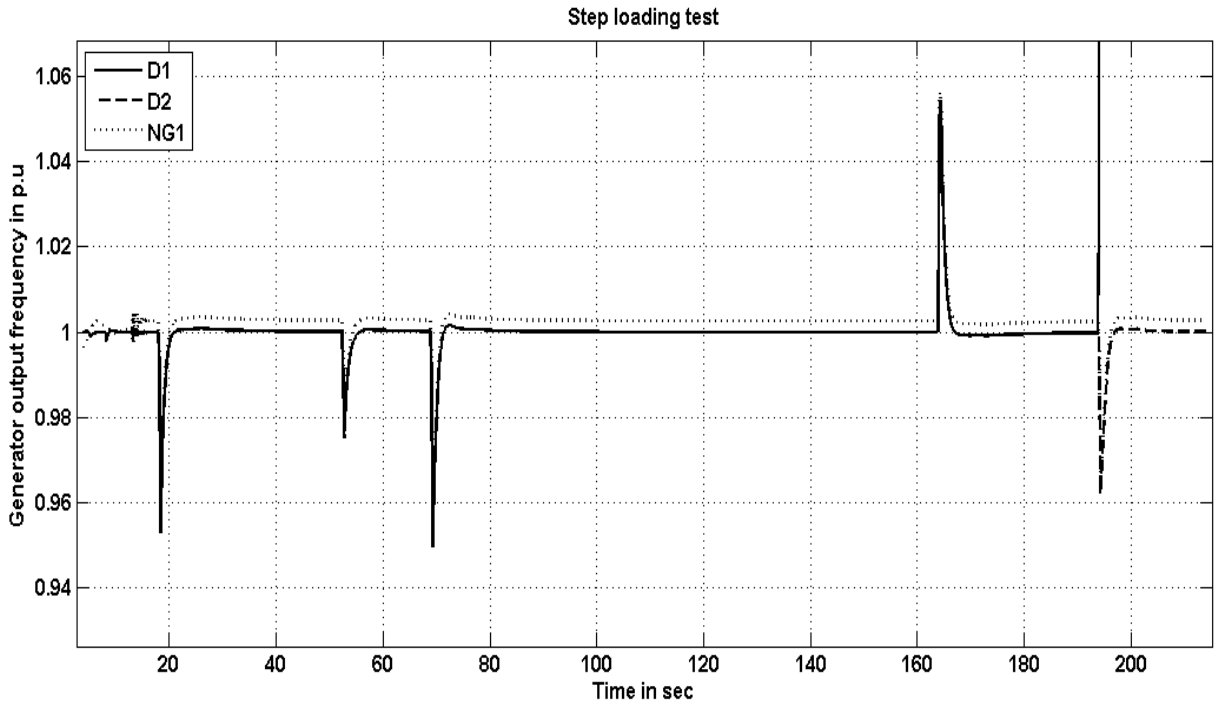

Fig. 4.14 Output frequency response of 2 Diesel 1 NG generator step load test.

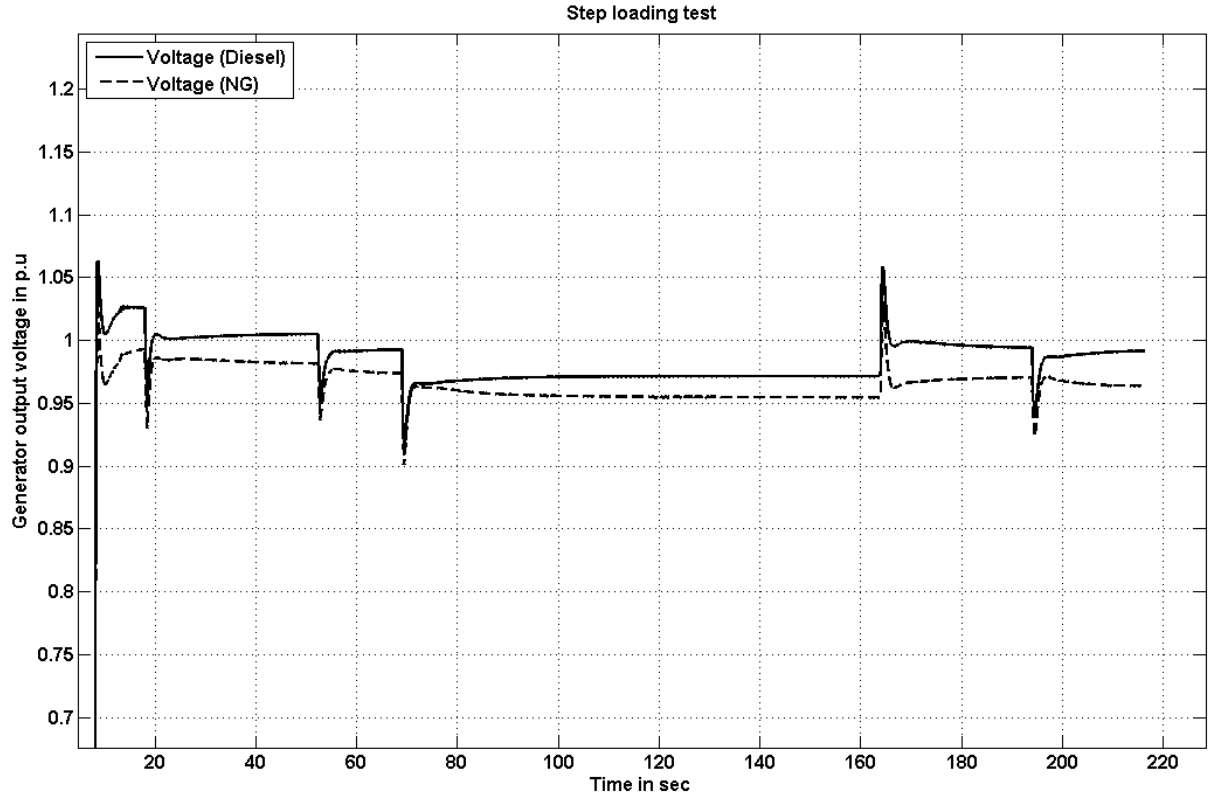

Fig. 4.15 Output voltage response of 2 Diesel 1 NG generator step load test.

- At time t = 0.5 sec all machines are turned on and brought to a stable idle state.
- At t = 5 sec, the machines are connected to the microgrid and service parasitic plant loads.
- At t = 20 sec, feeder 1 is connected to the system. As can be noticed in Fig. 4.12, the diesel machines respond first load addition, while the baseload machine returns to its baseload setpoint after a small inertial deviation when the load was added. The supervisor control then changes the baseload setpoint, and the baseload machine steadily ramps toward that setpoint. As observed in Fig. 4. 13 and 4.14, the frequency disturbances are larger than Case 1, the 3 diesel system. In this case load step is picked up primarily by the two fast responding machines (the diesels), while the relatively slow baseload machine (the NG machine) does not immediately pick up load. Since the diesels provide most of the disturbance response and there are only two diesels in this case, versus three in Case 1, voltage and frequency deviations are larger. In contrast, voltage deviations are nearly the same as Case 1 due to fast action of all voltage regulators, including the regulator on the NG machine. The response time of the regulator is largely independent of the governor dynamics of the engine.
- Feeders 2 and 3 are added at t = 50 sec and t = 70 sec respectively. The voltage and frequency deviations are observed in Fig. 4.13 and 4.14 respectively. While the frequency deviates by 3% and 5% respectively, the voltage shows a deviation of over 10% at t = 70 sec.
- At t = 160 sec, the largest load feeder in the system is opened to simulate a loss of load. As observed in Fig. 4.13 and 4.14, this causes both voltage and frequency swells in the system. Fig. 4.12 shows the power output response of the generators. The diesel machines respond almost instantly to the load change, while the NG machine, operating as a baseload machine, responds slowly to set-point changes (approximately 29 seconds).
- At t = 190 sec, the breaker of a diesel generator is opened, to simulate the loss of generation. The other diesel generator that is still online, responds by increasing its power output quickly while the NG machine responds slowly, and increases the power output over 30 seconds

while unloading the diesel machine. The large frequency deviation observed is again attributed to the slow response of the base load NG machine.

4.6.3 2 Diesel 2 Biomass machines

The biomass machines are modeled similarly to the NG machines with the difference that they have lower output power. A very specific requirement in the notional microgrid studied in this work was that the biomass machines must be operated between 87% and 100% of rated capacity to avoid undesirable combustion issues. The operating sequence of this case is somewhat different than the sequence utilized for Cases 1 and 2. Fig. 4.15, 4.16 and 4.17 describe the step responses of this machine configuration.

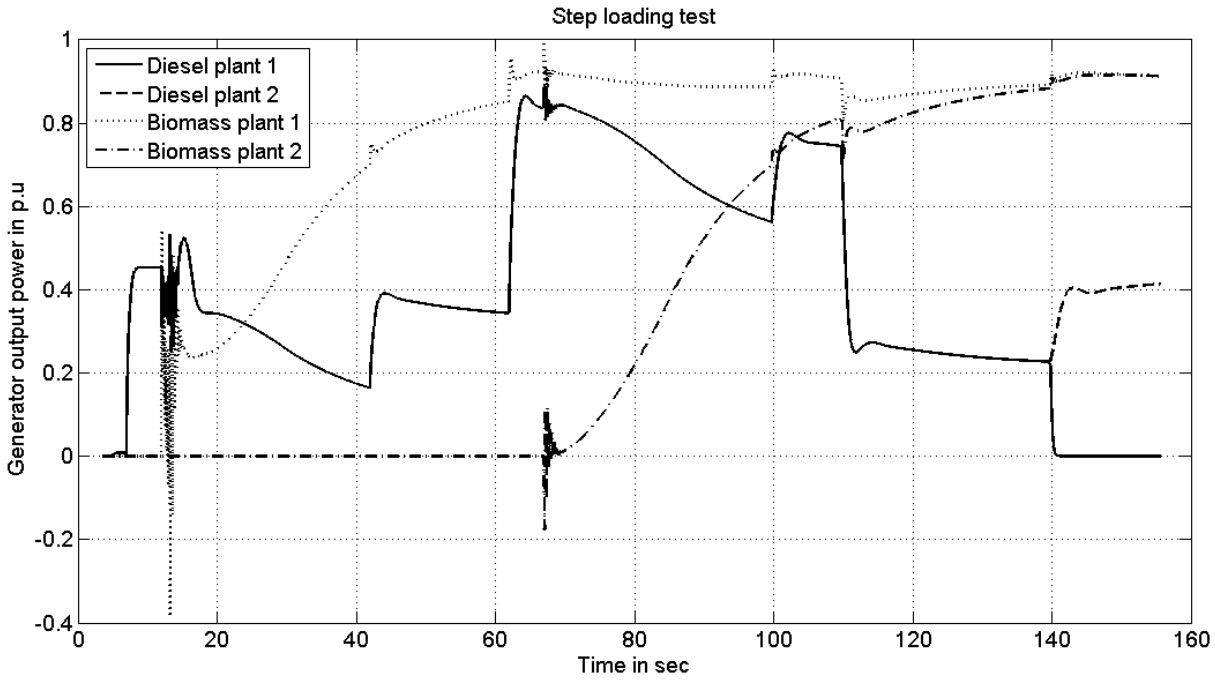

Fig. 4.16 Output power response of 2 Diesel 2 Biomass generator step load test.

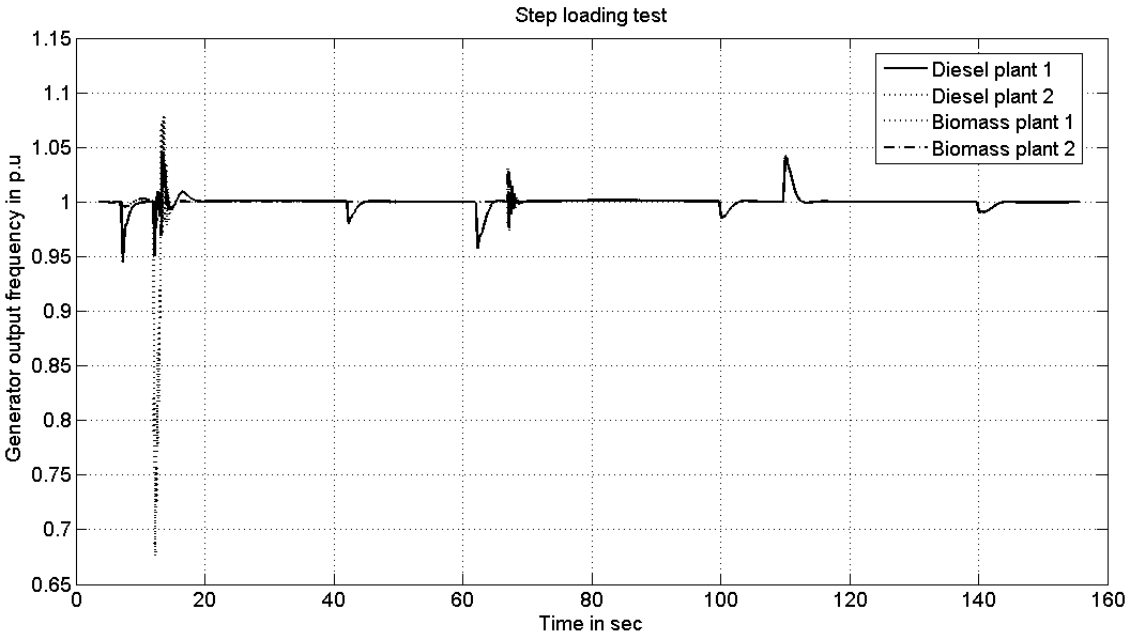

Fig. 4.17 Output frequency response of 2 Diesel 2 Biomass generator step load test.

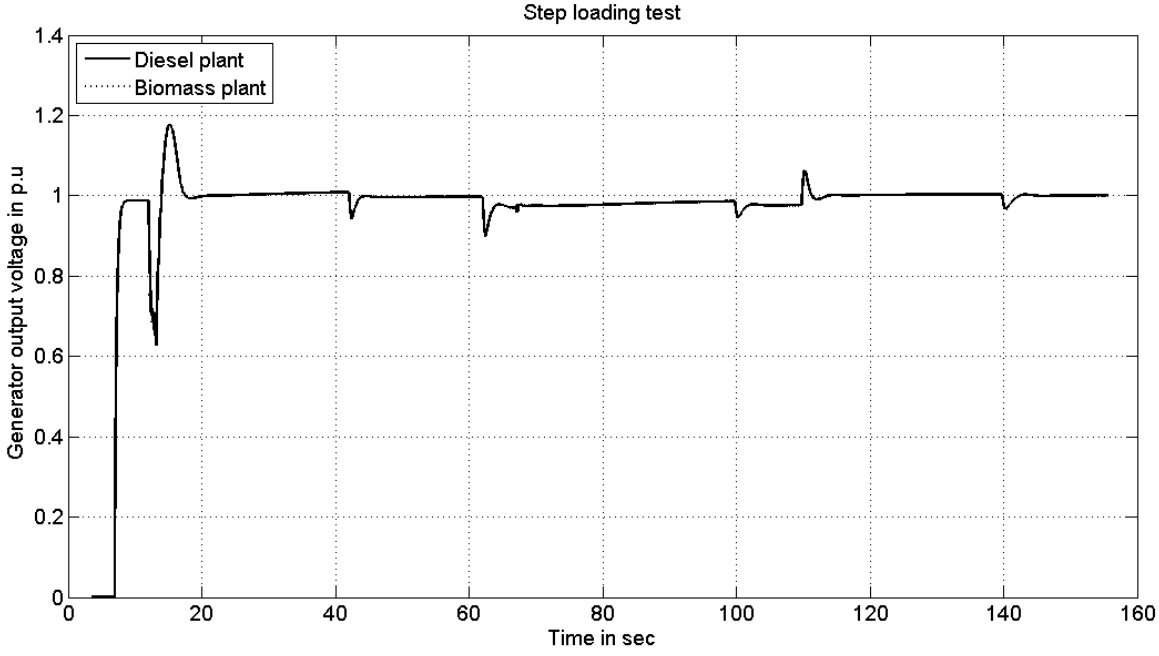

Fig. 4.18 Output voltage response of 2 Diesel 2 Biomass generator step load test.

- At t = 0.5 sec, all machines are turned on and are in idle state. This is a simplification to reduce the simulation time. In an actual implementation, the biogas machines would not be started until required to carry load.
- At t = 5 sec, diesel machines are connected to the generator bus, and supplies parasitic loads. At t = 7 sec Feed_Load_P1 is connected to the load bus, and is supplied by the generators that are online.
- At t = 15 sec, the biomass generator is connected to the generator bus. Connection transients can be observed in Fig. 4.16 and 4.17. The synchronizer is not modeled in this analysis, to reduce modeling complexity, and the connection transient is hence not representative of the actual operation. PSCAD automatically synchronizes the out of sequence components, and quickly restores stability on the bus. The starting transients are permitted to settle prior to proceeding with the test. After the transient settles, the biomass generator set-point is adjusted to ramp-up towards 88% of its capacity.
- At t = 40 and t = 60 sec, loads Feed_Load_P2 and Feed_Load_P3 are added. The frequency and voltage transients are observed in Fig. 4.16 and 4.17 respectively. The voltage and frequency deviations are similar to Fig. 4.13 and 4.14 respectively, since the system configuration is similar. As explained earlier, the biomass generator is modeled similar to the NG generator.
- At t = 65 sec, the second biomass generator is turned on. As before, the initial transients are ignored, as it is largely composed of synchronization transients. The second biomass generator is also ramped up to 88% of its rated capacity, due to the operational constraint.
- At t = 95 sec, Feed_Load_P4 is connected to the load bus. While the diesel generators quickly ramp to supply the load, it is observed from Fig. 4.15 that the biomass generator whose output is at 88% of rated capacity does not participate much in supplying this additional load. This is because, the set-point value of the biomass generator, does not permit

it to deviate from the operating point. Momentarily, when the load change causes a drift in the frequency of the system, the set-point value of the base load machine (biomass generator) changes, causing the output of the machine to change. This is the cause of the small spike in the machine power during load changes. This frequency deviation is identified and corrected by the isochronous machines (diesels). The biomass generators participate minimally in responding to load changes, and hence, the voltage and frequency deviations are mainly due to the diesel generators. The second biomass generator has not reached the 88% operating point at this time, and continues to ramp-up its output.

- At t = 110 sec, Feed_Load_P3 is disconnected from the load bus, and the system responds by a large drop in the output of the diesel generators. The biomass generators respond by a small dip in the output power, which is quickly recovered in the next 5 seconds.
- After approximately 70 seconds, at t = 135 seconds, the second biomass generator finally reaches the operating set-point of 88% of rated capacity.
- At t = 140 sec, a diesel generator is disconnected from the generator bus, in order to simulate loss of generation. The other diesel generator that is online, ramps up to meet the deficiency in generation, while the biomass generators respond minimally, as expected.

4.7 3-NG machines

This system consists on only 3 NG machines. All three machines are configured in isochronous load sharing mode of operation. The machine responses are slower due to higher fuel command-to-combustion ratio, as explained earlier. On adjusting the gain of the controller, it is observed that the system frequency begins to oscillate at step loads, and takes longer duration to settle to set-point values. A step loading and unloading test is performed on the machines. The results of the tests are presented in Fig. 4.18, 4.19 and 4.20 respectively.

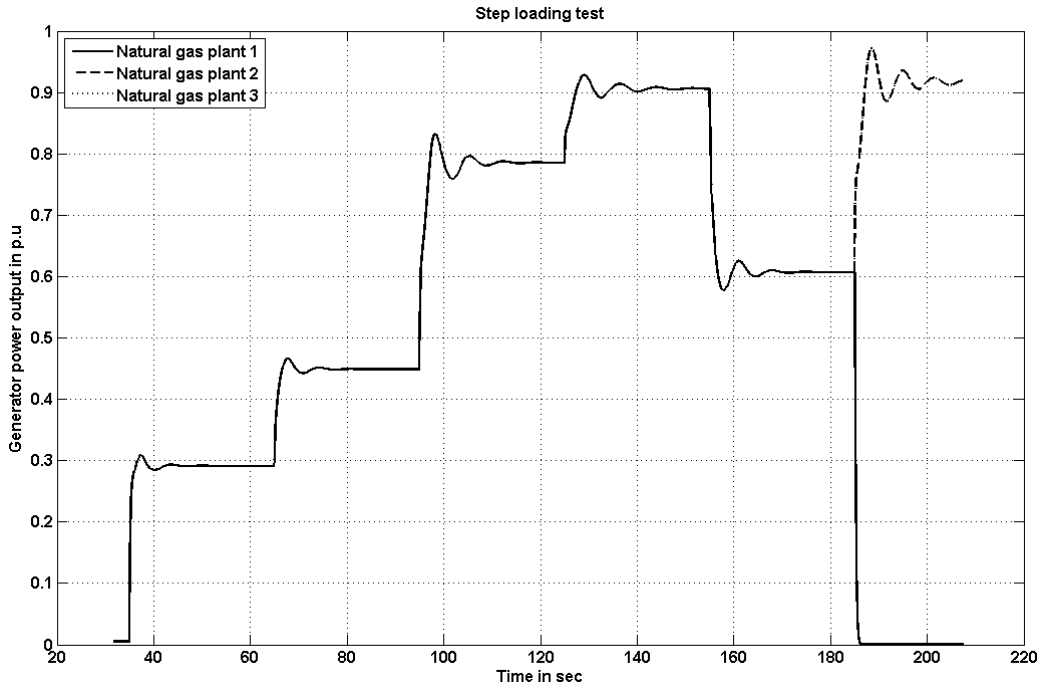

Fig. 4.19 Output power response of 3-NG generator step load test.

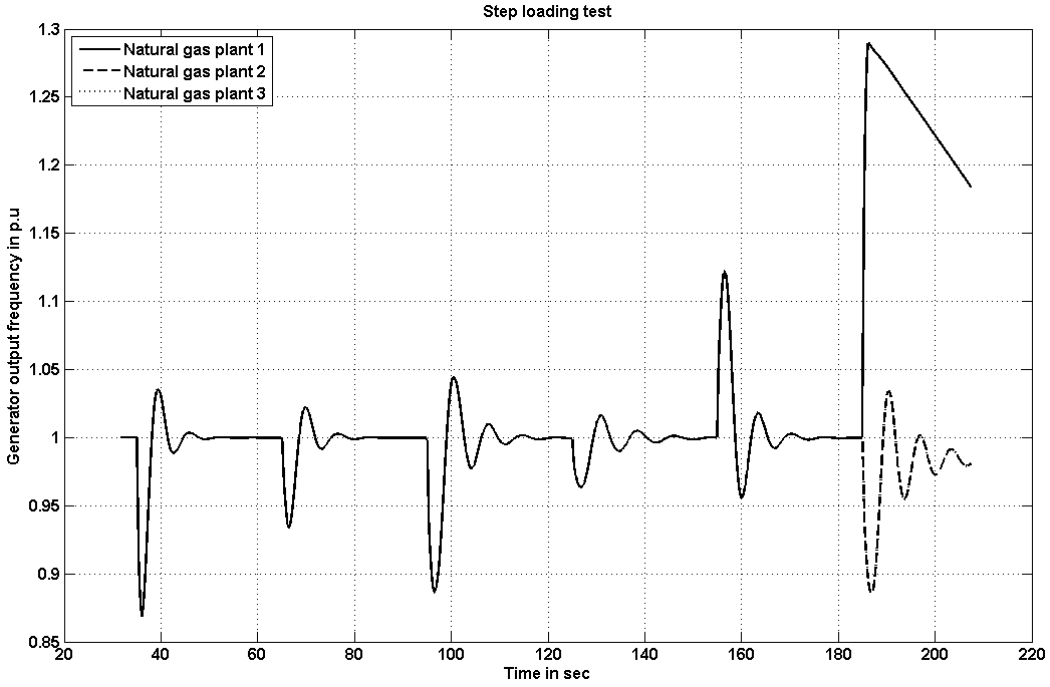

Fig. 4.20 Output frequency response of 3-NG generator step load test.

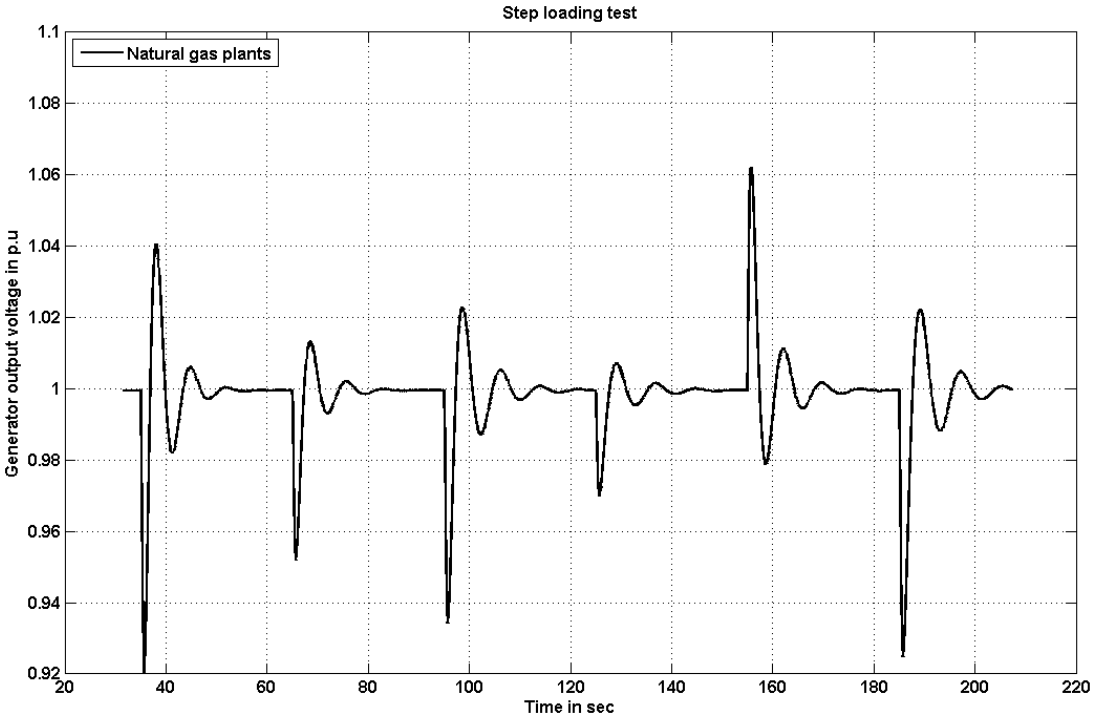

Fig. 4.21 Output voltage response of 3-NG generator step load test.

- At t = 0.5 seconds, all generators are turned on, and at t = 5 sec, the generators are connected to the generator bus to supply a parasitic load.
- Loads Feed_Load_P1, Feed_Load_P2, Feed_Load_P3 and Feed_Load_P4 are added successively at t = 35 sec, t = 65 sec, t = 95 sec, and t = 125 sec respectively. The frequency and voltage deviations are observed in Fig. 4.19 and 4.20 respectively. As expected, the system undergoes large voltage and frequency deviations, due to the slower response of the NG engines. Also, as can be seen in Fig. 4.19, the system frequency oscillates for approximately 15 seconds due to high gain values, as explained earlier. At t = 155 sec, the largest feeder in the system (Feed_Load_P3) is disconnected. Fig. 4.19 shows that the frequency deviation due to this loss of load is approximately 15%. Also, a 6% deviation is noticed in the voltage from Fig. 4.20.
- At t = 185 sec, an NG generator is disconnected to simulate loss of generation. In addition to voltage and frequency deviations, this also causes damped oscillations in the system.

The frequency and voltage deviations of the different generator configurations are summarized in Fig. 4.21 and 4.22 respectively. In the figures, testcases 1, 2, and 3 show addition of load feeders, testcase 4 depicts the deviation due to loss of a feeder, and testcase 5 depicts the deviation due to loss of a generation unit. Thus, the analyses only correspond to the dynamic response of the microgrid to expected load steps for different generator configurations. Also, the testcases present the worst case conditions during islanded mode of operation. It can be observed that the voltage and frequency deviation for the 3-Diesel machine configuration is the lowest. Quick response makes the diesel machine an ideal isochronous machine for microgrid operations. But this configuration does not use any of the available renewable resources, and hence will not be a recommended configuration in the microgrid. Relatively slower response of gas engines to load variation leads to larger frequency deviations in the system when used in a microgrid. The microgrid must be configured to be able to handle ± 10% load steps, as well as the deviations due to loss of the largest feeder and loss of a generation unit. Since loss of largest feeder causes up to 5 times greater deviation, sensitive equipment may be disconnected to this event. The study also shows that gas engines cannot be run alone in islanded mode of operation due to their slow response rate. At low loads, it is seen that the gas machines can carry the load, as long as voltage and frequency support is provided by as fast responding machine, such as the diesel machine. Voltage deviations depend on the response of the voltage regulator on each machine, and is unaffected by the presence or absence of a gas machine. Hence, the 2-Diesel 2-Biomass machine configuration is the next best choice, due to its relatively low voltage and frequency deviation characteristics. In this configuration, the diesels are configured in isochronous load sharing, hence providing quick response to load changes, and the gas engines are configured as base load machines.

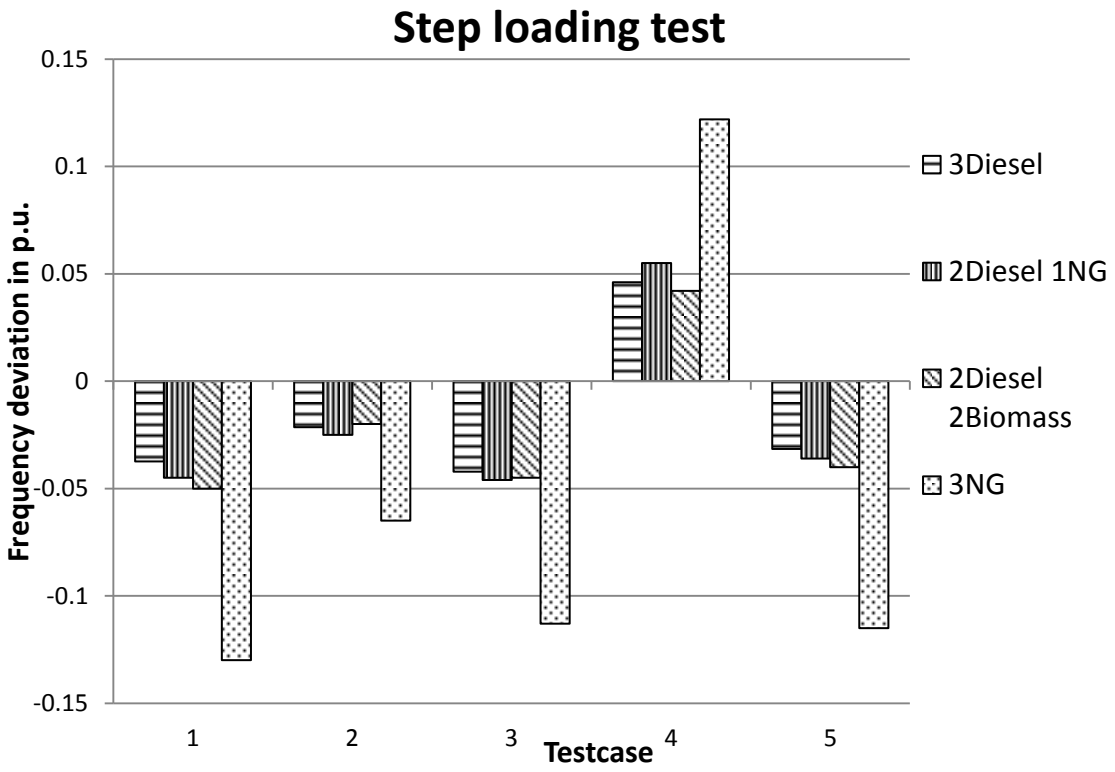

Fig. 4.22 Output frequency responses of all generator configurations.

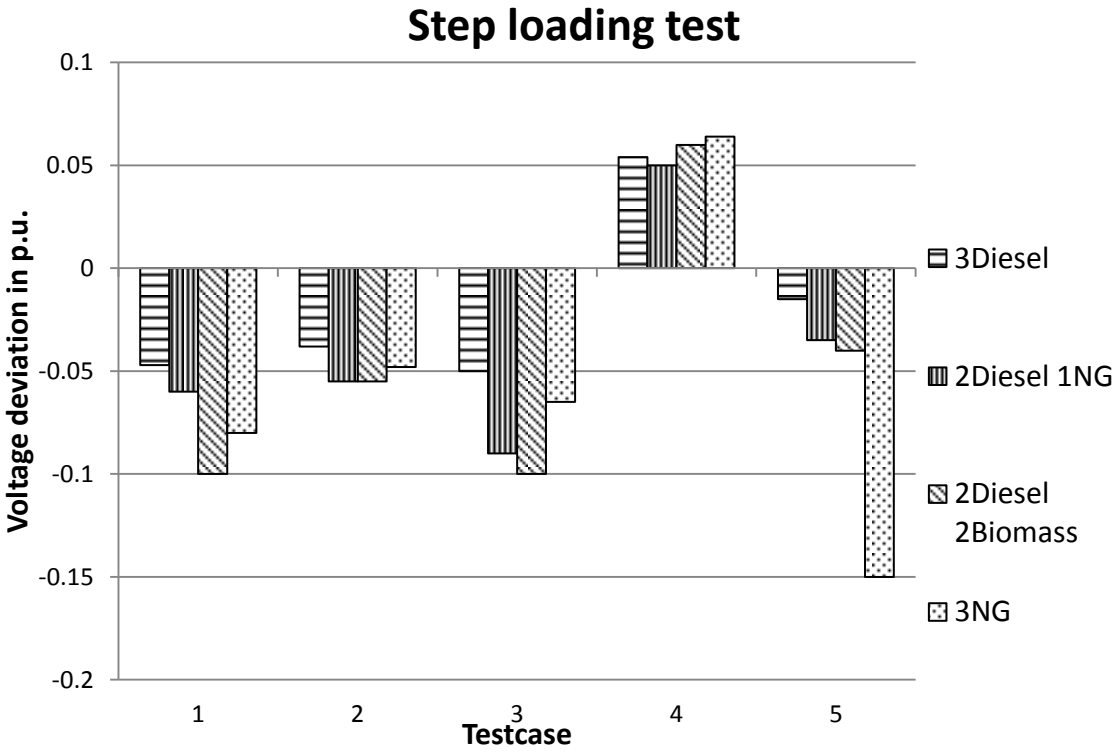

Fig. 4.23 Output voltage responses of all generator configurations.

As mentioned earlier, the machine configurations were chosen based on both load and observed deviations in voltage and frequency.

Hence the study concludes that, among the tested machine configurations, the 2-Diesel 2-Biomass and the 2-Diesel 1-NG generator configurations are the most favorable configuration due to two reasons: 1) it permits the use of renewable energy resources (biomass) and 2) due to relatively smaller deviations in frequency and voltage deviations at load steps. Large voltage and frequency deviations of the 3-NG model make it unsuitable for most applications. Greater deviations in voltage and frequency will require reprogramming of protection systems to avoid false tripping. It could also potentially cause damage to sensitive power electronic interfaces.

Chapter 5
Conclusions and Future Work

The work presented in this thesis was divided into two parts. The first part involved discussion on the distribution feeder reconfiguration problem and the second part involved the discussion on the notional microgrid that was modeled as a part of this work.

5.1 Conclusion

Distribution feeder reconfiguration, presented in chapters 2 and 3, advanced some of the existing work of using GAs for finding the Pareto front of solutions to the distribution feeder reconfiguration problem. Chapter 2 provided an understanding of how search problems can be classified based on the complexity of the problem. The lower and upper bounds on the growth of the distribution feeder reconfiguration problem were also found in this work. Further, using the standard reduction technique, **the problem was classified as an *NP* problem**. This means, that the problem cannot be solved in polynomial time using any of the conventional search algorithms such as descent methods, Dijkstra's algorithm, or A* algorithm. This proof also explains why prior work in feeder reconfiguration use heuristic based algorithms such as simulated annealing or genetic algorithms. The computational complexity of a problem must be identified before researching an algorithm to solve the problem. This is because, attempts to find efficient polynomial time algorithms to ***NP*** problems, have been futile. On the other hand, the use of heuristics based algorithms to solve polynomial time problems, may lead to pseudo-optimal solutions.

Chapter 3 focused on advancing a prior algorithm that is used to solve the distribution feeder reconfiguration problem. Prior techniques to solve the reconfiguration problem were found to take a long execution time to converge to the solutions. Analysis of the code revealed what factors led to the long code executions. Based on these observations, **an efficient technique was developed to accelerate the code execution of the feeder reconfiguration problem**. This technique led to savings in time of an order

of magnitude. The results of the various formulations of the problem were shown to be in agreement with the results obtained from the unaccelerated codes.

Chapter 4 introduced the concept of microgrids, and provided details on the implementation of a notional mission-specific microgrid. A microgrid may be developed at a site based on the local load needs. Situated close to the loads, the main purpose of the microgrid could be to improve the overall efficiency of the system. This is achieved by use of CHP systems by reusing the waste heat produced as a by-product of power generation for internal heating of nearby residential or small scale commercial buildings. Another important application of a microgrid is to maintain power supply to critical infrastructure in the event of loss of power supply from the main grid. The main grid is vulnerable to attacks, both physical and cyber. Maintaining power supply to certain critical resources such as military bases in the event of loss of supply from the main grid may be important. In such a case, a microgrid serves as an ideal resource. While some microgrids have distributed storage resources to seamlessly transform the microgrid from a grid connected to islanded mode of operation, most microgrids must rely on blackstart capability. Blackstart defines a sequence of steps that must be followed to bring up the loads in the microgrid. Blackstart sequences are very specific to each microgrid, since most microgrids differ in the mix of power generation resources that are available at the microgrid site, or the capacity of the resources. In this work, **studies were conducted on the various generation resources available at the site of a notional microgrid, and a blackstart sequence was developed**. Microgrids are also capable of exporting power to the main grid during periods of peak loads. This aids in peak shavings for the utilities supplying the main grid.

5.2 Future work

The distribution feeder reconfiguration algorithm can now be applied to much larger systems, which closely resemble real world power networks. The algorithm can also be used to study the effects and the role of potential impact of technologies such as PHEVs on the larger grid.

Future work in the field of microgrids includes the development of a SCADA system for control and operation of the notional microgrid. The SCADA system could have the capability to be updated on

the real-time prices of power on the main grid. Through this the system could decide for or against exporting power from the microgrid to aid in peak shaving efforts on the main grid.

Since plans are underway to include renewable energy in the mix of generation in the notional microgrid, another avenue of future work could be to study the effects of renewables on the notional microgrid and on blackstart sequence.

REFERENCES

[1] S. Abraham and R. J. Efford, "Final Report on the August 14 2003 Blackout in the United States and Canada: Causes and Recommendations," U.S - Canada Power System Outage Task Force, Apr 2004.

[2] Smart Grid: Enabler of the new energy economy. A report by the Electrical Advisory Committee, Dec 2008. [Online] {Available}: http://energy.gov/sites/prod/files/oeprod/DocumentsandMedia/final-smart-grid-report.pdf

[3] 110th Congress of the United States, "Title XIII (Smart Grid)," in *Energy Independence and Security Act* of 2007. Washington, DC: Dec. 2007, pp. 292 – 303.

[4] M. M. Foss, "Electricity Restructuring in Texas – A Status Report," Centre for Energy Economics, October 2003.

[5] Smarter Grids: The Opportunity – Dept. of Energy and Climate Change. [Online] {Available}: http://www.decc.gov.uk/assets/decc/what%20we%20do/uk%20energy%20supply/futureelectricitynetworks/1_20091203163757_e_@@_smartergridsopportunity.pdf

[6] M. Sánchez, "Overview of microgrid research and development activities in the EU," [Online] {Available} http://der.lbl.gov/presentations/overview-microgrid-research-development-activities-eu

[7] P. Acharjee and J. Gunda, "Development prospect of Smart Grid in India," IEEE International Conference on Power and Energy (PECon), 2010.

[8] E. Santacana, G. Rackliffe, L. Tang, and X. Feng, "Getting Smart," *IEEE Power and Energy Magazine*, Mar-Apr 2010.

[9] The UK Low Carbon Transition Plan: national strategy for climate and energy. - Dept. of Energy and Climate Change. [Online] {Available}: http://www.decc.gov.uk/publications/basket.aspx?FilePath=White+Papers%2fUK+Low+Carbon+Transition+Plan+WP09%2f1_20090724153238_e_%40%40_lowcarbontransitionplan.pdf&filetype=4#basket

[10] A vision for the modern grid. – Prepared by the Office of Electricity Delivery and Energy Reliability, Apr 2007. [Online] {Available}: http://www.ilgridplan.org/Shared%20Documents/A%20Vision%20for%20the%20Modern%20Grid.pdf

[11] R. E. Brown, "Impact of Smart Grid on distribution system design," IEEE Power & Energy Society General Meeting, Pittsburgh, PA, 2008.

[12] X. Mamo, S. Mallet , T. Coste , and S. Grenard , "Distribution automation: The cornerstone for Smart Grid development strategy," IEEE Power & Energy Society General Meeting, Calgary, Alberta, Canada, 2009.

[13] J. Fan and S. Borlase, "The Evolution of Distribution," *IEEE Power and Energy Magazine*, vol.7, pp. 63-68, 2009.

[14] *IEEE Draft Guide for Design, Operation, and Integration of Distributed Resource Island Systems with Electric Power Systems*, IEEE P1547.4 Draft 4, 2008.

[15] R. Lasseter, A. Akhil, C. Marnay, J. Stephens, J. Dagle, R. Guttromson, A. S. Meliopoulous, R. Yinger, and J. Eto, "Integration of Distributed energy resources: The CERTS microgrid concept," Apr 2002.

[16] A. Shipley, A. Hampson, B. Hedman, P. Garland, and P. Bautista, "Combined Heat and Power - Effective Energy Solutions for a Sustainable Future," [Online] {Available} http://www1.eere.energy.gov/manufacturing/distributedenergy/pdfs/chp_report_12-08.pdf

[17] R. H. Lasseter and P. Paigi, "Microgrid: a conceptual solution," IEEE Power Electronics Specialists Conference, Aachen, Germany, 2004.

[18] California distributed energy resource grid on microturbines. [Online] {Available} http://www.wbdg.org/resources/microturbines.php

[19] H. E. Brown, "Implications on the Smart Grid Initiative on Distribution System Engineering: Improving Reliability on Islanded Distribution Systems with Distributed Generation Sources," M.S dissertation, Dept. of Elec. Eng., Colorado School of Mines, 2010.

[20] J. G. Miner, "Planning distribution system resource islands considering reliability, cost and the impact of penetration of Plug-in Hybrid electric vehicles," M.S dissertation, Dept. Elec. Eng., Colorado School of Mines, 2011.

[21] J. Giráldez, A. Jaiantilal, J. Walz, S. Suryanarayanan, S. Sankaranarayanan, H. E. Brown, and E. Chang, "An Evolutionary Algorithm and Acceleration Approach for Topological Design of Distributed Resource Islands," IEEE Power and Energy Society PowerTech 2011, Trondheim, Norway, 2011.

[22] GRID 2030: A National Vision for Electricity's Second 100 Years, U.S Dept. of Energy (2003) [Online] {Available} http://climatevision.gov/sectors/electricpower/pdfs/electric_vision.pdf

[23] Electric Reliability Council of Texas (ERCOT) [Online] {Available} http://www.ercot.com/

[24] Edison SmartConnect, Southern California Edison [Online] {Available} http://www.sce.com/info/smartconnect/smartenergy/smart-energy.htm

[25] PG&E SmartMeter Leads the Nation, Pacific Gas & Electric Co. [Online] {Available} http://www.pge.com/mybusiness/customerservice/meter/smartmeter/

[26] The Future Smart Grid: Smart Meters Are Just the Beginning, CenterPoint Energy [Online] {Available} http://www.centerpointenergy.com/services/electricity/competitiveretailers/smartmeters/thefuturesmartgrid/

[27] Smart Texas: Rethinking Energy, Oncor, [Online] {Available} http://www.txuelectricdelivery.com/tech_reliable/smarttexas/

[28] Automated Meters: Austin Energy and the Smart Grid, Austin Energy [Online] {Available} http://www.austinenergy. com/Customer%20Care/Billing/AM/index.htm

[29] H. E. Brown, S. Suryanarayanan, and G. T. Heydt, "Some characteristics of emerging distribution systems considering the Smart Grid Initiative," *The Electricity Journal*, vol. 5, pp. 64-75, 2010.

[30] C. W. Gellings, *The Smart Grid: Enabling Energy Efficiency and Demand Response*, 1st ed., CRC Press, 2009.

[31] A. H. Rosenfeld, D. A. Bulleit, and R. A Peddie, "Smart Meters and Spot Pricing: Experiments and Potential", *IEEE Technology and Society Magazine*, vol. 5, pp. 23-28, 2009.

[32] K. Herter, "Residential implementation of critical-peak pricing of electricity," *Energy Policy*, vol. 4, pp. 2121-2130, 2007.

[33] S. Borenstei, M. Jaske, and A. Rosenfeld, "Dynamic Pricing, Advanced Metering and Demand Response in Electricity Markets," Center for the Study of Energy Markets, University of California at Berkeley, Oct. 2002
[Online] {Available} http://escholarship.org/uc/item/11w8d6m4

[34] C. S. Chen and J. T. Leu, "Interruptible load control for Taiwan power company," *IEEE Transactions on Power Systems*, vol. 5, pp. 460-465, 2002.

[35] J. F. Gómez, H. M. Khodr, P. M. de Oliveira, L. Ocque, J. M. Yusta,R. Villasana, and A. J. Urdaneta, "Ant Colony System Algorithm for the Planning of Primary Distribution Circuits," *IEEE Transactions on Power Systems*, vol. 19, no. 2, pp. 996–1004, 2004.

[36] V. Parada, J. A. Ferland, M. Arias, and K. Daniels, "Optimization of Electrical Distribution Feeders using Simulated Annealing," *IEEE Transactions on Power Delivery*, vol. 19, pp. 1135–1141, 2004.

[37] A. Augugliaro, L. Dusonchet, and E. R. Sanseverino, "An Evolutionary Parallel Tabu Search Approach for Distribution Systems Reinforcement Planning," *Advanced Engineering Informatics*, vol. 16, pp. 205–215, 2002.

[38] T. J. Hartranft, "Sustainable Energy for Deployed Military Bases," Proceedings of 2nd International Conference on Energy Sustainability, Jacksonville, Florida, 2008.

[39] M. Barnes, J. Kondoh, H. Asano, J. Oyarzabal, G. Ventakaramanan, R. Lasseter, N. Hatziargyriou, and T. Green, "Real-World MicroGrids - An Overview," IEEE International Conference on System of Systems Engineering, San Antonio, TX, 2007.

[40] N. DeForest, J. Lai, M. Stadler, G. Mendes, C. Marnay, and J. Donadee, "Integration & Operation of a Microgrid at Santa Rita Jail," [Online] {Available}
http://der.lbl.gov/sites/der.lbl.gov/files/jeju_deforest_poster.pdf

[41] [Online] {Available}
http://www.fuelcellmarkets.com/fuel_cell_markets/molten_carbonate_fuel_cells_mcfc/4,1,1,2505.html

[42] M. Gauthier, C. Abbey, F. Katiraei, J. Pepin, M. Plamondon, and G. Simard "Planned Islanding as a Distribution system operation tool for Reliability Enhancement," 19th International Conference on Electricity Distribution, Vienna, Austria, 2007.

[43] G. Reitenbach, "Smart Power Generation at UCSD". [Online] {Available} http://ssi.ucsd.edu/index.php?option=com_content&view=article&id=416:smart-power-generation-at-ucsd-november-1-2010&catid=8:newsflash&Itemid=20

[44] J. Lynch, "Update on Mad River MicroGrid and Related Activities," Northern Power Systems, 2005. [Online] {Available} http://der.lbl.gov/presentations/update-mad-river-microgrid-related-activities

[45] D. Zimmerle, "A Community-Scale Microgrid Demonstration: FortZED/RDSI," Colorado State University, Fort Collins, CO, 2011.

[46] M. Quah, "Feasibility Study of Micro-grids for Southeast Asia," [Online] {Available} http://der.lbl.gov/sites/der.lbl.gov/files/jeju_quah_poster.pdf

[47] E. Hirotoshi, S. Hiroaki, S. Shigeyuki, M. Saburou, S. Eisuke, M. Kimio, L. Shirong, and H. Qiguo, "Simulation of supply-demand control in Micro-Grid with fluctuating natural power supply," The International Conference on Electrical Engineering, San Francisco, U.S, 2008.

[48] C. Marnay, "Microgrids and Heterogeneous Power Quality and Reliability," [Online] {Available} http://eetd.lbl.gov/ea/ems/reports/LBNL-777E.pdf

[49] E. Strickland, "A Microgrid That Wouldn't Quit," *IEEE Spectrum*, Oct. 2011.

[50] H. M. Liu, "The Development of Microgrid in China," IEEE Power and Energy Society Innovative Smart Grid Technologies European, Manchester, United Kingdom, 2011.

[51] I. Kungulovski, D. Kungulovski, A. Krkoleva, R. Taleski, M. Todorovski, V. Taseska, and N. Markovska, "Advanced Architectures and Control Concepts for more Microgrids," [Online] {Available} http://www.microgrids.eu/documents/664.pdf

[52] S. S. Skiena, *The Algorithm Design Manual*, 1st ed., Springer 1997.

[53] O. Goldreich, *P, NP, and NP-Completeness: The Basics of Computational Complexity,* 1st ed., Cambridge University Press 2010.

[54] S. Dasgupta, C. H. Papadimitriou, and U. V. Vazirani, *Algorithms* - [Online] {Available}: http://www.cs.berkeley.edu/~vazirani/algorithms.html

[55] A. M. Leite da Silva, W. S. Sales, L. C. Resende, L. A. F. Manso, C .E. Sacramento, and L. S. Rezende, "Evolution Strategies to Transmission Expansion Planning considering Unreliability Costs," In Proc. of the 9th PMAPS, Stockholm, Sweden, 11-15 June, 2006. [Online] {Available} http://citeseerx.ist.psu.edu/viewdoc/download?doi=10.1.1.92.3907&rep=rep1&type=pdf

[56] J. Zhu and M. Chow, "A Review of Emerging Techniques on Generation Expansion Planning," *IEEE Trans. Power Syst*., vol. 12, no. 4, pp. 1722-1728, Nov. 1997.

[57] S. Suryanarayanan and R. G. Farmer, "Load modeling for stability studies," A white paper for Power Systems Engineering Research Center, Arizona State University, Tempe, AZ, Dec. 2002

[58] F. Woolf, *Global Transmission Expansion; Recipes for Success*, Tulsa Oklahoma: Penn Well Corporation, 2003.

[59] M. K. Deshmukh and S. S. Deshmukh, "Modeling of hybrid renewable energy systems," *Renewable and Sustainable Energy Reviews*, volume 12, Issue 1, pp. 235–249, 2008.

[60] R. Billinton and R. N. Allan, *Reliability Evaluation of Power Systems*, 2nd ed., New York: Plenum Press, 1996.

[61] R. T. Marler and J. S. Arora, "Survey of multi-objective optimization methods for engineering," *Structural and Multidisciplinary Optimization*, vol. 26 no. 6, pp. 369-395, 2007.

[62] C. A. C. Coello, G. B. Lamont, and D. A. VanVeldhuizen, *Evolutionary Algorithms for Solving Multiobjective Problems*, 2nd ed. New York: Springer, 2007.

[63] F. Y. Kocer and J. S. Arora, "Optimal design of H-frame transmission poles for earthquake loading," *Journal of Structural Engineering*, vol. 125, Issue 11, 1999.

[64] D. Whitley, "A genetic algorithm tutorial," [Online] {Available} http://www.cs.colostate.edu/~genitor/MiscPubs/tutorial.pdf

[65] T. Cormen, C. Leiserson, R. L. Rivest, and C. Stein, *Introduction to Algorithms*, 3rd ed., The MIT Press, 2009.

[66] R. Billinton, S. Kumar, et al., "A Reliability Test System for Educational Purposes - Basic Data," *IEEE Transactions on Power Systems*, vol. 4, pp. 1238-1244, August 1989.

[67] R. Billinton and S. Jonnavithula, "A Test System for Teaching Overall Power System Reliability assessment," *IEEE Transactions on Power Systems*, vol. 11, pp. 1670-1676, November 1996.

[68] "PowerWorld Simulator - Automation Server (SimAuto)," PowerWorld Coporation, Champaign, IL, 2009.

[69] H. E. Brown, D. A. Haughton, G. T. Heydt, and S. Suryanarayanan, "Some Elements of Design and operation of a Smart Distribution System," IEEE T&D Conference and Exposition, pp.1-8, April 2010.

[70] T. P. Wagner, A. Y. Chikhani, and R. Hackam, "Feeder Reconfiguration for Loss Reduction: An Application of Distribution Automation," *IEEE Transactions on Power Delivery*, vol. 6, pp. 1922-1933, October 1991.

[71] D. T. Ton., W. M Wang, and W. Wang, "Smart Grid R&D by the U.S. Department of Energy to optimize distribution grid operations," IEEE Power & Energy Society General Meeting, pp. 1-5, 2011.

[72] [Online] {Available} http://www.cecer.army.mil/td/tips/docs/EnergySurety.pdf

[73] J. Langston, S. Suryanarayanan, M. Steurer, M. Andrus, S. Woodruff, and P. F. Ribeiro, "Experiences with the simulation of a notional all-electric ship integrated power system on a large-scale high-speed electromagnetic transient simulator," IEEE Power & Energy Society General Meeting, pp. 1-5, 2006.

[74] C. Niannian, X. Xufeng, and J. Mitra, "A hierarchical multi-agent control scheme for a black start-capable microgrid," IEEE T&D Conference and Exposition, pp. 1-8, April 2011.

[75] [Online] {Available} http://www.eia.gov/forecasts/archive/aeo11/chapter_executive_summary.cfm#domestic

[76] [Online] {Available} http://www.eia.gov/oiaf/analysispaper/biomass/

[77] [Online] {Available} http://www.ucsusa.org/clean_energy/technology_and_impacts/energy_technologies/how-biomass-energy-works.html.

[78] J. Benneche et al, "Annual Energy Outlook 2002," Dec. 2001. [Online] {Available} ftp://ftp.eia.doe.gov/forecasting/0383(2002).pdf.

[79] Z. Ding, S. K. Srivastava, D. A. Cartes, and S. Suryanarayanan, "Dynamic Simulation-Based Analysis of a New Load Shedding Scheme for a Notional Destroyer-Class Shipboard Power System", *IEEE Transactions on Industrial Applications,* vol. 45, pp. 1166 – 1174.

[80] N. Senroy, S. Suryanarayanan, and P. F. Ribeiro, "An Improved Hilbert–Huang Method for Analysis of Time-Varying Waveforms in Power Quality," *IEEE Transactions on Power Systems*, vol. 22, no. 4, pp. 1843-1850, Nov. 2007.

[81] K. Ogata, *Modern Control Engineering*, 5th ed., Prentice Hall, 2009.

[82] A.L Dimeas and N. D. Hatziargyriou, "Operation of a Multiagent System for Microgrid Control," *IEEE Transactions on Power Delivery*, vol. 6 issue 3, pp.1447 – 1455.

[83] D. Zimmerle, "RE: Regarding the NG machine" Official e-mail (Mar. 23, 2012).

Appendix A

Accessing PowerWorld™ from Matlab™

- Accessing PowerWorld™ files from Matlab™ through a COM connection.

```
Aux_connx = actxserver('pwrworld.SimulatorAuto');

% Set the current directory to working folder
Aux_connx.CurrentDir = '/*Provide the absolute path of the working
folder here*/';

%PowerWorld file that is to be accessed from Matlab
file = '/*Provide the absolute path of the PowerWorld file that
contains the network to be reconfigured*/';

Output = Aux_connx.OpenCase(file);

%Check if there was an error in opening the file
if ~(strcmp(Output{1},''))
    fprintf('OpenCase error: ')
    disp(Output{1})
    return
end
```

- Sample script for running multiple generations through a single Aux file on Matlab™. Call script commands from Matlab™ using the Aux_connx.RunScriptCommand command.

```
SCRIPT script_1
{
     OpenCase("'/*Provide the absolute path of the PowerWorld file
that contains the network to be reconfigured*/");
     EnterMode(EDIT,CASE);
     EnterMode(POWERFLOW);
     ResetToFlatStart (YES, NO,NO,NO);
     SolvePowerFlow (POLARNEWTON);
     CTGProduceReport("CTG_Filters_AfterReport");
     OPFWriteResultsAndOptions("'/*Provide the absolute path of the
AUX file that PowerWorld reads to reconfigure the network*/");
     EnterMode(EDIT,CASE);
}

DATA data_1(Branch, [BusNum, BusNum:1, BusName_NomVolt,
BusName_NomVolt:1, LineAMVA, LineBMVA, LineCMVA, LineR, LineX, LineC,
LineCircuit, LineStatus], CSV, True)
{
1, 4, 1_ 12.5, 4_ 12.5, 15.42, 0, 0, 0.0011309, 0.0033048, 0, 1,
Closed
}
```

```
SCRIPT script_2
{
      EnterMode(RUN,POWERFLOW);
      ResetToFlatStart (YES, NO,NO,NO);
      SolvePowerFlow (POLARNEWTON);
      OPFWriteResultsAndOptions("filename");
}

SCRIPT script_3
{
      OPFWriteResultsAndOptions(“/*Provide the absolute path of the
PowerWorld file that contains the network to be reconfigured */”);
}

SCRIPT script_4
{
      OpenCase(“/*Provide the absolute path of the PowerWorld file that
contains the network to be reconfigured*/”);
      EnterMode(EDIT,CASE);
      EnterMode(POWERFLOW);
      ResetToFlatStart (YES, NO,NO,NO);
      SolvePowerFlow (POLARNEWTON);
      CTGProduceReport("CTG_Filters_AfterReport");
      OPFWriteResultsAndOptions(“/*Provide the absolute path of the AUX
file that PowerWorld reads to reconfigure the network*/”);
      EnterMode(EDIT,CASE);
}

DATA data_2(Branch, [BusNum, BusNum:1, BusName_NomVolt,
BusName_NomVolt:1, LineAMVA, LineBMVA, LineCMVA, LineR, LineX, LineC,
LineCircuit, LineStatus], CSV, True)
{
1, 6, 1_ 12.5, 4_ 12.5, 15.42, 0, 0, 0.0012309, 0.0033048, 0, 1,
Closed
}

SCRIPT script_5
{
      EnterMode(RUN,POWERFLOW);
      ResetToFlatStart (YES, NO,NO,NO);
      SolvePowerFlow (POLARNEWTON);
      OPFWriteResultsAndOptions("filename");
}

SCRIPT script_6
{
      OPFWriteResultsAndOptions(“/* Provide the absolute path of the
AUX file that PowerWorld reads to reconfigure the network */”);
}
```

Appendix B

Steps to run MOGA on Matlab™

- Create the distribution feeder system that is to be studied on PowerWorld™.
- Open file RunMoga.m. This file contains a call to the GA toolbox function "gaoptimset", which contains the following information. These fields can be modified as required.
    - Population type
    - Size of a population
    - The initial population. This can be defined to be random or a specific population specified by the user
    - Pareto fraction: This limits the number of individuals on the Pareto front.
    - Maximum number of generations to run the genetic algorithm
    - PlotFcn: Use default value.
- The function "gamultiobj" has the following information that can be modified.
    - objectval: A reference to the function that evaluates the objective function for each string. There are two objectives modeled in this problem. First is the ENS, and next is the cost. Both the objectives are computed for each individual string in each population, in this function. To start, Matlab first establishes a connection with SimAuto using the Aux command [Appendix A].
        - Next, the current network configuration is obtained using the "DevListDisp" function. The total load in the system is obtained using the SimAuto's "GetParametersMultipleElement" command.
        - The functions "branchEX" and "genEX" are used to get parameters of the various elements (loads, generators, and branches) from PowerWorld. While the function "DevListDisp" uses SimAuto's "ListOfDevices" command to obtain the key field values only, the "branchEX" and "genEX" commands use SimAuto's

"GetParametersMultipleElement" command to obtain any specified parameters of an element.

- Next the "genFormat" and "branchFormat" commands are used to format the input to PowerWorld, as PowerWorld can read in a specific format only.
- The command "ChangeParametersMultipleElementFlatInput" is used to reconfigure the network on PowerWorld through Matlab.
- Based on the output of the load flow analysis, the ENS is calculated. Cost of the reconfigured network is calculated directly, from the cnxns matrix. Functions loading, v_level and penalty are used to evaluate the penalty function of each configuration. Penalty functions are used to find the fitness of a string in a population.

- The second command to gamuliobj, is the length of each string in a population. This value changes based on total number of interties, and number of possible generator locations.
- All other inputs to the function gamultiobj are retained as default values.
- This function returns after completion of all generations of the GA. It returns the final population.

- Further processing can be done, as desired by the user, based on outputs received. In this work, the population returned from the GA is used to print results on the command window in Matlab™.